



GE Energy

David H. Hinds  
Manager, ESBWR

PO Box 780 M/C L60  
Wilmington, NC 28402-0780  
USA

T 910 675 6363  
F 910 362 6363  
david.hinds@ge.com

MFN 06-428

Docket No. 52-010

October 29, 2006

U.S. Nuclear Regulatory Commission  
Document Control Desk  
Washington, D.C. 20555-0001

Subject: **Response to Portion of NRC Request for Additional Information  
Letter No. 43 Related to ESBWR Design Certification Application –  
Containment Fragility – RAI Numbers 6.2-96, 19.2-39, 19.2-40, 19.2-  
42, 19.2-43, 19.2-47, 19.2-48, 19.2-51, 19.2-52, 19.2-53, 19.2-54, 19.2-55,  
19.2-66, 19.2-67 and 19.2-68**

Enclosure 1 contains GE's response to the subject NRC RAIs transmitted via the  
Reference 1 letter.

If you have any questions about the information provided here, please let me know.

Sincerely,

David H. Hinds  
Manager, ESBWR

D068

Reference:

1. MFN 06-237, Letter from U.S. Nuclear Regulatory Commission to David Hinds, *Request for Additional Information Letter No. 43 Related to ESBWR Design Certification Application*, July 18, 2006

Enclosure:

1. MFN 06-428 – Response to Portion of NRC Request for Additional Information Letter No. 43 Related to ESBWR Design Certification Application – Containment Fragility – RAI Numbers 6.2-96, 19.2-39, 19.2-40, 19.2-42, 19.2-43, 19.2-47, 19.2-48, 19.2-51, 19.2-52, 19.2-53, 19.2-54, 19.2-55, 19.2-66, 19.2-67 and 19.2-68

cc: AE Cabbage USNRC (with enclosures)  
GB Stramback GE/San Jose (with enclosures)  
eDRF 0059-0213

**ENCLOSURE 1**

**MFN 06-428**

**Response to Portion of NRC Request for**

**Additional Information Letter No. 43**

**Related to ESBWR Design Certification Application**

**Containment Fragility**

**RAI Numbers 6.2-96, 19.2-39, 19.2-40, 19.2-42, 19.2-43,  
19.2-47, 19.2-48, 19.2-51, 19.2-52, 19.2-53, 19.2-54,  
19.2-55, 19.2-66, 19.2-67 and 19.2-68**

**NRC RAI 6.2-96**

*In ESBWR DCD Tier 2, rev 01, Section 6.2.5.4, which addresses 10 CFR50.44(c)(5) - Hydrogen Rule, GE states that the pressure capability of the containment's limiting component is higher than the pressure (GE does not quantify this pressure) that results from assuming 100% fuel clad-coolant reaction. Provide the following information:*

- a) the estimate of the internal pressure loading on the ESBWR containment structure, assuming an "accident that releases hydrogen generated from 100 percent fuel clad-coolant reaction accompanied by hydrogen burning."*
- b) where the estimate is in response to question (a), above, documented in DCD Tier 2.*
- c) what the estimated temperature of the containment structure is at the time of this event discussed in question (a).*
- d) a justification for the use of ambient temperature material properties, in the case that the estimated temperature is higher than ambient temperature, or a revision to the Service Level C pressure capabilities for each containment structural component, consistent with its estimated structural temperature.*
- e) details of the analysis described in the last paragraph of ESBWR DCD Tier 2, rev 01, Section 6.2.5.4.2, for the concrete containment, "A nonlinear finite element analysis of the containment concrete structure including liner plates is performed for over-pressurization." If the analysis is contained in another section of the DCD, provide the reference.*
- f) the estimate of the Level C pressure capability of the drywell head if evaluation of instability is NOT included? Provide details of the calculation.*
- g) the estimate of the Level C pressure capability of the drywell head if the method of Code Case N-284-1 (linear bifurcation buckling prediction, capacity reduction factor for imperfections, capacity reduction factor for inelastic response, SF=1.67 for Level C) is used, instead of DCD Tier 2, rev 01, Section 6.2.5.4.2, Eq. (6.2-2). Provide details of the calculation.*

**GE Response**

- a) Burn of hydrogen was not considered because of inerting. There is residual oxygen (~3%), but burning this makes the containment pressure lower. The concentration is too low for detonation so no pressure is added, only heat. This amount of heat is small compared with decay heat, so it can be effectively removed by the PCCS - which is not at its heat removal limit 4 hours into the scenario (the earliest time of core melt that was calculated).
- b) It is not in Tier 2.

- c) Temperature is not relevant because of the PCCS. The saturation temperature at pressure should be used.
- d) As a first stage, room temperature material properties were used in determining Containment Ultimate Capacity and the results extrapolated for higher temperatures (see NEDO-33201 Rev. 1 Table B.8-2, and response to RAI 19.2-45 and 46). In addition, the way high temperature Drywell Head material is considered is explained in response to RAI 19.2-55.

A confirmatory analysis was performed taking into account high temperature effects explicitly. The results are shown in response to RAI 19.2-47.

- e) Details of the nonlinear finite element analysis of the containment concrete structure performed for over-pressurization are contained in report 092-134-F-C-0004, which is available for NRC review at GE San Jose offices.
- f) The estimate of the Level C pressure capability of the drywell head excluding instability is 1.684MPa which is the pressure required to result in the primary membrane stress equal to Service Level C allowable based on the ASME B&PV Code Sec. III, Subsection NE-3324.8(b). The details of calculation are described in DC-OG-0052, "Structural Design Report for Containment Metal Components", Revision 1, which is available for NRC review at GE San Jose offices.
- g) The method of Code Case N-284-1 is not used since evaluation of instability is not a RG 1.7 Rev. 3 requirement for demonstration of containment structural integrity to meet NE-3220, Service Level C Limits.

No DCD changes will be made in response to this RAI.

**NRC RAI 19.2-39**

*In DCD Tier 2, Section 19.2.4, General Electric (GE) provides a containment performance assessment for the ultimate pressure capability. This assessment was described in the context of the containment pressure fragility estimates. However, it is the staff's expectation that deterministic containment performance assessment addressing the criteria in SECY 93-087 and 10 CFR 50.44(c)(5) be located in this section and the structural calculations and assumptions need to be presented in Chapter 19 or in Section 3.8. All relevant structural assessments of the critical elements necessary to maintain containment performance and integrity, such as reinforced concrete containment structure, drywell head and its connections, critical bellows and their connections, large diameter piping connections, instrumentation or power supply penetrations should be described and discussed in Chapter 19.*

*Provide the following information for the deterministic containment performance assessment in this section:*

- a) A discussion of the deterministic containment performance assessment of the ultimate pressure capability of all relevant critical elements of containment integrity and performance.*
- b) In order to ensure that the as-built plant implements the containment performance as reviewed by the staff for the design certification, it is necessary to provide essential details and drawings of critical sections of all critical components and connections in the table of Inspection, Test, Analyses and Acceptance Criteria (ITAAC) with clear statements related to as-procured engineering specifications, certified as-built engineering reports, test data and results, walk down and measurements of dimensions, as appropriate.*
- c) A discussion of how 10 CFR 50.44(c)(5) is met, and, if the issue is addressed in other sections of the DCD Tier 2, provide a direct reference.*
- d) SECY-93-087 requires satisfaction of Service Level C limits, including considerations of structural instability, for the more likely severe accident challenges for approximately 24 hours following the onset of core damage under the most likely severe accident challenges, and, following this period, the containment should continue to provide a barrier against the uncontrolled release of fission products. Provide:*
  - 1) a discussion of how the SECY-93-087 requirements are addressed in the GE deterministic containment performance analysis, include any transient condition in which the containment could be subjected to negative external pressure caused by condensation of internal hot gases and,*
  - 2) the estimate of the Service Level C pressure capability of the ESBWR containment and associated failure modes for the challenges discussed in response to question (1) above.*

**GE Response**

- a) PRA report NEDO-33201 Rev 1, Appendix B.8 contains evaluation of ultimate pressure capability for all critical elements (concrete shell, drywell head, PCCS heat exchangers, liner plates, and penetrations), along with the uncertainties in the prediction of the failure pressure.
- b) Inclusion of design details and drawings in ITAAC Tables is not warranted. DCD Tier 1 ITAAC Table 2.15.1-1 already contains sufficient requirements to ensure that the containment is built according to design configuration.
- c) 10 CFR 50.44(c)(5) regulation is met following RG 1.7 Revision 3 requirements for demonstration of containment structural integrity by meeting ASME Service Level C/Factored Load Category limits. Service Level C pressure capability evaluation is contained in DCD Section 6.2.5.4.2.
- d) It is GE's understanding that the SECY-83-087 requirements are reflected in RG 1.7 Revision 3. The structural evaluation performed in accordance with RG 1.7 as stated above also satisfies SECY-83-087.

No DCD changes will be made in response to this RAI

**NRC RAI 19.2-40**

*In DCD Tier 2, 6.2.5.4 and 19.2.4, respectively, GE provides a deterministic analysis and a fragility analysis for the containment performance under internal pressurization. However, neither information nor discussion of adequate anchorage of the drywell head into the top concrete slab to ensure the anchorage capacity exceeds the load capacity of the drywell head is provided in these sections. The design pressure for the ESBWR containment is 0.31 MPa (45 psi); the stated Service Level C pressure capability for the drywell head is 1.182 MPa (171 psi), which is about 4 times the design pressure. Provide the following information:*

- a) In determining the Service Level C pressure capability for the drywell head, how was the primary axial load path through the bolted flange closure (DCD Figure 3G.1-51, Detail B), to the anchored support cylinder (DCD Figure 3G.1-51, Detail C), and into the concrete evaluated?*
- b) Include in the DCD details of the calculation which demonstrates that the Service Level C pressure capability for the bolted flange closure, anchored support cylinder, and supporting concrete exceeds 1.182 MPa (171 psi), including: (1) a description of the load transfer from the drywell head, through the bolted closure, to the overall concrete upper slab; (2) the location and magnitude of the maximum radial shear load due to internal pressure; (3) the location and magnitude of the maximum shear stress in the concrete; (4) a discussion of potential leakage through the bolted flange closure at 1.182 MPa (171 psi) internal pressure; and (5) a discussion of potential bolt failure due to combined axial tension and transverse shear loading.*

**GE Response**

- a) The primary axial load of the drywell head under internal pressure is resisted by the bolted flange closure in the form of bending, by the anchored support cylinder through the lower flange and gusset plate in the form of bending and shear, and by the concrete in the form of bearing.
- b) The Service Level C pressure capability of the bolted flange closure, anchored support cylinder and supporting concrete was evaluated by stress analysis under internal pressure loading equal to 1.182 MPa, the controlling Service Level C capability. The results are summarized in Tables 19.2-40(1) through (4). All stresses satisfy Service Level C allowable based on the ASME B&PV Code Section III, Subsection NE and CC; hence their Service Level C pressure capabilities are higher than 1.182 MPa. The details of calculation are described in DE-ES-0024, "Stress Analysis Report for Drywell Head under Severe Accident Condition", Revision 1, which is available for NRC review at GE San Jose offices. It should be noted that under internal pressure load, no transverse shear is developed in the

flange bolts and no radial shear in the anchorage system. See response to RAI 19.2-52 for potential leakage through the bolted flange closure.

Figure 3G.1-51 of DCD Tier 2 Appendix 3G will be revised in the next update as noted in the attached markup.

**Table 19.2-40(1) Summary of Stress Evaluation for Flange**  
 unit: MPa

Condition	Stress	Result	Limit	
Level C	SH	201	$1.5S_{mc}$	227
	SR	99	$1.0S_{mc}$	151
	ST	-24	$1.0S_{mc}$	151
	$(SH+SR)/2$	150	$1.0S_{mc}$	151
	$(SH+ST)/2$	89	$1.0S_{mc}$	151

**Table 19.2-40(2) Summary of Stress Evaluation for Flange Bolt**  
 unit: MPa

Condition	Stress	Result	Limit	
Level C	$\sigma_B$	212	2.2S	439

**Table 19.2-40(3) Summary of Stress Evaluation for Other Metal Parts**  
 unit: MPa

Evaluation Point	Service Level	$P_L+P_b$		
		Result	Limit	
Lower Flange Plate	Level C	386	$1.8S_{mc}$ or $1.5S_y$	393
Gusset Plate of Lower Flange Plate	Level C	334	$1.8S_{mc}$ or $1.5S_y$	393

**Table 19.2-40(4) Summary of Stress Evaluation for Concrete Portion**  
 unit : MPa

Evaluation Point	Compressive Stress	Limit	
Concrete Portion near the Lower Flange Plate	16.4	$0.6f_c'$	20.7

**NRC RAI 19.2-42**

*What provision has GE made in the DCD to ensure that the containment structure geometry, critical dimensions and details, and materials of construction will not be subject to change without prior review and approval by the staff?*

**GE Response**

Critical sections will be identified in the next update of DCD Tier 2 as Tier 2\* items which will require NRC Staff approval prior to implementing a change.

**NRC RAI 19.2-43**

*In DCD Tier 2, Section 19.2.2.4, GE provides a brief summary of the seismic fragility evaluation using the Zion method in NUREG/CR-2300. However, the details of the fragility results are presented in Section 15.0 of the PRA. These fragility results should be included in this DCD section. Further, the seismic fragility results and the ultimate containment pressure capability results should be adequately included in ITAAC tables of DCD Tier 1. Provide the following information:*

- a) Include the seismic HCLPF values from Tables 15-1 through 15-13 of the ESBWR PRA in DCD Tier 2, Section 19.2.2.4 and make appropriate entries into DCD Tier 1, ITAAC tables.*
- b) Also make appropriate entries into DCD Tier 1, ITAAC tables that address the ultimate containment pressure capability results from both the deterministic and fragility containment performance assessments.*

**GE Response**

- a) A summary of HCLPF margins is included in Table 19.2-4 of DCD Tier 2 Chapter 19 Rev. 1. Such information will not be included as ITAAC items in Tier 1 since the existing ITAAC items for various SSCs will ensure that the plant has adequate seismic margin beyond the design basis SSE due to the various conservatism introduced in the normal design process.
- b) Inclusion of ultimate containment pressure capability results in ITAAC Tables is not warranted. DCD Tier 1 ITAAC Table 2.15.1-1 already contains sufficient requirements to ensure that the containment is built according to design configuration.

No DCD changes will be made in response to this RAI.

**NRC RAI 19.2-47**

*In PRA Appendix B.8.2.1, GE provides an estimate of containment pressure capacity at 500 °F temperature. This estimate was based on an ANL study, which concluded that the failure pressure for RCCV at temperatures up to 700°F was reduced by about 11% from that predicted at ambient temperature, for pressure load alone. Provide:*

- a) a discussion of the applicability of the ANL study to the ESBWR containment.*
- b) a discussion of an estimate of the containment pressure capacity at 500°F, if the ANSYS model had been used (Repeat the ANSYS analysis with degraded material properties at 500°F), and a comparison of the ANSYS analysis result for 500°F with the pressure capacity reduction estimate of 10% based on the ANL study.*
- c) a justification for using 500°F, based on the NUREG-1540 analysis of Oyster Creek drywell. This analysis considered an accident scenario where the uniform temperature was 800°F. Is 500°F just "typical", or is it the true maximum accident temperature that needs to be considered? Does 500°F represent a creditable upper bound to the temperature challenge?*
- d) a discussion of any available test data of containment pressure capacity at high temperatures for containments similar to ESBWR.*

**GE Response**

- a) The cited ANL study considered an axisymmetric analytical model of the 1:6 scale model of a reinforced concrete containment structure tested for over-pressurization capacity at Sandia National Labs. The axisymmetric model used in the study was based on a "clean" slice through the structure away from penetrations and thus considered a global failure mode of the RCCV, namely failure of the hoop rebar at mid-height of the barrel. Comparative analyses were considered for increasing internal pressure at ambient temperature (70 °F everywhere) and for 3 thermal conditions; steady state temperature distributions (linear through the wall thickness) with the liner at 400 °F and at 700 °F, and a simulated transient condition (bilinear temperature distribution through the wall) with the liner at 700 °F. The analyses showed that the internal pressure that would cause failure of the hoop rebar splices dropped from 185 psig for ambient temperatures to 165 psig for the 700 °F steady state condition. Note that the tested specimen did not fail in this global failure mode, but rather reached a limit of 145 psig when liner tears prevented further pressurization in a "leak before burst" mode. The lowest failure pressure in the ANL study corresponded to the steady state thermal condition with 700 °F liner temperature because the rebar had about 23% degradation in ultimate strength due to the higher penetration of temperatures into the RCCV wall. The ANL study concluded that the global failure mode for over-pressurization would not change due to the associated thermal conditions, and that the reduction in capacity is

mainly associated with material property degradation at temperature. For the mode of failure considered in the ANL study, the capacity was governed by the ultimate strength of the hoop rebar and splices.

The results are applicable to the ESBWR analyses provided in Appendix B.8.2.1 because they are applied in a consistent manner. This static capacity analysis is based on an axisymmetric model for the global failure of the RCCV. The capacity of the RCCV is not expected to be the limiting capacity of the ESBWR primary containment system, and the mode of this global failure under internal pressure is not expected to change with temperature. While the failure mode in the axisymmetric model for the ESBWR is found to be section shear capacity at a horizontal floor connection (rather than hoop rebar capacity), a similar reduction in capacity due to concrete and rebar property degradation at temperature was deemed appropriate. Some conservatism is included in adapting the 10% reduction in pressure capacity at elevated temperature from the ANL study to the ESBWR axisymmetric global analysis. The ANL study found an 11% reduction at 700 °F, whereas the ESBWR analysis considers a 10% reduction for a 500 °F condition. In addition, for the section shear capacity failure mode, the thermal loading also has a counteracting effect to the material property degradation. Any additional compressive stress acting on the section due to restraint against thermal expansion will increase the shear capacity of the section.

- b) To better assess the true pressure capacity of the RCCV and the effects of temperature on this capacity for the ESBWR containment system, an independent and a more detailed analysis using 3D modeling is performed. This analysis employs the ANACAP-U concrete and steel model coupled to the ABAQUS general purpose finite element program, and is based on the modeling performed for the thermal stress analysis of the LOCA conditions as part of the design basis. Thermal-stress analyses are performed for a half-symmetric, 3D model for the RCCV and reactor building using temperature dependent material properties. As a best estimate calculation, this analysis is based on median or expected values of material properties. This 3D model is better equipped to capture the non-axisymmetric configuration of the top slab and upper pools. The pressure capacity is determined for normal operating thermal conditions and then for the 500 °F accident condition case using a steady state temperature distribution with the drywell liner temperature increased to 500 °F. The wet well is considered to have a 3 psi differential (lower) pressure than the drywell and with a temperature corresponding to that of saturated water vapor at that pressure in the suppression pool.

Figures 19.2-47(1) and 19.2-47(2) plot the temperature contours for the normal operating condition and for the 500 °F condition, respectively, to illustrate the modeling. Figures 19.2-47(3) and 19.2-47(4) plot contours for the maximum principal strains in the concrete (with steel liners removed) with deformations magnified by 10 at an internal pressure of 4 times the design pressure for the normal operating and 500 °F cases, respectively. These figures illustrate the deformation

patterns and that the critical location for pressure capacity of the RCCV is at the connection of the top slab to the upper drywell wall. Cracking damage and trauma in the upper pool girders are also evident in the figures. It is found that the pressure capacity of the RCCV component of the primary containment system is limited by shear failure in the pool girders that span the top slab. This loss of structural integrity in these girders will then lead to rapid failure of the containment boundary at the connection of the RCCV wall to the top slab. For normal operating conditions, shear failure in the pool girders occurs at an internal pressure of 2.135 MPa or 6.88 times design pressure. For the 500 °F accident condition, the pool girders fail in shear at an internal pressure of 1.915 MPa or 6.17 times design pressure. Note that the mode of failure does not change because of the elevated temperatures, and that the reduction in the pressure capacity due to temperature is about 10%. This confirms that the 10% reduction factor used in the ANSYS analysis is appropriate.

- c) The design envelope for temperature, which is a bound on possible maximum anticipated temperatures, during a LOCA includes an initial spike to 171 °C (340 °F) and a long term temperature of 150 °C (302 °F). The best estimate temperature history for a large break leading to DCH conditions, see response to RAI 19.2-57(1), considers a temperature spike of ~1600 °C lasting only a few seconds, with a long term equilibrium temperature of about 200 °C (392 °F). Based on these severe accident temperature histories, the steady state temperature distribution with the liner at 500 °F is considered a representative maximum accident temperature distribution with regards to the containment pressure capacity. The pressure capacity for the RCCV is most affected when temperatures penetrate well into the wall depth because the strength reduction is most affected by material degradation at elevated temperature. Even a much higher temperature spike that lasts only a few seconds will have little effect on the pressure capacity because the temperatures within the RCCV wall are not affected. Note that in the ANL study, the pressure capacity for the 700 °F transient thermal distribution case was higher than the 400 °F steady state distribution case.
- d) We are unaware of any available test data for containment pressure capacity at high temperatures for containments similar to ESBWR. However, refer to response to RAI 19.2-41 c) for some discussion of available test data for containment pressure capacity at ambient temperature relative to the ESBWR containment design.

No DCD changes will be made in response to this RAI.

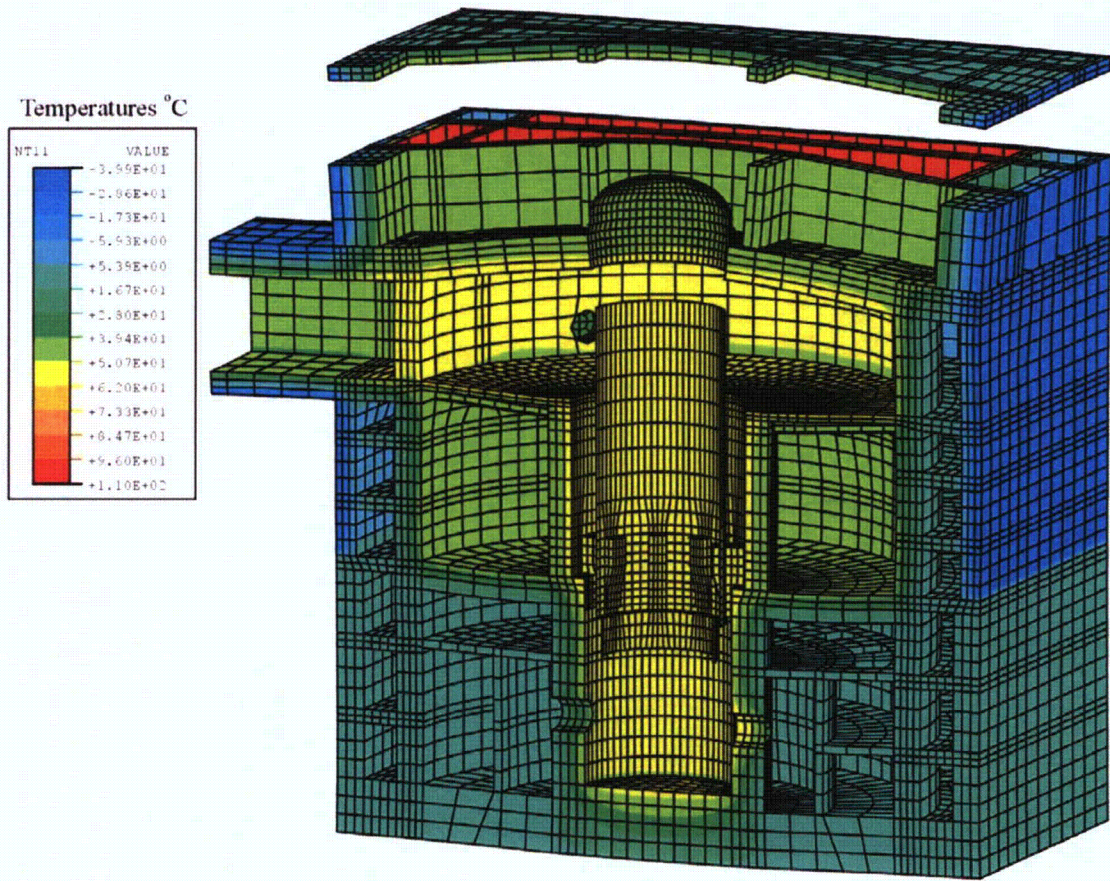


Figure 19.2-47(1) Temperature Distributions for Normal Operating Thermal Conditions

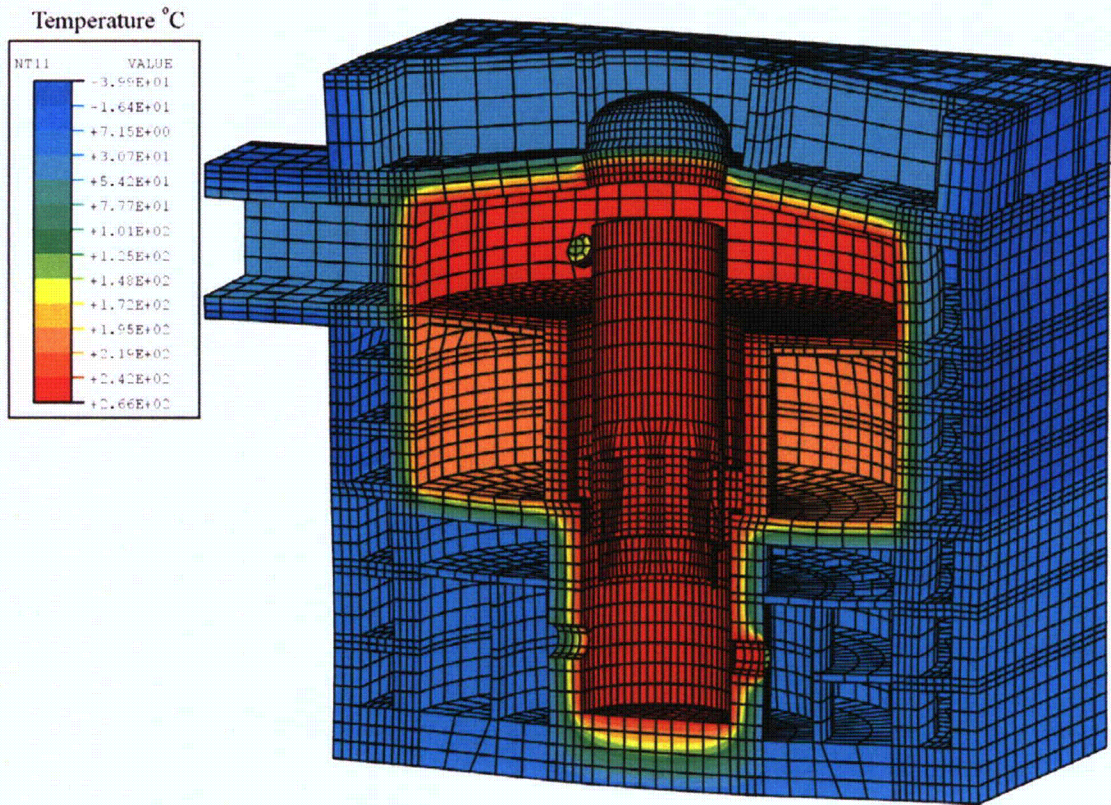


Figure 19.2-47(2) Temperature Distributions for 500 °F Thermal Conditions

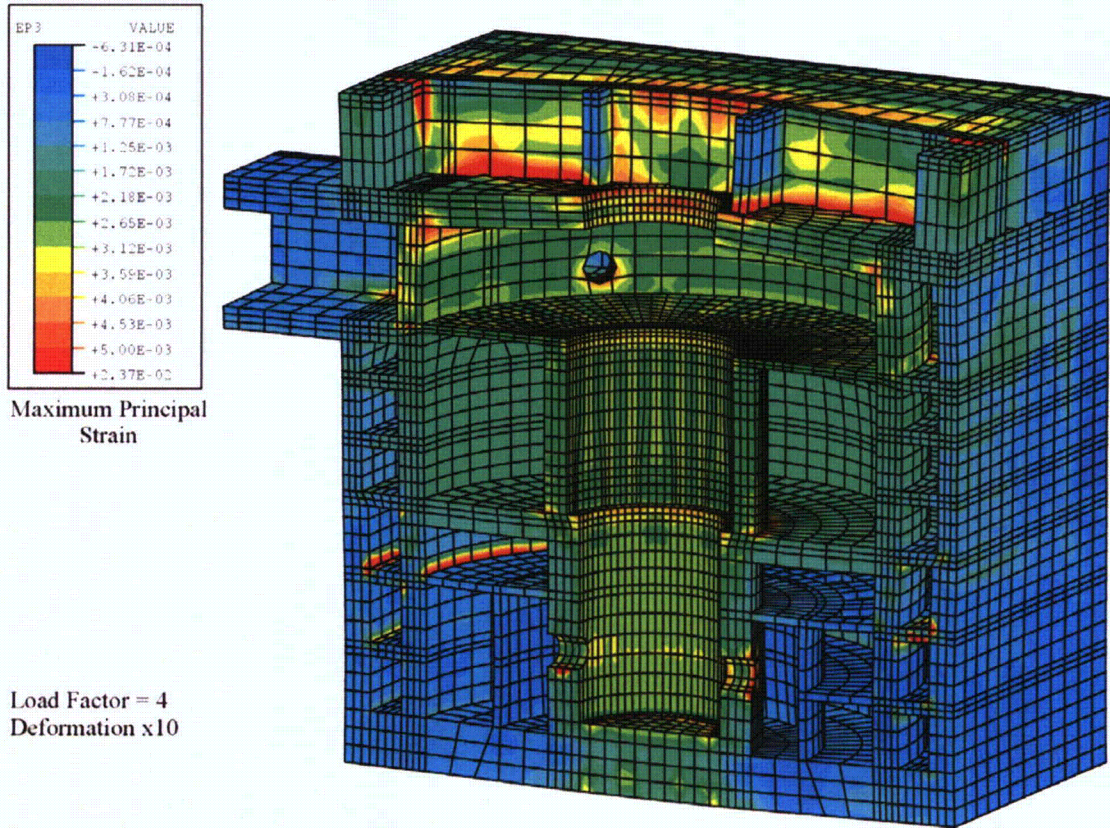


Figure 19.2-47(3) Maximum Principal Strains in RCCV for Normal Operating Conditions at 4 P<sub>d</sub>

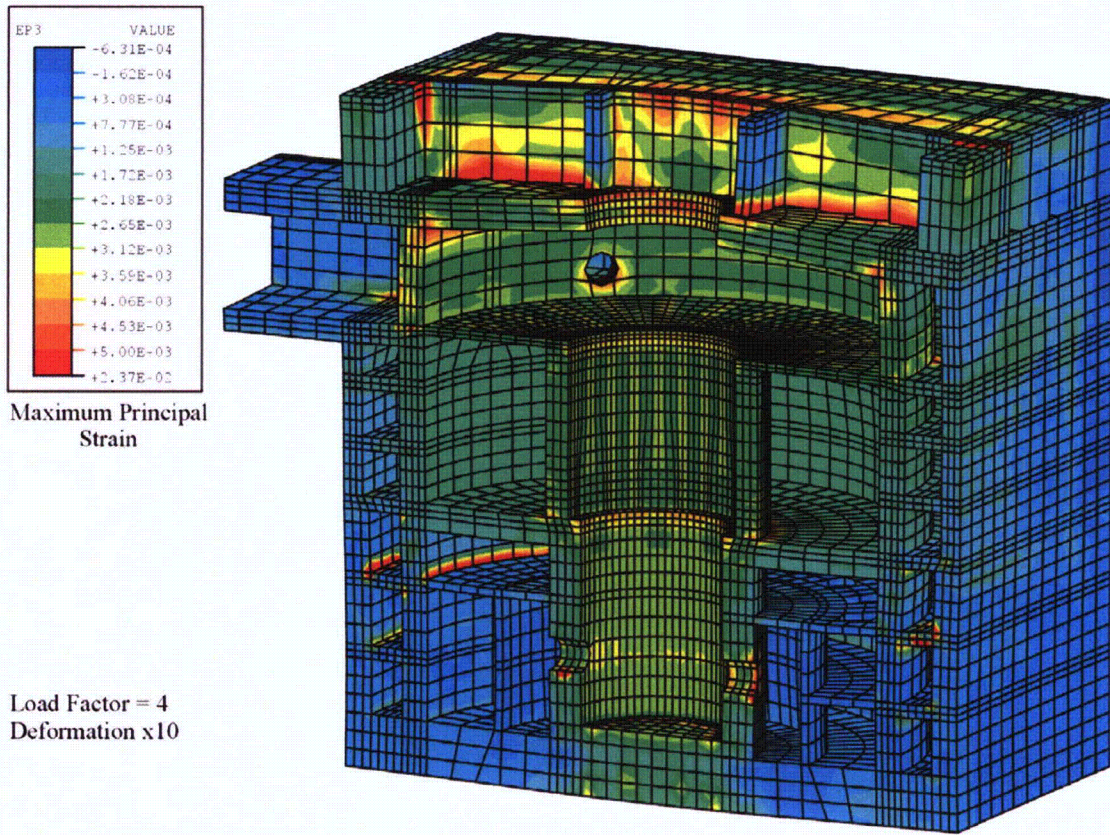


Figure 19.2.47(4) Maximum Principal Strains in RCCV for 500 °F Conditions at 4 P<sub>d</sub>

**NRC RAI 19.2-48**

*In PRA Appendix B.8.2.1.2, GE presents the results of its analysis for estimating the ultimate pressure capacity for the drywell head at 500°F. Failure of the drywell head is either by buckling (elastic or inelastic) in the knuckle (toroidal) region or rupture due to tensile strains approaching the material ultimate strain limit. GE's analysis relies on the use of two (2) approximate equations. GE claims that the Shield and Drucker equation (B.8-1) addresses plastic yielding, and the Galletly equation (B.8-3) addresses buckling. Please address the following:*

- a) The staff noted that the Shield and Drucker equation (B.8-1) and the Galletly equation (B.8-3) give essentially identical results. Using the geometric parameters from DCD Figure 3G.1-51, equation (B.8-1) predicts 0.005156 Sy and equation (B.8-3) predicts 0.00503 Sy. The staff also noted that both equations include the yield strength, but not the elastic or tangent modulus. It is unclear to the staff that these equations consider 2 different and distinct modes of failure. GE is requested to submit the 2 referenced papers for staff review, and to provide additional documentation in the DCD that supports its claims.*
- b) GE has compared the Galletly equation (B.8-3), taken from Reference B.8-3, to "all known test results (43 in total)" taken from Reference B.8-2. Reference B.8-2 is dated June 1961. This reference also contains the Shield and Drucker equation (B.8-1). GE is requested to submit the test data used, including geometry and materials of the test specimens, and to confirm that there is no new test data available on failure of torispherical heads since this compilation in 1961.*
- c) The first step in accessing the applicability of the test results to the ESBWR drywell head is to compare the key geometric ratios tested and the materials tested to the ESBWR drywell head parameters, to ensure inclusion in the test database. If included, then the factor of conservatism should be developed using only the subset of test data that applies to the ESBWR drywell head. If excluded, then there is no basis to develop a factor of conservatism based on this test data. The staff noted that in PRA Figure B.8-2, it appears that the highest ratio of predicted pressure to yield strength for any of the test specimens is about 0.0026. For the ESBWR drywell head, this ratio is 0.00503. GE is requested to provide its technical justification why this test data is applicable to the ESBWR drywell head.*
- d) Explain how the Reference B.8-2 test data was used to develop and/or correlate with the Shield and Drucker equation (B.8-1), which is presented in the same reference.*
- e) In the absence of buckling in the elastic stress range, the actual failure mode will likely be either gross yielding at the apex of the head or inelastic buckling in the knuckle region, depending on the specific material plastic behavior and the geometric parameters of the torispherical head. As the material yields at loads above the elastic limit, the stiffness is reduced due to a decrease in the tangent modulus. For mild steels, exhibiting a pronounced yield point and plateau up to*

*about 3% strain, a buckling instability in the knuckle region, in the presence of a compressive stress field, would be expected. However, there may be residual post buckling strength because the stress field in the head is predominantly tensile. GE has relied on simple semi-empirical formulas to predict the ultimate pressure capacity of the limiting structural element of the containment. There is a long history of study of failure of torispherical heads under internal pressure. Many options exist for conducting computer-based numerical analysis, including consideration of inelastic behavior, buckling failure, and even post-buckling behavior. GE is requested to discuss the correlation between the semi-empirical equations used and available numerical analysis methods (e.g., BOSOR5) in estimating the ultimate pressure capacity of the ESBWR drywell head.*

- f) *At the end of PRA Section B.8.2.1.2, in the comparison of failure pressures between the plastic yielding failure and buckling, the pressure for the buckling failure mode was estimated based on a best estimate value (factor of 2.27 applied to Equation B.8-3), while the plastic yielding failure pressure was computed directly from Equation (B.8-1). Discuss whether Equation (B.8-1) was intended for design purposes, and represents a lower-bound prediction, or if it is considered to be a best-estimate prediction. If it is intended to be a lower-bound prediction, explain the technical basis for the comparison of the lower bound yield pressure with the best estimate (median) buckling pressure.*

### **GE Response**

- a) The requested papers are attached in response to this RAI.
- b) Reference B.8-2 is attached to this RAI. As stated in NEDO-33201 Rev. 1, the Galletly equation (B.8-3) and the 43 cited results are based on References B.8-3, B.8-4 and B.8-5 dated November 1986, August 1979 and August 1985, respectively. All these papers were published well after June 1961.
- c) The Galletly equation B.8-3 was developed to prevent internal pressure buckling (unsymmetric buckling mode) in fabricated carbon steel or stainless steel torispheres. That effect occurs typically for D/t ratios greater than 400 or 500 (D is the diameter of the attached cylinder, and t the thickness of torispherical shell). The ESBWR design has a D/t ratio equal to 260, well below 400 (the material is SA-516 Gr. 70 with clad).

The Galletly equation is checked in Reference B.8-3 against 44 experimental buckling tests. The key geometric ratios tested were; D from 1.35 m to 20.3 m, D/t from 373 to 2,325, r/D from 0.04 to 0.173, and Rs/D from 0.72 to 1.10. In addition, yield points ranged from 197 N/mm<sup>2</sup> to 293 N/mm<sup>2</sup> (r is the radius of the cylindrical shell, and Rs the radius of the spherical cap).

The actual values for the ESBWR drywell head are: D = 10.4 m, D/t = 260, r/D = 0.173, and Rs/D = 0.90 and yield point equal to 260 N/mm<sup>2</sup>. All the ratios are within the range of applicability, with the exception of D/t ratio, which is slightly

out of the range of the tested geometry ratios, but conservatively so (more thickness).

Accordingly, PRA Figure B.8-2 is not the range of applicability of the equation. This means only that the predicted yield pressure and the tested yield pressure are in relation 1 to 1.5 as a lower bound.

As for the applicability of the Shield-Drucker equation B.8-1, it was derived in accordance to Reference B.8-2, for values of  $r/D$  between 0.06 and 0.16,  $R_s/D$  between 0.6 and 1.0,  $t/D$  between 0.002 and 0.014 and  $H/D$  between 0.16 and 0.28 ( $H$  is the height of the non-cylinder-shaped part of the head). Again, all the ESBWR ratios are within the range, with the exception of  $r/D$  ( $=0.173$ ), which is slightly out of the range, but conservatively, as shown in References B.8-2 figures. The ESBWR  $H/D$  ratio is 0.249.

- d) See attached Reference B.8-2 for details on the developing of Equation B.8-1 (Shield and Drucker).
- e) BOSOR 5 computer program was already used to develop the Galletly equation as stated in References B.8-4 and compared to available data (Reference B.8-5) Note that they yield a reasonable agreement.
- f) Shield and Drucker formula B.8-1 is considered a best-estimate prediction for plastic yielding. Some comparisons between the Shield-Drucker formula and average of upper and lower bounds on limit pressures can be found in Reference B.8-2. They show a good agreement with data. Accordingly, Shield-Drucker formula B.8-1 is considered a best-estimate prediction and its result can be compared to that from 2.27 times the Galletly equation value (best-estimate for buckling pressure).

No DCD changes will be made in response to this RAI.

**NRC RAI 19.2-51**

*In PRA Appendix B.8.2.2.1, GE stated that the thermal induced loading would not pose a challenge to liner buckling since the increase in internal pressure could be much faster than the heat conduction through the containment wall for the typical temperature load (GE stated that the representative severe accident temperature for the ESBWR containment is 500°F). However, a postulated direct containment heating (DCH) event could induce much higher temperature than 500°F within a short period of time due to particle entrainment. In PRA, Section 21.3.4.5, GE stated that strains in liners due to DCH induced thermal stresses are about 8% (which could be considered high for carbon steels). Provide:*

- a) a description of the characteristics of a DCH induced temperature load in liners above 500°F;*
- b) a discussion of the possible DCH induced thermal load build-up before the build-up of internal pressure sufficient to prevent the thermal induced buckling in liners;*
- c) a discussion of liner materials to sustain high strains, especially near penetrations;*
- d) discussion of thermal induced local liner tearing, including any test data if available.*

**GE Response**

- a)& b) Detailed analysis of DCH is described in Section 21.3 of NEDO-33201 Rev 1. A discussion on DCH induced temperature loads is also presented in the response to RAI 19.2-57 and a resulting drywell temperature history is shown Figure 19.2-57(1). The associated drywell pressure history is shown in Figure 19.2-51(1). Detailed model calculation presented in NEDO-33201 Rev 1 Section 21.3 and related physical understanding show that in a hypothetical DCH event the pressure and temperature transients in the upper drywell and the wet-well atmospheres would develop in tandem, with the pressure transient “leading the way”. Note that in the lower drywell we assume localized liner failure due to direct contact with the melt.
- c) The liner material used in the ESBWR containment is SA-516 Gr. 70 carbon steel, which has a long history of application as a liner material in reinforced concrete containment designs where the design requirement is to provide a strong, ductile material as the leak tight boundary for the concrete. This material has a specified minimum elongation of 17% at room temperature, and the expected median value will be 20%. While no specific elongation data on A516 Grade 70 at high temperature has been found, the available data indicates that for temperatures over 800 °F, the ductility of carbon steel increases significantly. Figure 19.2-51(2) illustrates median data for A36 structural steel, developed from testing on steel taken from the World Trade Center [Ref 1], and median data for SA533 pressure

vessel steel from testing following the Three Mile Island accident [Ref 2]. Based on this data, the expected median elongation of A516 steel would be about 39% at temperatures around 1100 °F.

To evaluate calculated strains from finite element analyses against material elongation data for tearing, two additional factors must be considered. First, the actual ductility of the material depends on the biaxial or triaxial state of stress, so that the elongation data from uniaxial tension tests must be reduced to account for the biaxial loading in the liner. For liner connections with thickened plates at penetrations, where tearing is likely to occur, the ductility is generally taken as 60% of the uniaxial elongation data. This assumes that the material is in biaxial tension where the hoop direction is 2 times the axial direction, i.e. pressure loading for the barrel portion of the containment. Secondly, the calculated strains must be factored to account for strain concentrations that are not captured by the mesh at these types of connections. This factor depends on the fidelity of the mesh and the refinement detail of the model. For global, axisymmetric type models, a factor of 10-15 on the far field liner strain is needed to estimate the local strain in the liner at a penetration. For 3D global models that include some representation of the penetration, a factor of 4 to 5 on the calculated liner strain near the penetration of interest is sufficient to establish the peak local strain. For detailed local models that include the connection of interest, a factor of 1.5 to 2 is generally appropriate.

For the liner buckling model described in Section 21.3.4.5 of NEDO-33201 Rev 1, the peak strain occurs midway between the anchor studs remote from any connection or discontinuity, and the modeling has good mesh refinement. Thus, the calculated strain of about 8% could be compared to the expected ductility of about 23% under biaxial loading at elevated temperature. This shows a large margin against tearing. However, the reported calculation is not representative of the liner anchorage configuration specified for the ESBWR. The referenced calculation assumes the liner is anchored with studs, whereas the ESBWR anchorage design is for continuous vertical T stiffeners spaced 50 cm apart.

Thus, a detailed local model for the liner, T anchors, and thickened plate near a representative equipment hatch for the ESBWR design was developed to evaluate strain and possible tearing near the penetration under hypothetical DCH conditions. This model is a sub-model from a local model of the penetration and portion of the RCCV wall that is currently being used to further assess the capacity of the containment system to internal pressure. Figure 19.2-51(3) illustrates the local model of the penetration and RCCV wall, and Figure 19.2-51(4) illustrates the more detailed local model of the liner and anchorage system. This model takes boundary conditions along the cut surfaces from the local penetration model (Figure 19.2-51(3)), and the local penetration model takes its boundary conditions from a global model of the ESBWR primary containment system. The temperature and pressure histories, representative of a large break DCH condition, are used to evaluate liner strains near the equipment hatch penetration under DCH conditions. The temperature history used is provided as

Figure 19.2-57(1). The associated drywell pressure history is shown in Figure 19.2-51(1). The models are initialized to steady state operating conditions, and a nonlinear, dynamic thermal stress analysis is performed using the temperature and pressure transients. Figure 19.2-51(5) plots contours for the effective plastic strains in the liner at the time of peak temperature when the temperature on the inside surface of the liner is 1629 °C. This figure shows that general yielding is widespread in the liner due to the high compressive stresses with somewhat larger plastic strains along the connections of the liner with the T-anchors. Also, clearly, the highest plastic deformations occur around the connection of the liner with the thickened plate at the penetration with peak plastic strains of 4%. Considering a strain concentration factor of 2 for the mesh refinement used, the calculated strains are well within the ductility of 23% for the liner at the elevated temperature. Furthermore, a check of the principal membrane stresses shows that the material is yielding in compression. Membrane tension is needed before liner plates will tear. Therefore, liner tearing at the penetration will not develop under this DCH condition.

- d) The expected performance of the ESBWR liner and anchorage system can also be illustrated based on full-scale test data as described below.

Full scale testing of a steel lined RCCV wall was performed in Japan [Ref 3] to evaluate the liner and anchorage performance under LOCA conditions in association with the ABWR design. The liner and anchorage design for the ABWR is the same as that for the ESBWR, namely 6.4 mm thick A516 Grade 70 steel liner plate attached to vertical T-bar embedded anchors 50 cm apart. A section of a 2 m thick concrete wall and a liner anchored with vertical T sections were tested by heating the liner to 171 °C for 6 hours as representative of LOCA conditions. The test was performed with the liner unconstrained for out-of-plane deformation and also for cases where the liner is pressed against the concrete wall. These tests showed bulging of the liner between the anchors under the elevated temperatures. A maximum bulge at the midspan of the liner between anchors of 6 to 13 mm was found for the unconstrained cases, and a maximum bulging of only 2-3 mm was found for the constrained cases. Moreover, for the unconstrained case having 13 mm bulging at temperature, the maximum bulge between stiffeners was only 3.4 mm after the liner cooled back down. This implies that the bulging causes some plastic deformation under the thermal induced compressive load, sufficient to prevent the liner from fully returning to the original configuration (no pressure on liner). However, the recovery was significant, indicating a good margin against tearing, and, indeed, no tearing of the liner was found in these tests.

For the DCH conditions, a much higher temperature spike would be anticipated, but this spike occurs and dissipates within a few seconds, as illustrated in 19.2-57(1). The longer-term temperature for the DCH condition is about 200 °C, which is very similar to the LOCA conditions that were tested. In addition, at the high temperatures, the material softens considerably, which means that it develops

less thermal stress and is more easily flattened against the concrete by the internal pressure. The pressure and temperature transients would develop in tandem, and the liner experiences two counteracting effects under the DCH conditions, namely, in-plane compression due to restrained thermal expansion, and in plane tension (limited by the RCCV wall) due to internal pressure, which acts to push the liner against the concrete wall. Consequently, thermal induced compressive yielding and bulging of the liner away from the wall is anticipated, but local liner tearing is unlikely to occur under the hypothetical DCH conditions.

### **References**

1. NIST NCSTAR 1-3D, "Mechanical Properties of Structural Steels," Federal Building and Fire Safety Investigation of the World Trade Center Disaster, National Institute of Standards and Technology, Washington, D. C. September 2005.
2. Chu, T. Y., et. al., "Lower Head Failure Experiments and Analyses," Sandia National Labs, NUREG/CR-5582, USNRC, Washington, D. C., February 1999.
3. Saito, H., Hirao, K., Muramatsu, Y., Nagata, T., Yamazaki, M., and Hasegawa, T., "Study on Behavior of Concrete with Steel Liner under High-Temperature Condition," Transactions of SMiRT 11, Vol. H, Paper H03/5, Tokyo, Japan, 1991.

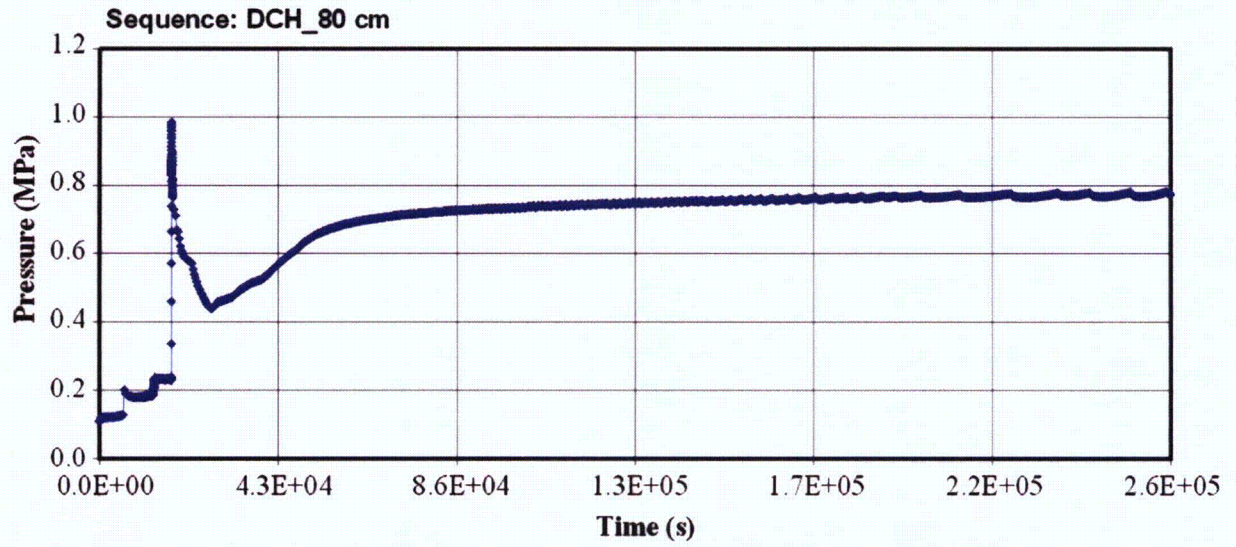


Figure 19.2-51(1) Drywell Pressure History for Large Break DCH Conditions

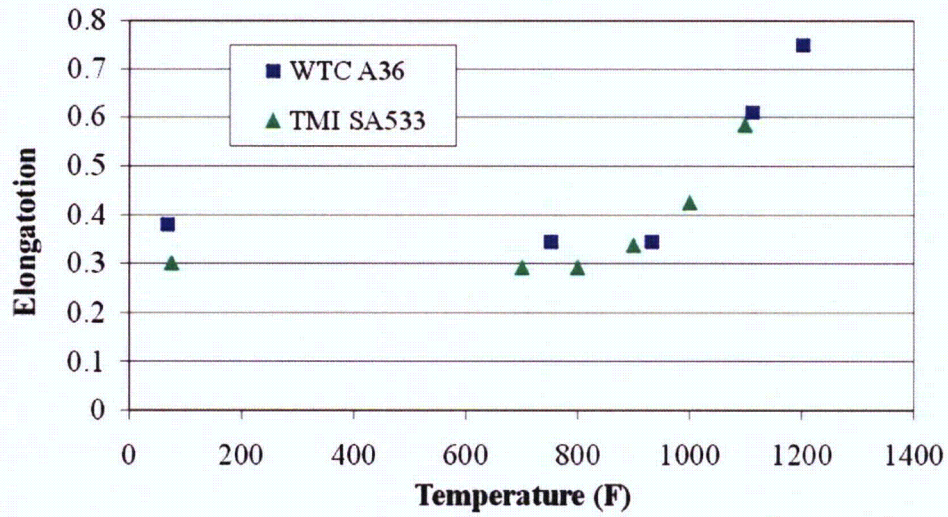


Figure 19.2-51(2) Representative Elongation Test Data for Carbon Steel at Elevated Temperatures

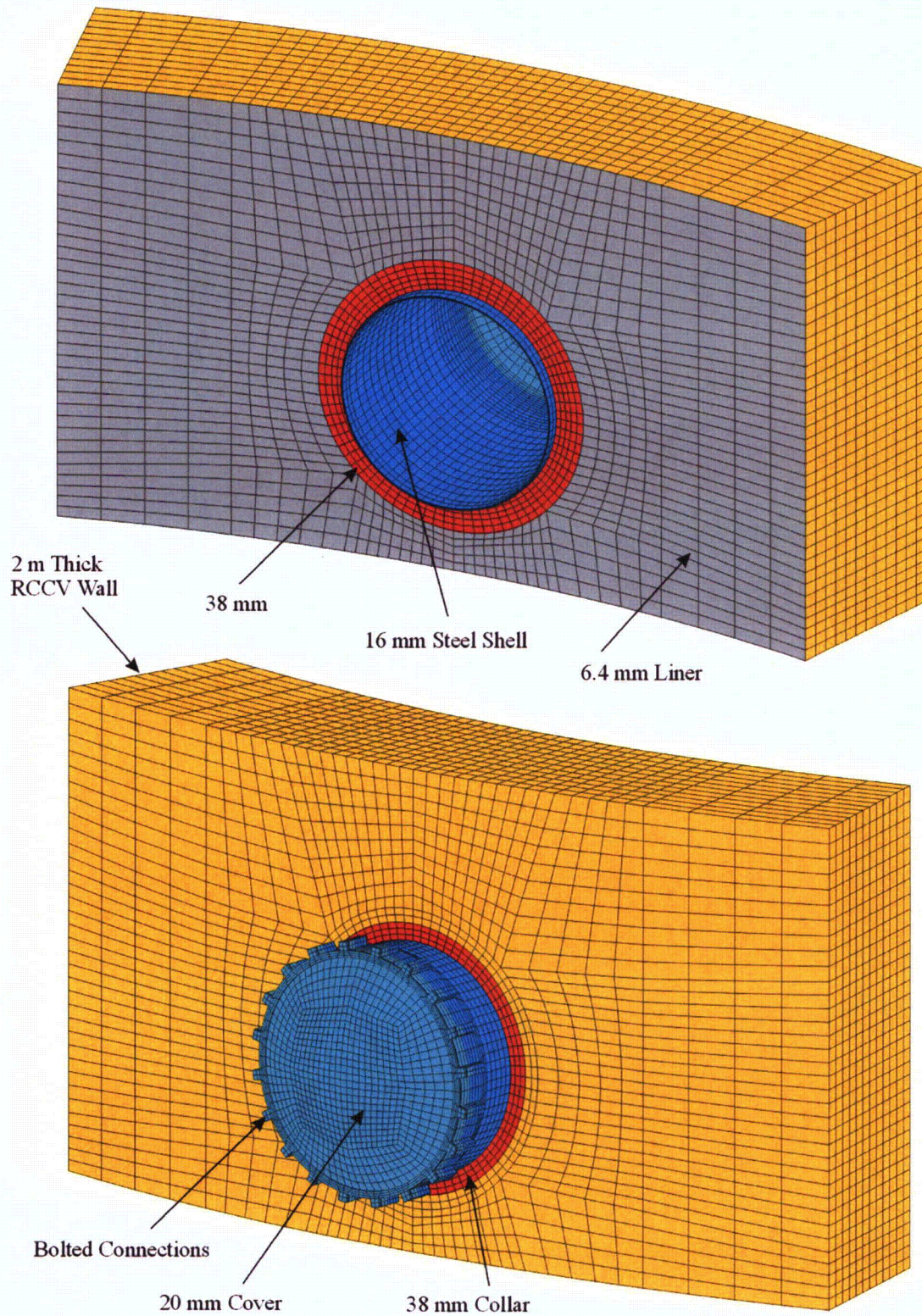


Figure 19.2-51(3) Local Model of Representative Equipment Hatch for ESBWR

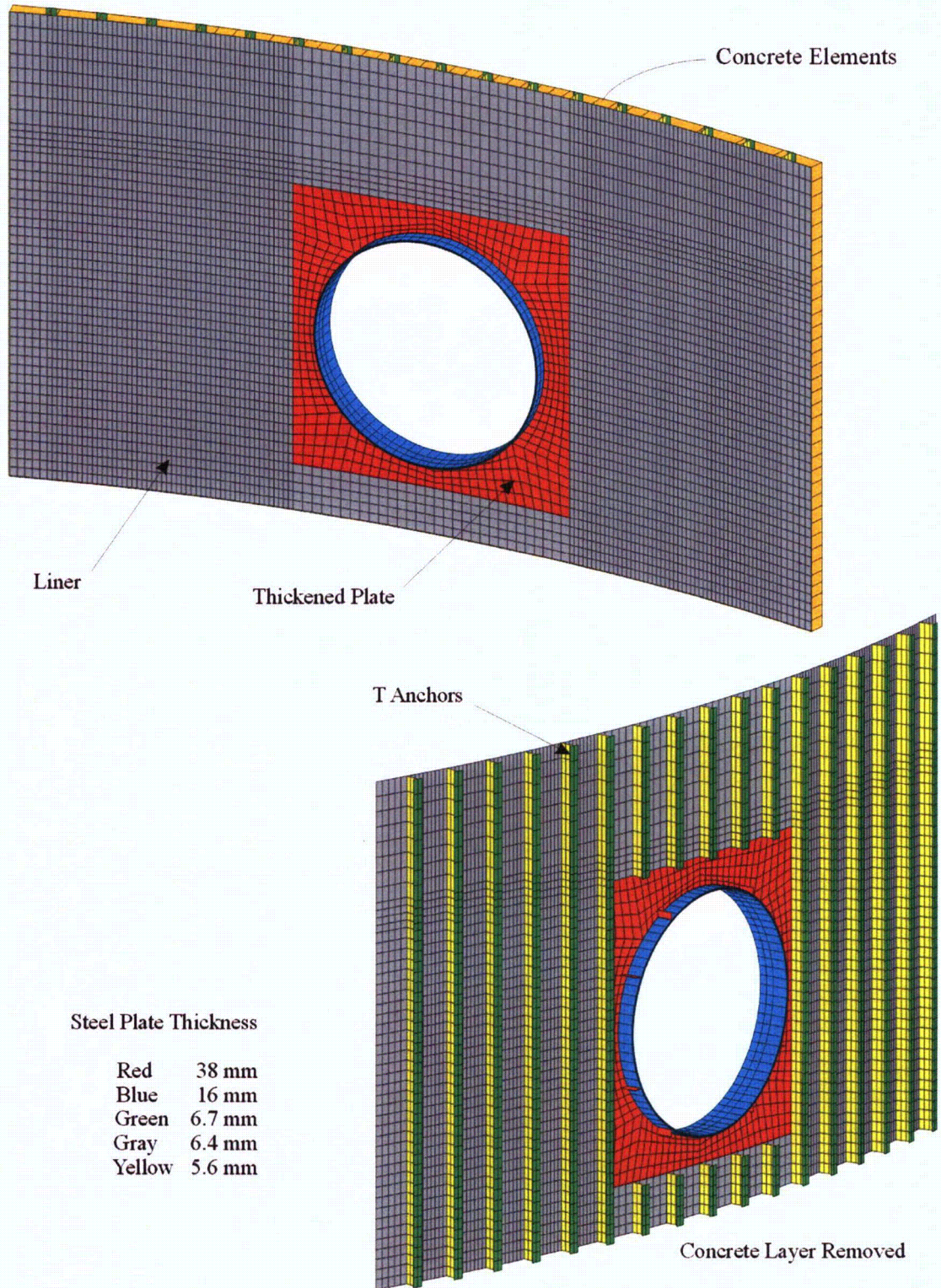
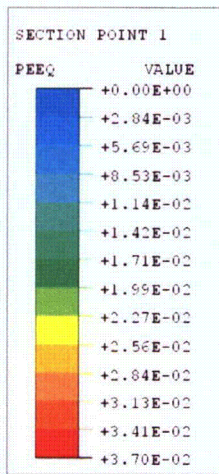
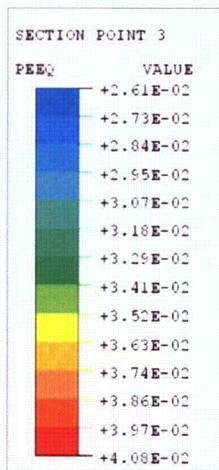
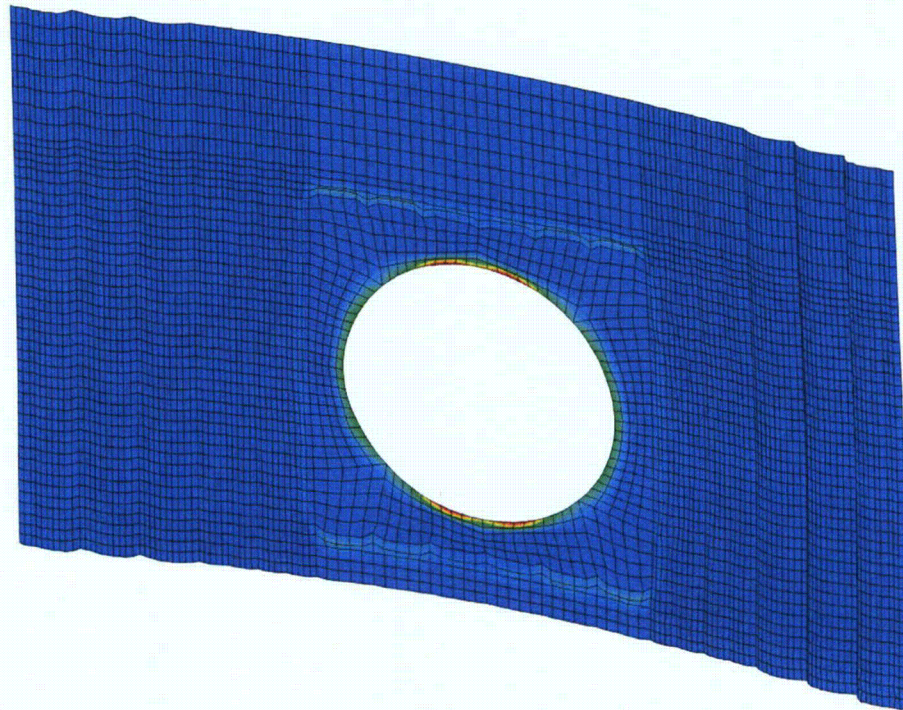


Figure 19.2-51(4). Local Model of Liner and Anchorage System at Equipment Hatch



At Back Face  
(Concrete Side)



At Inside Surface

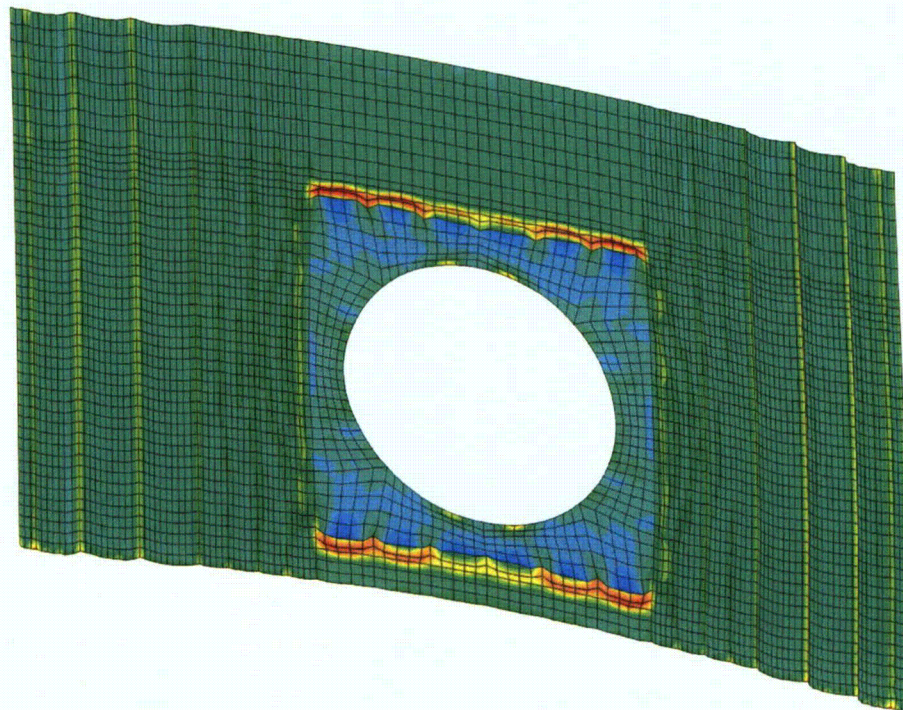


Figure 19.2-51(5) Accumulated Plastic Strain at Time of Peak Temperature

**NRC RAI 19.2-52**

*In PRA, Revision 1, Appendix B.8.2.2.2, GE used a Sandia-proposed springback for leakage prevention at seals. According to PRA, Revision 0, Section 8.2.1.3, the allowable technical specification leakage is 0.5% of containment air volume per day at rated pressure. GE further stated in the same section that based on MAAP test runs, the effective flow area required to allow 0.5% of the containment air volume to leak per day at design pressure is approximately  $3.4E-6$  m<sup>2</sup> (3.4 mm<sup>2</sup>). However, in PRA, Revision 1, Appendix B.8.2.2.2, GE estimated that the seal gaps for the drywell head and both drywell and wetwell hatches exceed the springback limit and possibly have a flow area greater than the allowable technical specification leakage area. Provide justification for the statement that the resulting maximum gap of 0.077 mm is deemed small.*

**GE Response**

Bolted flanges of the drywell head, drywell and wetwell hatches have been strengthened to achieve no leakage potential under severe accidents for pressures up to the containment ultimate capability pressure. This is an example of design improvement resulting from PRA insights. PRA report Sections B8, B8.2.2.2 and B.8.2.3 will be revised in the next update as shown in the attached markups.

In addition, Figures 3G.1-51 through 3G.1-53 of DCD Tier 2 Appendix 3G will be revised in the next update as noted in the attached markup.

**NRC RAI 19.2-53**

*In PRA, Revision 0, Section 8.1, GE stated that "However, for source term calculations, leakage in terms of leak areas is conservatively estimated for pressures below the capability pressure." However, Section 8.1.2.2 "Leakage Potential" seems to conclude that the leakage potential for the liner and penetrations is negligible. Explain the apparent discrepancy.*

**GE Response**

The statement "However, for source term calculations, leakage in terms of leak areas is conservatively estimated for pressures below capability pressure" has been deleted from Section B.8 in Rev. 1 of PRA report.

No DCD changes will be made in response to this RAI.

**NRC RAI 19.2-54**

*In PRA, Appendix B.8.3, GE treated the failure pressure due to plastic failure mode calculated using Equation (B.8-10) as a median value. Provide justification for this judgement, including a description of the development of this equation, assumptions used, stress-strain relation assumed, and magnitude of failure strain, as well as test data available to support the median failure pressure capacity estimate.*

**GE Response**

The paper [19.2-54(1)] from which PRA Equation (B.8-10) was taken, came up with a formulation to account for internal buckling pressure and axisymmetric yielding pressure for perfect torispherical shells in the range;  $R_s/D = 1.0$  and  $0.8$ ,  $r/D = 0.05-0.20$ ,  $D/t=300-1500$ , yield point  $=207$  N/mm<sup>2</sup>,  $310$  N/mm<sup>2</sup>,  $414$  N/mm<sup>2</sup> and  $E = 207,000$  N/mm<sup>2</sup>, (conservatively bounding the ESBWR drywell head characteristics).

The authors made a series of calculations using BOSOR 5 computer program, to determine the values of both failure modes, which were then transformed, using curve-fitting techniques, into simple approximate equations. The approximate equation on axisymmetric yielding failure is PRA Equation (B.8-10).

Among others, a comparison was carried out there, between the suggested formula PRA (B.8-10) and the Drucker-Shield equation (PRA Equation (B.8-1), both dealing with axisymmetric yielding failure mode). It was found that Drucker-Shield equation leads to higher values (between 1.2 and 1.8 times). This is the reason to consider Drucker-Shield PRA Equation (B.8-1) as a best estimate, and PRA Equation (B.8-10) as median.

There are no stress-strain information or failure strain data available in the available paper.

Reference 19.2-54 (1):

Galletly, G.D., and Blachnut, J., Torispherical Shells Under Internal Pressure – Failure Due to Asymmetric Plastic Buckling or Axisymmetric Yielding, Proc. of Institution of Mech. Engineers, Vol. 199, No C3, 1985.

No DCD changes will be made in response to this RAI.

**NRC RAI 19.2-55**

*In PRA, Appendix B.8.3, GE described the development of a containment pressure capacity fragility curve using a lognormal distribution. Confirm that this fragility is developed for 500°F and it also bounds the ambient temperature.*

*Also provide a detailed description of the ultimate pressure capacity estimates for 1000°F as shown in Table B.8-2, including material models at 1000°F for both concrete and steels.*

**GE Response**

The containment pressure capacity fragility curve is developed for 500°F and conservatively covers the ambient temperature. Temperature effects are taken into account by means of the yield strength variation with temperature.

Refer to response of RAI 19.2-46 for details on calculation of RCCV ultimate pressure capacity at 1000°F. Refer also to RAI 19.2-47 about the confirmatory analysis for the effect of temperature.

No DCD changes will be made in response to this RAI

**NRC RAI 19.2-66**

*In PRA, Revision 0, Section 15.1.3.1.1, GE described a method for calculating the ultimate shear strength of reinforced shear walls. This method utilizes the Barda Equation, which applies to low rise flat reinforced concrete shear walls with the height/length ( $h/l$ ) ratio less than two. According to studies (Figure C4.2-1 of ASCE 43-05), which compared the Barda Equation with test data for shear walls with different aspect ratios ( $h/l$ ), the Barda equation gives results that are consistent with the median of the test data, when code-specified minimum material strengths are used in the equation.*

*However, GE stated that in computing ultimate shear strength with this equation, the median material strengths of the concrete and reinforcing steel are used. This appears to double count for the material strengths, since the Barda Equation has already taken the median effect into consideration.*

*Provide justification for applying median values of material strengths in the Barda Equation for the ultimate shear strength of reinforced concrete shear walls.*

**GE Response**

Note that the Barda equation uses actual properties of material and not code-specified minimum strength. Therefore, the use of median material strengths is correct when applying the Barda equation.

However, the associated strength factors will be updated as necessary in the HCLPF reevaluation due to the revision of the design spectra definition as mentioned in response to RAI 19.2-67.

**NRC RAI 19.2-67**

*In PRA, Revision 0, Section 15.1.3.1.1, GE described a method for calculating the ultimate shear strength of reinforced shear walls. GE also described the shear strength calculation for the reactor building as an example. In Table 15-3, GE presented the seismic fragility for containment walls, and the governing failure is described as the lower wall with shear failure mode. GE did not describe the detailed analysis for containment walls, which have cylindrical geometry (Note that the Baroda et al. equation does not apply to this geometry). Provide the following information:*

- a) Provide a detailed description of the calculation for the strength factor for the reinforced concrete containment, including assumptions and data applied.*
- b) Provide a description of criteria used for the ultimate strength determination for both shear and flexural modes of failure of the reinforced concrete containment.*
- c) Provide the containment HCLPF value in terms of spectral acceleration, and the fundamental frequency of the reinforced concrete containment structure.*

**GE Response**

As a result of the single envelop revision to the design spectra for the ESBWR, revision of the results for the fragilities will be submitted in the next revision of the DCD.

- a) To calculate the strength factor for the RCCV the SSE stresses calculated from the finite element stress analysis were used. Depending on the failure mode that controls, the appropriate ultimate capacity is used to establish the strength factor as a ratio of the demand to the capability.
- b) Methods of calculating ultimate capacity follows the guidance in EPRI-6041 document for containment structures. Tangential shear capacity guidance is obtained from Appendix N of the same EPRI report.

The containment HCLPF in terms of spectral acceleration will be provided in the planned revision described above due to changes in the generic spectra shape.

**NRC RAI 19.2-68**

*In PRA, Revision 0, Section 15.1.3, GE used a fragility method for calculating structural HCLPFs, based on scaling the design seismic response with safety factors and associated aleatory and epistemic uncertainty values. The determination of these uncertainty values typically requires substantial subjective inputs as compared to the deterministic engineering approach such as CDFM (Conservative Deterministic Failure Margin).*

*Provide a discussion of the selection and basis for the aleatory and epistemic uncertainty values in Table 15-3 used for the RCCV HCLPF calculation.*

**GE Response**

The selection of aleatory and epistemic uncertainty values follows the guidance in EPRI Report TR 103959s. The values will be updated as necessary in the HCLPF re-evaluation due to the revision of the design spectra definition as mentioned in response to RAI 19.2-67.

## B.8 CONTAINMENT ULTIMATE STRENGTH

This section describes the analysis and evaluation used to estimate the containment internal pressure capability and associated failure mode and location. The ultimate pressure capability of the containment structure is limited by the drywell head whose failure mode is plastic yielding of the torispherical dome. The pressure capability is 1.204 MPa gauge at 533K (500°F). It is a typical temperature for most severe accident sequences. The containment is conservatively assumed to depressurize rapidly when the pressure capability is reached. No leakage through penetrations is anticipated before the capability pressure is reached.

The primary function of the containment structure is to serve as the principal barrier to control potential fission product releases. The design basis event for this function is a postulated loss-of-coolant accident (LOCA). Based on this functional requirement, the containment pressure vessel is designed to withstand the maximum pressure and temperature conditions which would occur during a postulated LOCA. The ESBWR containment system employs pressure suppression, which allows a design pressure of 0.310 MPa and a design temperature of 444°K (340°F) for the primary containment pressure vessel. In addition, the suppression pool retains fission products that could be released in the event of an accident. In this section the capability of the containment structural system of the ESBWR standard plant to resist potentially higher internal pressures and temperatures associated with severe accidents is evaluated.

Primary containment, also referred to as "RCCV" for reinforced concrete containment vessel, is a cylindrical structure of steel-lined reinforced concrete. The containment is integrated with the reactor building (RB) walls from the basemat up to the elevation of the containment top slab. The top slab, together with pool girders and building walls, form the IC/PCCS pools and the services pools for storage of Dryer/Separator, fuel handling, new fuel storage and other uses. The elevation view of the reactor building/containment structural system along 0°–180° direction is shown in Figure B.8-1. The containment is divided by the diaphragm floor and the vent wall into a drywell chamber and a suppression chamber or wetwell chamber. The drywell chamber above the diaphragm floor is called the upper drywell (U/D). The drywell chamber enclosed by the RPV support pedestal (a part of RCCV) beneath the RPV is called the lower drywell (L/D). The major penetrations in the containment wall include:

- (1) Drywell head
- (2) The upper drywell equipment and personnel hatches at azimuth 307° and 52°
- (3) The lower drywell personnel and equipment hatches at azimuth 0° and 180°
- (4) The wetwell hatch at azimuth 115°
- (5) The main steam and feedwater pipe penetrations at the level of the steam tunnel

Additional detail of the containment design is provided in Section 4.0.

The pressure boundary of the containment structure consists of the reinforced concrete containment vessel (RCCV) and the steel drywell head. The structural integrity of the RCCV is investigated for its global strength under internal pressure beyond the design basis using the ANSYS computer program, which is based on the nonlinear finite element method of analysis for 3D reinforced concrete structures. During various severe accident conditions, the ESBWR

containment could also be challenged by high temperatures with a typical temperature of 533°K (500°F) for most accident sequences). At typical accident temperature of 533°K (500°F), the controlling pressure capability is 1.204 MPa associated with the plastic yielding of the drywell head.

In order to evaluate liner response to over-pressurization, liner plates are included in the ANSYS analysis. The analysis results show that the liner strains are much smaller than the ASME code allowable for factory load category when the internal pressure is as high as 1.468 MPa. A separate evaluation further demonstrates that at the governing containment failure pressure of 1.204 MPa at 533°K (500°F), the liner and anchor system will maintain its structural integrity and no liner tearing will occur.

No leakage potential through penetrations is expected.

In conclusion, the ultimate pressure capability is limited by the drywell head. The postulated failure mechanism is the plastic yield of the drywell head. The pressure capability is 1.204 MPa gauge at 533°K (500°F). The pressure capability evaluation described above is based on the deterministic approach. The uncertainties associated with the failure pressure are assessed in Section B.8-3.

### **B.8.1 RCCV NON-LINEAR ANALYSIS**

This subsection describes the non-linear analysis performed for the reinforced concrete containment vessel (RCCV) of the ESBWR Standard Plant. Computer code ANSYS was used for evaluation of the RCCV.

#### **B.8.1.1 Finite Element (FE) Model Description**

The containment and the containment internal structures (excluding GDSCS pools structures) are axi-symmetric while the RCCV top slab together with the reinforced concrete girders even though not axi-symmetric, are idealized and included in the axi-symmetrical model. Solid elements are used to represent the girders at the top of the RCCV, approximating the stiffness of the actual structure from a detailed model of the walls and slabs in the upper pools.

To represent the restraining effects of the floors outside the containment, horizontal restraining slabs are used with equivalent material properties. The model includes concrete elements, the reinforcing steel, the steel liner plate of the drywell, the drywell head, the wetwell with the vent wall and diaphragm floor structures.

The model consists of 3780 nodal points and 2160 elements. There are 1497 elements representing concrete, whereas 249 elements are isotropic, representing steel plates. The soil below the foundation mat was modeled as 72 spring constants, 342 concentrated mass elements. See Figure B.8-1 for the model.

The ANSYS computer program permits the specification of bi-linear, brittle or ductile material properties. The concrete and soil elements are specified to have properties with no or low tensile capability. The steel plate elements and the rebar elements are specified to have ductile material properties with the same strength in tension and compression. The capability of the ANSYS program to accommodate ductile material behaviors permits both concrete cracking and yielding of steel and rebar. This allows the program to consider redistribution of forces throughout the structure due to the non-linear behavior such as concrete cracking.

Equation B.8-4 is based on the assumption that significant leakage can be prevented as long as positive compression of the gasket is maintained. Equation B.8-5 is empirical based on test results that even a degraded gasket can effectively prevent leakage if the separation of the sealing surfaces is equal to or less than 0.127 mm (0.005 in).

For the pressure-unseating drywell head closure and equipment hatches, the pressure required to separate the sealing surfaces is a function of the bolt preload, axial stiffness of the bolts and the compression flanges, and the differential thermal expansion between the bolts and the compression flanges. The separation pressure ( $P_s$ ) for operable penetrations is calculated in accordance with the following formula, as per Reference B.8.8, even the seal degradation temperature of about 533°K (500°F) has reached.

$$P_s = \frac{\left[ (K_b + K_f) \frac{F_i}{K_f} + K_b (\varepsilon_{Tf} - \varepsilon_{Tb}) L \right]}{\left( 1 + 2\nu \frac{K_b}{K_f} \right) \pi r^2} \quad \text{B.8.6}$$

Where the subscripts f and b denote the compression flanges and bolts respectively.

$F_i$ : total bolt preload

$K$ : total axial stiffness

$\varepsilon_T$ : thermal strain

$L$ : bolt grip

$N$ : Poisson's ratio (0.3)

$r$ : inside radius of penetration

The adequacy of this approach has been recently confirmed by the Sandia hatch leakage tests (Reference B.8-9) in that the predicted leakage onset pressures were in favorable agreement with the test results. The drywell head anchorage to the top slab has a pressure capability higher than the drywell head shell and the leakage path of the drywell head assembly before the failure pressure is reached is through the flanges.

The drywell head is a 10.4-m diameter closure with double seal. One hundred twenty 80-mm diameter bolts hold the head in place. There are 2 drywell equipment hatches and 1 wetwell hatch in the containment wall. The diameters are 2.4 m for drywell equipment hatches and 2.0 m for the wetwell hatch. The drywell equipment hatches have twenty 43 mm diameter bolts, and the wetwell hatch has twenty 38 mm diameter bolts. According to Equation B.8-6, the separation pressures are: 1.3 MPa for the drywell head, 1.4 MPa for the drywell equipment hatches and 1.6 MPa for the wetwell hatch. All of them are higher than the 1.204 MPa capability pressure. This means that no separation of the flange surfaces can be expected, and no leaks through the penetrations.

For equipment hatches, another potential leakage mechanism is ovalization of the sleeve which causes the sleeve to slide relative to the tensioning ring (or the cover flange). An initiation of leakage due to sleeve ovalization, however, requires significant deformations of the containment shell around the equipment hatch. The average circumferential membrane strain in the shell that is needed to result in the initiation of leakage from ovalization for equipment hatches identified

in the ANL survey (Reference B.8-8) was found to range from 2.5% to 7.3% by SNL (Reference B.8-8). For the equipment hatches under consideration, the ovalization leakage onset strain which is the ratio of the sleeve wall thickness at the sealing surface to the sleeve radius ranges, as a maximum, from about 5.8% to 7.0%. At a pressure of 1.468 MPa, the maximum radial deflection of the wetwell wall was calculated to be 13.02 mm (0.512 in.) from the ANSYS analysis (Table B.8-1). The corresponding hoop membrane strain is 0.072%. It is less than 1.2% and no leakage from sleeve ovalization of the equipment hatches will occur before the capability pressure is reached.

### B.8.2.3 Summary

The ultimate pressure capability of the containment structure is limited by the drywell head whose failure mode is plastic yield of the torispherical dome. The pressure capability is 1.204 MPa at 533°K (500°F). No liner leakage will occur before the capability pressure is reached. No leakage through penetrations is expected.

### B.8.3 UNCERTAINTY IN THE FAILURE PRESSURE

The uncertainties in the prediction of the failure pressure generally result from uncertainties in the two general areas listed below:

Material Strength (yield strength, tensile strength, modulus of elasticity, etc.)

Modeling (differences between the model and reality, use of simplified models or empirical correlations, uncertainty in dead-loads, etc.)

In a number of the areas listed above very little data may be available to guide the structural analyst in characterizing the uncertainty. Consequently, it is generally necessary to rely to a large extent on engineering judgment and past results to quantify these uncertainties.

As noted above a significant contributor to the uncertainty in the prediction of ultimate capacity derives from uncertainties in the material properties. For most structural materials the lognormal distribution has been shown to be a good model for the variability in material strength. Largely for this reason the lognormal distribution is generally selected to characterize the uncertainty in the prediction of the ultimate pressure capacity for structural components.

The most common form of the lognormal probability density function is:

$$p_f(p) = \frac{1}{p\sqrt{2\pi}\beta_c} \exp\left[-\frac{1}{2}\left[\frac{1}{\beta_c}\ln\left(\frac{P}{P_{med}}\right)\right]^2\right] \quad (B.8-7)$$

where:

$p_f(p)$  = the lognormal probability density function for failure pressure,

$\beta_c$  = logarithmic standard deviation on the pressure capacity  $p$ ,

$P_{med}$  = the median pressure capacity.

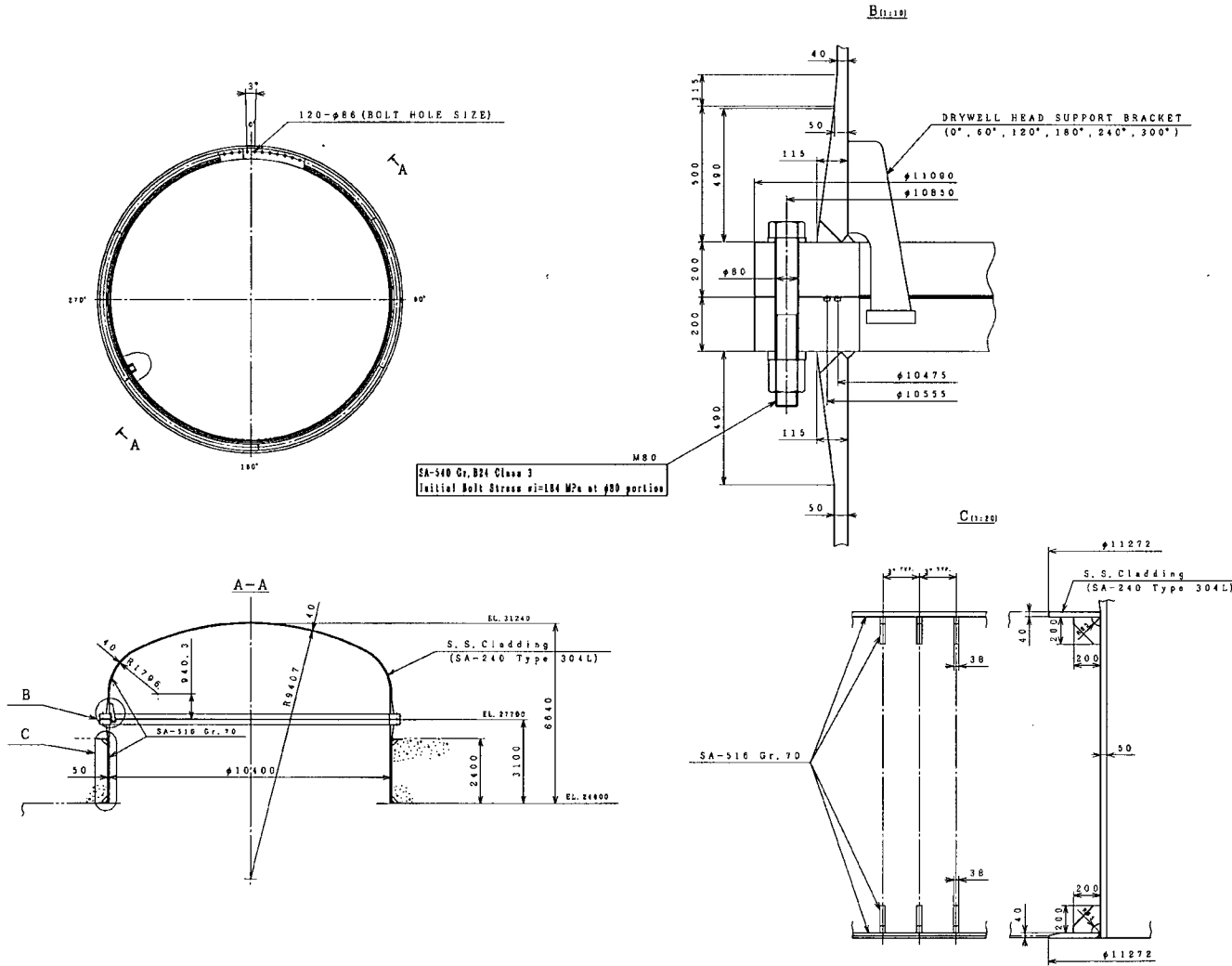


Figure 3G.1-51. Drywell Head

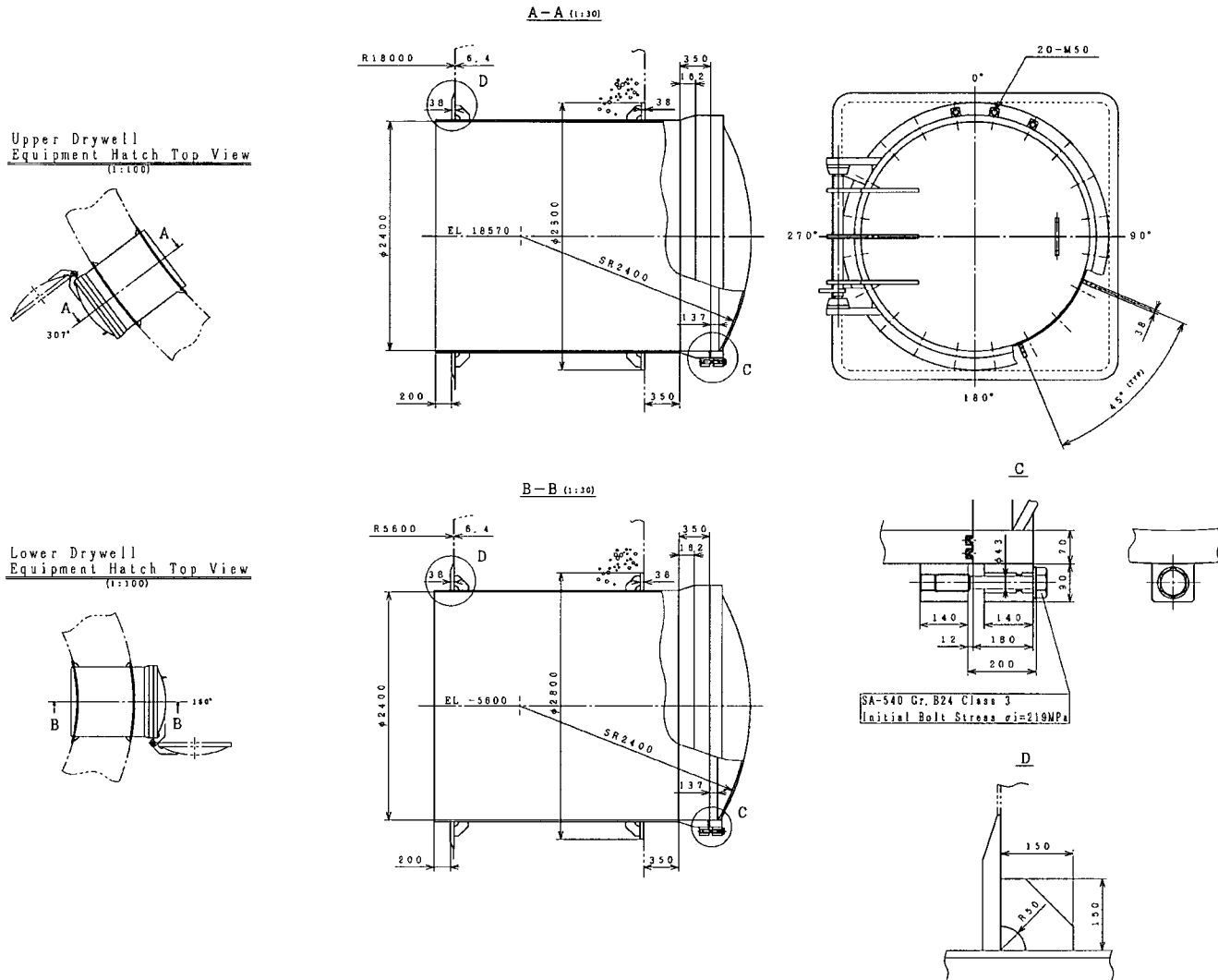


Figure 3G.1-52. Equipment Hatch

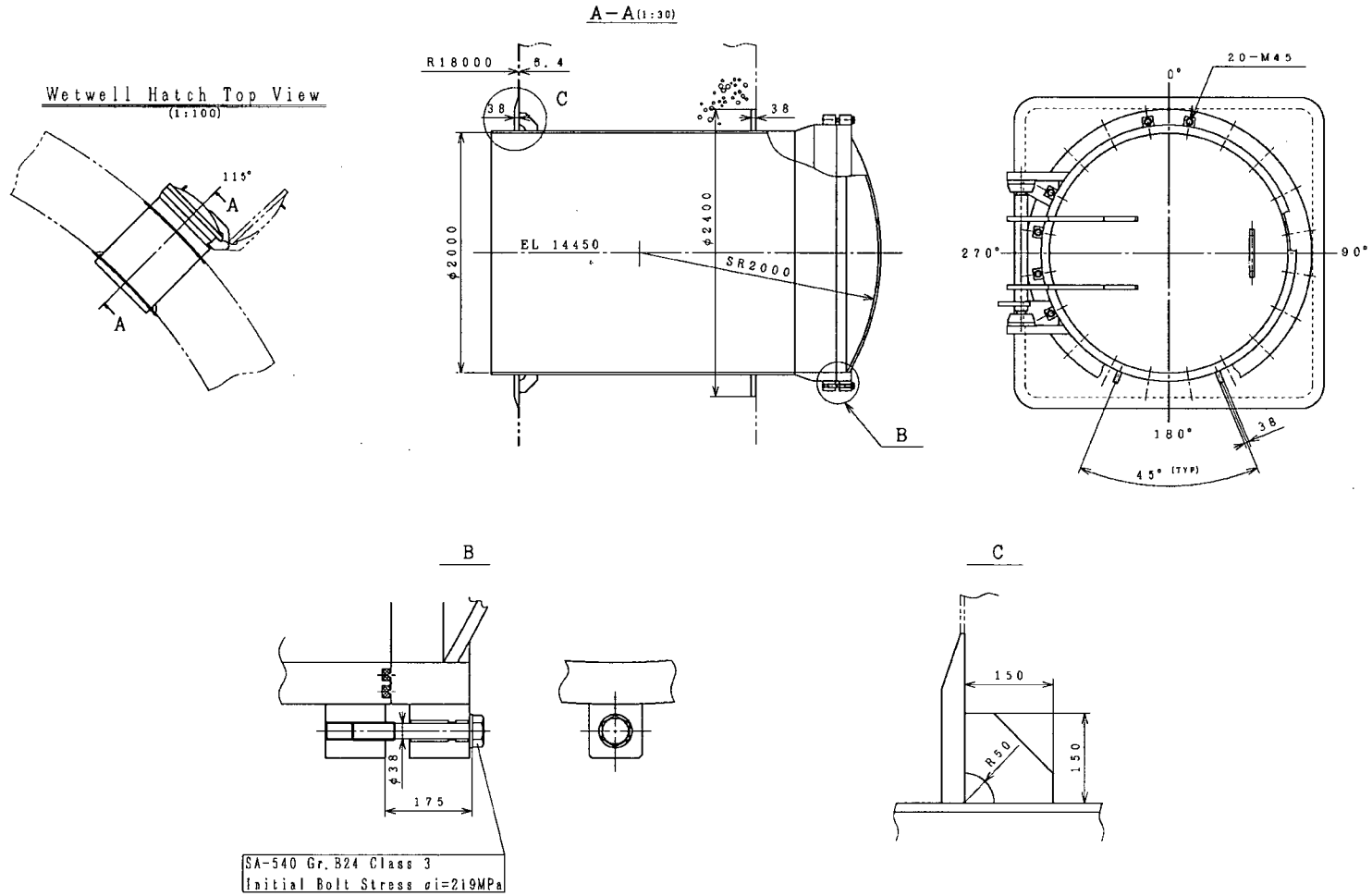


Figure 3G.1-53. Wetwell Hatch

Security-Related Information - Withhold Under 10 CFR 2.390

### A Simple Design Equation for Preventing Buckling in Fabricated Torispherical Shells Under Internal Pressure

G. D. Galletty<sup>1</sup>

*A simple equation is proposed which will enable a designer to estimate the onset of buckling in internally pressurized steel torispherical end closures. The equation applies to both crown and segment ends and spun ones. Apart from a factor which accounts for strain hardening, the same equation applies to both carbon steel and austenitic stainless steel torispheres. The proposed equation for the allowable internal pressure was checked against all known experimental buckling results and a minimum factor of safety of 1.5 was found. The equation was also checked against a number of full-scale vessels, some of which had failed in service. Once again, the equation was found to be satisfactory.*

#### Nomenclature

- $p$  = internal pressure
- $p_{cr}$  = internal buckling pressure of perfect torispherical shell (plastic buckling herein)
- $p_c$  = axisymmetric yield pressure of perfect torispherical shell
- $p_{DS}$  = Drucker-Shield limit pressure of perfect torispherical shell
- $p_D$  = design (allowable) pressure of fabricated torispherical shell (equation (1))
- $r$  = radius of toroidal portion (knuckle) of torisphere (see Fig. 2)
- $t$  = thickness of cylinder and torispherical shell (in design equation,  $t$  is minimum thickness in knuckle region)
- $D$  = diameter of attached cylinder (see Fig. 2)
- $E$  = modulus of elasticity
- $F$  =  $\sigma_{yp}$ , or 0.2 percent proof stress, of material
- $H$  = height of head (see Fig. 2)
- $L$  = length of attached cylinder (see Fig. 2)
- $R_s$  = radius of spherical portion of torisphere (see Fig. 2)
- $\gamma$  = strain-hardening factor modifying  $F$  (see equation (1))
- $\sigma_{yp}$  = yield point of material

NOTE:  $1 \text{ N/mm}^2 = 145 \text{ lbf/in}^2$

<sup>1</sup>Professor of Applied Mechanics, Department of Mechanical Engineering, University of Liverpool, Liverpool, U.K.

Contributed by the Pressure Vessels and Piping Division for publication in the JOURNAL OF PRESSURE VESSEL TECHNOLOGY. Manuscript received by the Pressure Vessels and Piping Division, November 26, 1985; revised manuscript received December 11, 1985.

#### Introduction

Fortunately, there have not been many failures of large internally pressurized dished ends. One well-known case was the 45-ft- (= 14-m-) dia fluid coker which failed in a brittle manner during its hydrostatic proof test at Avon, California in 1956. An elastic stress analysis of this vessel by Galletty [1, 2] showed that the direct hoop stresses in the knuckle region of the torispherical shell were compressive and exceeded the yield point of the material in several locations. It was also pointed out that buckling of the head was a possibility for some vessel geometries.

A limit analysis of the Avon vessel by Drucker and Shield [3] agreed with the basic findings of the elastic analysis; subsequently, the limit pressures of many torispheres and toricones were determined and the results were presented in the form of charts [4]. As a result of this work, the provisions relating to torispherical shells were modified in several Codes to take account of the limit pressures.

In recent years, the application of large-deflection shell theories to the problem has shown that the limit pressures are sometimes conservative for the higher values of  $\sigma_{yp}$ . However, the limit pressures do have the merit of being safe.

The foregoing results on limit pressures apply to the axisymmetric failure mode, which has yield circles at three locations in the vessel. However, they do not apply to the unsymmetric buckling mode, which has waves, or wrinkles, in the hoop direction in the knuckle (see Fig. 1). As rules to prevent this buckling mode are not available, Codes have tried to circumvent its occurrence by limiting the  $D/t$ -ratios of the heads which may be constructed. In the U.K. and the U.S., the limit is normally  $D/t = 500$  (or  $t/D = 0.002$ ). Heads are, of course, fabricated which have  $D/t$ -ratios greater than 500; but, in such cases, special arrangements are usually made with insurance companies in relation to the safety of the heads.

With the very thin heads (say,  $D/t > 1000$ ), buckling of torispheres due to internal pressure is certainly a possibility. One occasion on which it happened was with a 60-ft-(18.6-m-) dia oil storage vessel; it has also occurred several times with brewing tanks of about 3 m diameter which had  $D/t$ -ratios of about 900. Very recently, plastic buckling of internally-pressurized torispheres has occurred with  $D/t$ -ratios of 350 [5]; these cases are not catered for by the present Codes.

Although there have been few major accidents so far which have involved ellipsoidal or torispherical shells under internal pressure, it seems clear that it is time that Code rules on the subject of internal pressure buckling were formulated. The use of such shells as roof structures on PWR containment vessels and in LMFBR primary tanks (e.g., in France) gives added incentive to the development of these rules.

In this note, a possible design equation to prevent internal pressure buckling in fabricated steel torispheres is suggested. It applies both to crown and segment heads and spun ones. The same equation holds for carbon steel and stainless steel heads (other materials have yet to be studied). The equation



(a) Outward buckles



(b) Inward buckle

Fig. 1 Buckling due to internal pressure in a 3-m-dia stainless steel torispherical shell

was also applied to several vessels which had failed in service. If the equation had been available before, some of these vessels might have survived.

#### Brief Background to the Problem

In 1972 and 1976, experimental results on the buckling of austenitic stainless steel internally pressurized torispheres were published in references [6 and 7]. Both crown and segment and spun heads were tested and the diameters of the shells varied from 1.4 to 4.0 m. The situation with regard to carbon steel heads is not as good and the only test results available are the

recent ones published in [5] on 0.5-m spun heads. There have also been some tests on small torispherical models (0.14-m diameter) machined from aluminum alloys but these latter tests will not be considered further herein.

With the Kemper [6] and Stanley/Campbell [7] models, test coupons were not taken from the heads in the as-formed knuckle regions. With the Roche et al. tests [5], both the as-received and the as-formed properties were determined (it is necessary to have the latter if one is trying to check theory and experiment).

Besides strain-hardening effects, there are other difficulties in the way of good agreement between theory and experiment. These include residual stresses (forming and welding), information about actual radii of curvature, thickness variations and initial geometric imperfections. With the present buckling problem, the latter do not seem to have a very significant effect.

For the present purpose of obtaining an approximate buckling design equation, the experiments taken into account were those in [5-7]. In addition, the following procedure was adopted for the design equation:

- (i) the as-received (or minimum specified) mechanical properties and the nominal radii of curvature were used;
- (ii) the shell thicknesses were the minimum values measured in the toroidal, or knuckle, sections of the torispheres;
- (iii) all residual stresses and geometric imperfections were ignored; and
- (iv) strain hardening (of interest for cold-spun heads) was accounted for empirically via a factor  $\gamma$  (see equation (1)).

On the theoretical side, the publication of Bushnell's BOSOR 5 shell buckling program [8] in 1976 enabled the plastic buckling pressures of perfect shells of revolution to be calculated. This program was utilized by Galletly and Radhamohan in 1979 [9] and, from the computer results, they derived a simple equation for the plastic buckling pressures of perfect, constant-thickness, torispherical shells made from elastic, perfectly plastic material. This equation was applied to both the Kemper and the Stanley/Campbell models in [10-12] with reasonable success. The differences between perfect torispheres and those used in practice are discussed in the foregoing references.

The latest numerical results on this problem were published recently by Galletly and Blachut [13]. These authors extended the results of [9] down to  $D/t \approx 250$  and they also considered more values of  $\sigma_{yp}$ . The buckling equation for perfect torispheres which was proposed in [13] was similar to the one proposed in [9] but was not quite the same. Also, the buckling equation in [13] came from the results obtained with the deformation theory of plasticity while that in [9] utilized flow theory.

Two recent papers which also discuss design equations for this problem are [5, 14]. In [5] a design equation suggested in the 1982 edition of the French Pressure Vessel Code, i.e., CODAP [15], is mentioned but the derivation of it is not discussed. In the Appendix of [12], it is shown that the CODAP equation can be derived from the equation suggested by Galletly and Radhamohan [9], but with knock-down factors added.

The most recent paper on the subject [16] looked at three possible design equations which were based on equations for perfect torispheres proposed by the Liverpool group [11-13]. The constants in these equations were chosen so that the minimum value of the ratio  $p_{\text{exp}}/p_{\text{design}}$  was 1.5. All three equations were satisfactory for design purposes. As the exponents on  $(D/t)$ , etc., in the equations differed slightly, a composite (or average) buckling design equation was suggested. This equation is discussed in the next section.

**Proposed Design Equation for Preventing Buckling in Thin Torispherical Shells Subjected to Internal Pressure**

In this section the aforementioned design equation will be given and then its predictions will be compared with all known experimental results on fabricated torispheres. In addition, the equation will be applied to some large pressure vessels which failed in service, to see if use of the equation would have prevented the failures.

The proposed design equation is as follows:

$$p_D / \gamma F = \frac{80(r/D)^{0.825}}{(D/t)^{1.5}(R_s/D)^{1.15}} \quad (1)$$

where  $p_D$  = allowable internal design pressure (safety factor > 1.5)

$\gamma = \begin{cases} 1.0 & \text{for crown and segment steel heads} \\ 1.6 & \text{for cold spun steel heads} \end{cases}$

$F = \sigma_{sp}$ , or 0.2 percent proof stress, of the as-received plate material

$t$  = minimum thickness in the knuckle region of the torisphere and  $r$ ,  $R_s$ , and  $D$  are as shown in Fig. 2.

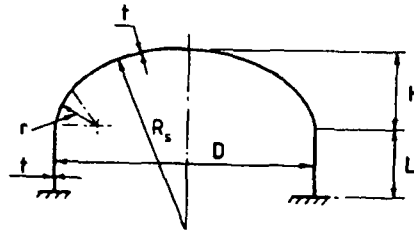


Fig. 2 Geometry of torispherical shell

In essence, equation (1) is based on the equations for perfect torispheres given in [9 and 13] and with knock-down, or reduction, factors added.

Equation (1) applies to both stainless steel and carbon steel heads. The factor  $\gamma$  allows for the enhancement of the mechanical properties in the knuckle due to thinning caused in the forming operation. If it is desired to use the 1.0 percent

**Table 1 Comparison of experimental buckling pressures with the predictions of the proposed design equation, i.e., equation (1)**

Head no.	$D/t_{min}$	Nom $r/D$	Nom. $R_s/D$	$\sigma_{sp}$ or 0.2 percent proof Stress $N/mm^2$	$P_{expt}$ $N/mm^2$	$P_D$ from equation (1) $N/mm^2$	$\frac{P_{expt}}{P_D}$
Stainless steel—crown and segment heads [6, 7]; 1.35 m < D < 4.0 m							
SC1	409	0.167	1.0	293	1.931	0.647	2.98
SC2	412	0.167	1.0	293	1.917	0.640	3.00
SC14	628	0.167	1.0	293	0.828	0.340	2.44
SC15	659	0.167	1.0	293	0.738	0.316	2.31
SC7	844	0.167	1.0	293	0.414 <sup>(a)</sup>	0.218	1.90
SC13	931	0.167	1.0	293	0.566	0.188	3.01
K1	825	0.159	0.91	293	0.366	0.242	1.51
K2	880	0.163	1.0	293	0.317	0.201	1.58
K3	915	0.166	1.0	293	0.290	0.192	1.51
K4	730	0.162	0.89	293	0.483	0.303	1.59
Stainless steel—pressed and spun heads [6, 7]; 1.35 m < D < 4.0 m							
SC3	482	0.111	1.0	293	1.710	0.578	2.96
SC4	535	0.074	1.0	293	1.366	0.354	3.86
SC5	505	0.074	0.83	293	1.917	0.478	4.01
SC6	495	0.074	0.78	293	1.917	0.529	3.62
SC16	730	0.074	1.0	293	0.655	0.222	2.95
SC17	717	0.074	0.83	293	0.738	0.282	2.62
SC8	1213	0.111	1.0	293	0.483	0.145	2.93
SC9	964	0.074	1.0	293	0.428	0.146	3.33
SC10	947	0.074	0.83	293	0.538	0.186	2.89
SC11	1049	0.074	0.72	293	0.593	0.188	3.15
SC12	947	0.056	1.0	293	0.455	0.119	3.82
K5	1045	0.083	1.0	293	0.228	0.142	1.61
Carbon steel—spun heads [5]; D = 0.5 m							
T1	543	0.06	1.10	230	0.425	0.205	2.07
T2	532	0.06	1.10	259	0.44	0.229	1.92
T3	373	0.06	1.10	290	1.13	0.453	2.49
T4	365	0.06	1.10	280	1.19	0.452	2.63
T5	538	0.04	1.0	263	0.36	0.190	1.90
T6	538	0.04	1.0	279	0.34	0.201	1.69
T7	1000	0.04	1.0	219	-	0.062	-
T8	1000	0.04	1.0	219	0.158	0.062	2.55
T9	365	0.04	1.0	239	0.75	0.308	2.44
T10	357	0.04	1.0	270	0.72	0.360	2.00
T11	1087	0.10	1.0	197	0.255	0.105	2.43
T12	1064	0.10	1.0	197	0.176 <sup>(b)</sup>	0.109	1.61
T13	556	0.10	1.0	253	0.617	0.370	1.67
T14	571	0.10	1.0	253	0.54	0.355	1.52
T15	385	0.10	1.0	262	1.15	0.664	1.73
T16	379	0.10	1.0	262	1.10	0.680	1.62

<sup>(a)</sup> This value seems low in comparison with SC13.

<sup>(b)</sup> This model had a large initial geometric imperfection.

proof stress, rather than the 0.2 percent proof stress, then the constant of 80 will need to be modified slightly.

As all the buckling tests considered herein were carried out at room temperature, equation (1) should not be used for elevated temperatures without further investigation.

The test results to be checked against the predictions of equation (1) are those in [5-7]. Details of the geometric ratios and material properties of the models are given in Table 1, together with the internal buckling pressures,  $p_{\text{expt}}$ , recorded in the tests. The thicknesses given are the minimum thicknesses in the knuckle region and the radii of curvature are the nominal specified ones. The design pressures,  $p_D$ , predicted by equation (1) are also given and the last column of Table 1 shows the ratios  $p_{\text{expt}}/p_D$ . As may be seen from a perusal of this column, the minimum ratios of  $p_{\text{expt}}/p_D$  occur with the carbon steel spun head T14 and the stainless steel crown and segment heads K1 and K3. The minimum ratio for the stainless steel spun head K5 is a little higher (1.61 instead of 1.5) but this could be reduced to 1.5 as well, if  $\gamma$  for stainless steel were to be changed to 1.7.

From Table 1, it will also be observed that the ratios of  $p_{\text{expt}}/p_D$  for the SC-heads are considerably higher than those for the K-heads. This was noted in [10] but the reason for it is not known. Both sets of heads were made by the same manufacturer (APV plc).

Since some of the  $p_{\text{expt}}/p_D$ -ratios are quite high ( $\approx 4.0$ ), it could be argued that the functional form of equation (1) is perhaps not the best one to use. It is quite possible that further study of the influence of strain hardening on the buckling pressures (included in equation (1) in only a very approximate manner) and residual stresses might produce a better buckling design equation.

#### Application of the Proposed Design Equation to Some Large Vessels Which Failed in Service

Another test of the usefulness of equation (1) is to apply it to some vessels which failed and to see what its predictions would have been. The vessels chosen for this purpose were:

- (i) the fluid coker ( $\approx 14$ -m diameter) at Avon which failed during its hydrostatic proof test [1, 2, 23]—even though this failure was ascribed to a weld defect, and the vessel failed in a brittle manner, it is instructive to determine its predicted buckling pressure;
- (ii) the large oil storage vessel ( $\approx 18$ -m diameter) which

buckled and which was discussed by Fino and Schneider [17]; (iii) two torispheres ( $\approx 5$ -m diameter) recently tested by CBI Industries [18];

(iv) a somewhat smaller vessel (2-m diameter) which buckled in service due to a gummed-up valve [19]; and

(v) a large vessel (20-m diameter) which was proof-tested but did not buckle [20]—this case only serves to check that equation (1) predicts a buckling pressure higher than the test pressure.

The geometric ratios, material properties, etc., for the foregoing torispherical shells are given in Table 2, together with the experimental and predicted buckling pressures. As may be seen from Table 2, all the values of  $p_D$  are lower than the experimental buckling pressures and the ratios  $p_{\text{expt}}/p_D$  are all greater than 1.5. Thus, if equation (1) had been available to check the operation of these vessels, some of them might not have failed.

#### Axisymmetric Yielding Versus Sinusoidal Buckling

It was noted earlier that the two static failure modes in internally pressurized torispherical heads are axisymmetric yielding (with the formation of yield circles) and buckling of the knuckle in the hoop direction (with the formation of waves or wrinkles). With very thin heads, buckling will be the controlling failure mode whereas yielding will control in the thicker heads. In the range  $300 < D/t < 500$ , buckling or axisymmetric yielding can occur, despite the fact that most Codes do not consider the occurrence of buckling in this  $D/t$ -range.

The experimental results in [5 and 7], and listed in Table 1, show that buckling can indeed occur for  $D/t < 500$ . The theoretical results of Gallety/Blachut [13] also predict that buckling can occur for  $D/t < 500$  and one of their figures is shown in Fig. 3 ( $p_c$  is the large-deflection axisymmetric yielding pressure and  $p_{\alpha}$  is the asymmetric, or sinusoidal, plastic buckling pressure). Depending on  $r/D$ ,  $R_s/D$  and  $\sigma_{yp}$ , either buckling or yielding may control the design.

In addition, the limit pressures  $p_{DS}$  obtained by a Drucker-Shield analysis [4] (and also associated with an axisymmetric failure mode), are shown in Fig. 3. It is clear that they are lower than both the values of  $p_{\alpha}$  and  $p_c$ . From the  $p_{DS}$ -curves, one would deduce that the failures would always occur by axisymmetric yielding in this  $D/t$ -range. However, from the Saclay test results [5], it is known that buckling failures can occur for  $D/t = 370$ ,  $\sigma_{yp} = 290$  N/mm<sup>2</sup>,  $r/D = 0.06$  and

Table 2 Buckling pressures ( $p_{\text{expt}}$ ) of several large crown and segment heads compared with the predictions of equation (1)

Reference	D (m)	Material	Nom. D/t	Nom. r/D	Nom. $R_s/D$	$\sigma_{yp}$ or 0.2 percent proof stress N/mm <sup>2</sup>	$p_{\text{expt}}$ N/mm <sup>2</sup>	$p_D$ from equation (1) N/mm <sup>2</sup>	$p_{\text{expt}}/p_D$
Fino-Schneider [28]	18.5	Carbon steel	2325	0.173	0.91	248	0.0862	0.0464	1.86
Avon [1,2,23]	13.8	Carbon steel	430	0.063	0.81	207	0.414 <sup>(a)</sup>	0.245	1.69
Blenkin [20]	20.3	Carbon steel	1420	0.106	1.0	241	0.0862 <sup>(b)</sup>	0.0567	1.52
CBI Ind. [18, 24]	4.92	Carbon steel	770	0.17	0.9	344	0.731	0.338	2.16
CBI Ind.	4.92	Carbon steel	1025	0.17	0.9	372	0.40	0.238	1.68
Stennett [19]	1.95	Stainless steel	950	0.105	1.0	293	0.276	0.125	2.21

<sup>(a)</sup> Brittle failure of head [23]

<sup>(b)</sup> Max test pressure; no buckling observed

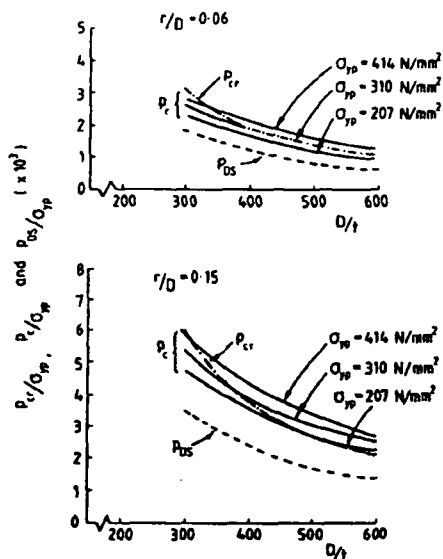


Fig. 3 Theoretical values of  $p_0$  and  $p_{DS}$  ( $\times 10^3$ ) for  $300 < D/t < 600$ ,  $R_s/D = 1.0$ ,  $r/D = 0.06$  and  $0.15$  (from [13])

$R_s/D = 1.10$ . From Fig. 3 (for  $R_s/D = 1.0$ ) it may be seen that (ignoring the  $p_{DS}$ -curve) either buckling or axisymmetric yielding can occur for  $r/D = 0.06$ ,  $D/t = 400$  and  $\sigma_{yp} = 310$  N/mm<sup>2</sup>. Test and theory are, therefore, in reasonable harmony for this case.

#### Elastic Buckling

With torispheres that have high  $D/t$ - or  $\sigma_{yp}/E$ -ratios, internal pressure buckling can occur in the elastic range. This topic has not been discussed in this note. However, elastic buckling formulae for perfect torispherical shells are given in [21]. Some experimental results obtained on plastic torispherical models are discussed in [22] and the relative magnitudes of the elastic and plastic buckling pressures of some steel torispherical shells are indicated in Fig. 8 of [11].

#### Discussion of the Proposed Design Equation

Equation (1) has the merits of being simple to apply and of giving a safety factor of at least 1.5 on all known internal pressure buckling tests on torispherical shells. It seems to be applicable to both crown and segment heads and to spun ones and the material of construction can be either carbon steel or stainless steel.

Residual stresses were, of course, ignored and strain-hardening was only treated in an approximate manner. In addition, there are criticisms which could be directed at the experimental data base. Some of these are:

(i) As the SC- and K- stainless steel heads were made by the same manufacturer, why were the values of  $p_{exp}$  for the SC heads so much higher than those for the K-heads? If one ignores the result for SC7, then the experimental results for the SC-heads were 1.5 to 2.5 times higher than those for the K-heads. In the absence of any adequate explanation for this result, the test results for the K-heads (being the lower) will control the constant in the design equation. This means that the design equation will give allowable design pressures which are sometimes very conservative.

(ii) The stainless steel buckling test results come from only one type of austenitic stainless steel (304 S65).

(iii) With the carbon steel spun heads, a number of the models had  $r/D = 0.04$  or  $R_s/D = 1.10$ . These geometric ratios are outside the limits allowed by some Codes. If the corresponding tests are excluded from consideration, then the number of relevant tests is very small.

(iv) There do not seem to be any tests of carbon steel crown and segment models.

Despite (iii), the range of values of  $p_{exp}/p_D$  for the T-heads in Table 1 was only 1.52 to 2.63 i.e. a factor of 1.73. This does not seem intolerable. In relation to (iv), the results in Table 2 for the larger vessels are at least reassuring.

However, it must be agreed that the number of relevant buckling test results is small. More tests are needed if a design equation which has been properly validated experimentally is to be obtained.

#### References

- 1 Galletly, G. D., "Stress Failure of Large Pressure Vessels—Recommendations Resulting From Studies of the Collapse of a 66 Ft. High  $\times$  45 Ft. Dia. Pressure Vessel," Technical Report No. 45-57, Shell Development Corporation, Emeryville, Calif., Mar. 1957.
- 2 Galletly, G. D., "Torispherical Shells—A Caution to Designers," ASME *Journal of Engineering for Industry*, Vol. 81, 1959, pp. 31-62; also, *Pressure Vessel and Piping Design—Collected Papers 1927-1959*, ASME, New York, 1960.
- 3 Drucker, D. C., and Shield, R. T., "Limit Analysis of Symmetrically Loaded Shells of Revolution," ASME *Journal of Applied Mechanics*, Vol. 81, 1959, pp. 61-68.
- 4 Shield, R. T., and Drucker, D. C., "Design of Thin-Walled Torispherical and Toriconical Pressure-Vessel Heads," ASME *Journal of Applied Mechanics*, Vol. 83, 1961, pp. 292-297.
- 5 Roche, R. L., and Antrusson, B., "Experimental Tests on Buckling of Torispherical Heads—Comparison with Plastic Bifurcation Analysis," presented at ASME PVP Conference, San Antonio, Tex., June 1984.
- 6 Kemper, M. J., "Buckling of Thin Dished Ends Under Internal Pressure," *Proceedings of the Symposium on Vessels Under Buckling Conditions*, I. Mech. E., London, 1972, pp. 23-32.
- 7 Stanley, P., Campbell, T. D., and Cooper, D., "Stresses and Deformations in Very Thin Pressure Vessel Ends," Technical Report, Department of Mechanical Engineering, University of Nottingham, 1975; see also, *Journal of Strain Analysis*, Vol. 16, 1981, pp. 171-203.
- 8 Bushnell, D., "BOSOR 5—Program for Buckling of Elastic-Plastic Shells of Revolution Including Large Deflections and Creep," *Computers and Structures*, Vol. 6, 1976, pp. 221-239.
- 9 Galletly, G. D., and Radhamohan, S. K., "Elastic-Plastic Buckling of Internally-Pressurized Thin Torispherical Shells," ASME *JOURNAL OF PRESSURE VESSEL TECHNOLOGY*, Vol. 101, 1979, pp. 216-225.
- 10 Galletly, G. D., "Plastic Buckling of Torispherical and Ellipsoidal Shells Subjected to Internal Pressure," *Proceedings of the Institution of Mechanical Engineers*, Vol. 193, 1981, pp. 329-345.
- 11 Galletly, G. D., "The Buckling of Fabricated Torispherical Shells Under Internal Pressure," *Buckling of Shells—Proceedings of a State-of-the-Art Colloquium*, Stuttgart, ed., E. Ramn, Springer-Verlag, Berlin, 1982, pp. 429-466.
- 12 Galletly, G. D., "A Design Procedure for Preventing Buckling in Internally-Pressurized Thin Fabricated Torispheres," *Journal of Const. Steel Research*, Vol. 2, No. 3, Sept. 1982, pp. 11-21.
- 13 Galletly, G. D., and Blachut, J., "Torispherical Shells Under Internal Pressure—Failure Due to Asymmetric Plastic Buckling or Axisymmetric Yielding," *Proceedings of the Institution of Mechanical Engineers*, Vol. 199, No. C3, 1985, pp. 225-238.
- 14 Roche, R. L., Alix, M., and Antrusson, B., "Design Rules Against Buckling of Dished Heads," *Proceedings of the 5th International Conference on Pressure Vessel Technology*, San Francisco, 1984, pp. 274-289.
- 15 CODAP, Code Francais de Construction des Appareils à Pression SNCT, AFIAF, Paris, 1982.
- 16 Galletly, G. D., "Design Equations for Preventing Buckling in Fabricated Torispherical Shells Subjected to Internal Pressure," *Proceedings of the Institution of Mechanical Engineers*, Vol. 200, No. A2, 1986, pp. 127-139.
- 17 Fino, A., and Schneider, R. W., "Wrinkling of a Large Thin Code Head Under Internal Pressure," *Bulletin of Welding Research Council*, Vol. 69, June 1961, pp. 11-23.
- 18 Raju, P. P., "An Overview of Buckling and Rupture Tests of Torispherical Heads Under Internal Pressure," *Pressure Vessel Components Design and Analysis*, PVP-Vol. 98-2, ASME, New York, 1985, pp. 77-82; see also, reference [24].

- 19 Stennett, R., "Gummed-Up Valve Causes Vessel Collapse," *Chartered Mechanical Engineer*, Oct. 1970, p. 404.
- 20 Blenkins, R., Whessoe Ltd. private communication.
- 21 Aylward, R. W., and Galletly, G. D., "Elastic Buckling of, and First Yielding in, Thin Torispherical Shells Subjected to Internal Pressure," *International Journal of Pressure Vessel and Piping*, Vol. 7, 1979, pp. 321-336.
- 22 Adachi, J., and Benisek, M., "Buckling of Torispherical Shells Under Internal Pressure," *Expt. Mech.*, Vol. 4, Aug. 1964, pp. 217-222.
- 23 Harding, A. G., and Ehmke, E. F., "Brittle Failure of a Large Pressure Vessel," *Proceedings of the American Petroleum Institute*, Sect. 3, Vol. 42, 1962, pp. 107-117.
- 24 Miller, C. D., Grove, R. B., and Bennett, J. G., "Pressure Testing of Large Scale Torispherical Heads Subject to Knuckle Buckling," Paper JK/10, Proceedings NUREG/CP-0065, Brussels, Aug. 1983, pp. 183-195.

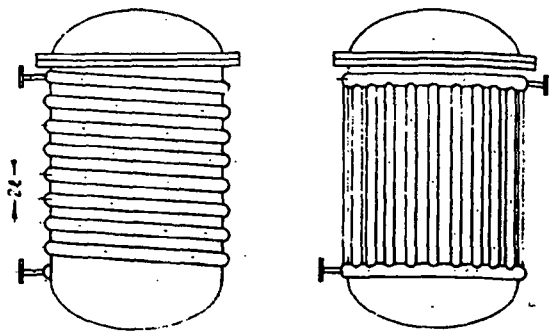


Fig. 1 Half-pipe heating channels

## Analysis of Half-Pipe Heating Channels on Pressure Vessel Shells

A. E. Blach<sup>1</sup>

*Half-pipe heating channels are used on the outside of pressure vessels such as agitators, mixers, reactors, etc., to avoid the high external pressure associated with heating jackets. No applicable method of analysis is contained in the ASME Code and proof tests are normally required for registration with governing authorities. An analytical method is presented which permits the evaluation of stresses in shell and half pipe; numerical examples are included.*

### Nomenclature

- $g$  = thickness of shell plate  
 $l$  = half-length between adjacent pipes  
 $p$  = internal pressure in heating pipes  
 $t$  = thickness of half-pipes  
 $E$  = modulus of elasticity  
 $E$  = ASME Code welding joint efficiency  
 $I$  = moment of inertia  
 $M$  = discontinuity moment  
 $\bar{M}$  = nondimensional moment  
 $Q$  = discontinuity force  
 $\bar{Q}$  = nondimensional force  
 $R$  = radius of half-pipe  
 $S_s$  = stress in shell plate  
 $S_p$  = stress in half-pipe  
 $\alpha$  = nondimensional parameter  
 $\beta$  = nondimensional parameter  
 $\delta$  = displacement  
 $\theta$  = rotation  
 $\nu$  = Poisson's ratio

### Introduction

Half-pipe heating channels as shown in Fig. 1, are often used on the outside of pressure vessels and tanks such as agitators, mixers, autoclaves and reactors, in order to avoid the high external pressures of heating jackets. The design and analysis of stresses in such heating channels is not covered by

ASME Code rules, except possibly by Appendix 13 of Section VIII, Division 1 [1], which gives rules for vessels with circular cross section and a longitudinal dividing plate through the center. Although similar in appearance, the problem of half pipe welded to a flat or slightly curved plate is quite different from the problem of a cylinder restrained from uniform deformation by a "tie" at the center.

This paper provides a method of analysis of stresses in both the half-pipe and the vessel shell to which it is welded. Numerical examples and values of proof tests conducted on test assemblies constructed for this purpose are also included.

### Method of Analysis

Both the half-pipe and the vessel plate are considered infinitely long in the axial direction and flat in the lateral direction; a reasonable assumption, since normally the ratio of heating pipe radius to vessel radius is very small. The pipe is analyzed as a curved beam subject to uniform pressure and the vessel wall as a continuous beam.

Using the nomenclature indicated in Fig. 2, equations for rotations and displacements are written and solved in terms of discontinuity forces and moments. A complete stress distribution in the assembly is then obtained.

### Half-Pipe Equations

For the half-pipe shown in Fig. 3, the radial expansion can be found from the membrane theory [2]

$$\delta_p = \frac{pR^2}{2tE} (2 - \nu) \quad (1)$$

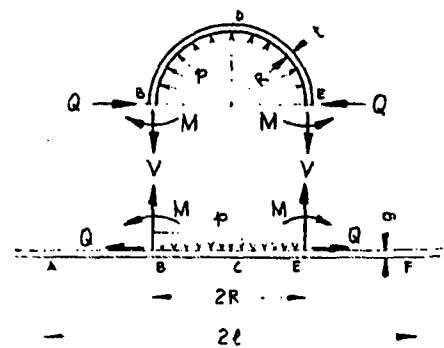


Fig. 2 Dimensions and free body diagram

<sup>1</sup>Concordia University, Montreal, Canada.

Contributed by the Pressure Vessels and Piping Division for publication in the JOURNAL OF PRESSURE VESSEL TECHNOLOGY. Manuscript received by the Pressure Vessels and Piping Division, February 7, 1985; revised manuscript received November 7, 1985.

It is important that the data contained in technical papers be made readily available to design engineers. In order to satisfy these needs of industry, this section of the Journal includes a concise presentation of data and information drawn chiefly from papers previously published by the Applied Mechanics Division of The American Society of Mechanical Engineers.

## Design of Thin-Walled Torispherical and Toriconical Pressure-Vessel Heads<sup>1</sup>

R. T. SHIELD<sup>2</sup> and D. C. DRUCKER<sup>3</sup>

### Summary

The failure under hydrostatic test of a large storage vessel designed in accordance with current practice stimulated earlier analytical studies. This paper gives curves and a table useful for the design and analysis of the knuckle region of a thin torispherical or toriconical head of an unfired cylindrical vessel. A simple but surprisingly adequate approximate formula is presented for the limit pressure,  $np^D$ , at which appreciable plastic deformations occur:

$$\frac{np^D}{\sigma_0} = \left(0.33 + 5.5 \frac{r}{D}\right) \frac{t}{L} + 28 \left(1 - 2.2 \frac{r}{D}\right) \left(\frac{t}{L}\right)^2 - 0.0006,$$

where  $p^D$  is the design pressure,  $\sigma_0$  is the yield stress of the material, and  $n$  is the factor of safety. The thickness  $t$  of the knuckle region is assumed uniform. Upper and lower bound calculations were made for ratios of knuckle radius  $r$  to cylinder diameter  $D$  of 0.06, 0.08, 0.10, 0.12, 0.14, and 0.16, and ratios of spherical cap radius  $L$  to  $D$  of 1.0, 0.9, 0.8, 0.7, and 0.6. Toriconical heads may be designed or analyzed closely enough by interpreting  $\phi_0$  in Table I as the complement of the half angle of the cone.

### Introduction

The design of pressure vessels requires the long experience distilled into the ASME Code to avoid overlooking many important factors. In principle, the most straightforward of the difficult problems is the design of an unreinforced knuckle region of uniform thickness in an unfired pressure vessel subjected to interior pressure. This topic is discussed at length in the Code and it might well be expected that little remained to be resolved. Surprisingly, analytical studies<sup>4,5</sup> stimulated by reports of a failure

under hydrostatic test demonstrated conclusively that the thickness required by the Code is inadequate for a range of designs. This range is one of small pressures and consequently of vessels whose wall thickness is small compared with the knuckle radius as well as the radius of the vessel itself. It did not, in all likelihood, engage the serious attention of the framers of the Code who were concerned primarily with pressures exceeding several hundred pounds per square inch. At these higher pressures, a sharply curved knuckle would have a radius which is not very large compared with the wall thickness, and so the knuckle would not be flexible and weak.

A design of adequate strength must provide a reasonable factor of safety against reaching the limit pressure, the pressure at which significantly large plastic deformation will take place. Many additional practical matters as well must be taken into account in the design. Among these are corrosion allowance, thinning allowance, and joint efficiency. They will not be considered here except by implication in the designation of the limit pressure as  $np^D$ , where  $n$  is a factor of safety and  $p^D$  is the design or working pressure.

The limit pressure is especially significant in a cold environment for those steels which are prone to brittle fracture. Appreciable plastic deformation below the transition temperature is almost certain to initiate a brittle fracture. Above this rather ill-defined transition temperature, the shape of a vessel of ductile material will be able to change sufficiently to carry the pressure without catastrophic failure. The pressure simply could form the head to a quite different but much better shape for containing pressure.

### A Qualitative Discussion of the Behavior of Pressure Vessels

A thin-walled vessel under interior pressure is most efficient when it can carry the pressure as a membrane in biaxial tension. However, the shape required for this desirable membrane behavior<sup>6</sup> has a height of head  $H = 0.26D$  which often appears too large from the fabrication or space utilization point of view. Torispherical heads are employed to reduce  $H$  appreciably, but they cannot act in biaxial tension; they must carry circumferential compression on the knuckle and also resist bending. Their local-

<sup>1</sup> The results presented in this paper were obtained in the course of research sponsored by the Office of Naval Research under Contract Nour 562(10) with Brown University, Providence, R. I.

<sup>2</sup> Professor of Applied Mathematics, Brown University, Providence, R. I.

<sup>3</sup> Professor of Engineering, Brown University. Mem. ASME.

<sup>4</sup> G. D. Galletly has studied elastic behavior in "Torispherical Shells—A Caution to Designers," *Journal of Engineering for Industry*—TRANS. ASME, vol. 81, Series B, 1959, pp. 51–62, and "On Particular Integrals for Toroidal Shells Subjected to Uniform Internal Pressure," *JOURNAL OF APPLIED MECHANICS*, vol. 25, TRANS. ASME, vol. 80, 1958, pp. 412–413.

<sup>5</sup> D. C. Drucker and R. T. Shield have studied plastic behavior in "Limit Strength of Thin-Walled Pressure Vessels With an ASME Standard Torispherical Head," Proceedings, Third U. S. National Congress of Applied Mechanics, ASME, 1955, pp. 665–672, and "Limit Analysis of Symmetrically Loaded Thin Shells of Revolution," *JOUR-*

*NAL OF APPLIED MECHANICS*, vol. 26, TRANS. ASME, vol. 81, Series E, 1959, pp. 61–63.

<sup>6</sup> R. A. Struble, "Biaxial Pressure Vessel Heads," *JOURNAL OF APPLIED MECHANICS*, vol. 23, TRANS. ASME, vol. 78, 1956, pp. 642–645.

Discussion of this paper should be addressed to the Secretary, ASME, 29 West 39th Street, New York 18, N. Y., and will be accepted until July 10, 1961, for publication at a later date. Discussion received after the closing date will be returned.

Manuscript received by ASME Applied Mechanics Division, September 20, 1960.

Table 1

$L/D$	$r/D$	$\varphi_0$ (deg)	$H/D$	$p^u D / 2\sigma_d$	$L/D$	$r/D$	$\varphi_0$ (deg)	$H/D$	$p^u D / 2\sigma_d$
1.0	0.06	27.91	0.1694	0.064	0.9	0.06	31.59	0.1844	0.079
	0.08	27.16	0.1815	0.087		0.08	30.81	0.1957	0.108
	0.10	26.39	0.1937	0.111		0.10	30.00	0.2072	0.139
	0.12	25.58	0.2053	0.136		0.12	29.16	0.2188	0.171
	0.14	24.75	0.2190	0.163		0.14	28.27	0.2306	0.205
	0.16	23.88	0.2319	0.190	0.16	27.35	0.2427	0.240	
0.8	0.06	36.48	0.2050	0.101	0.7	0.06	43.43	0.2353	0.134
	0.08	35.60	0.2152	0.139		0.08	42.64	0.2440	0.184
	0.10	34.85	0.2256	0.179		0.10	41.81	0.2528	0.238
	0.12	33.97	0.2360	0.221		0.12	40.93	0.2619	0.296
	0.14	33.06	0.2468	0.265		0.14	40.01	0.2710	0.357
	0.16	32.09	0.2577	0.312	0.16	39.02	0.2804	0.423	
0.6	0.06	51.57	0.2869	0.185					
	0.08	53.87	0.2934	0.256					
	0.10	53.13	0.3000	0.333					
	0.12	52.34	0.3068	0.417					
	0.14	51.50	0.3136	0.507					
	0.16	50.60	0.3207	0.606					

$$H = L - (L - r) \cos \varphi_0$$

$$\sin \varphi_0 = \left( \frac{1}{2} - \frac{r}{D} \right) / \left( \frac{L}{D} - \frac{r}{D} \right)$$

$$\frac{p^u D}{2\sigma_d} = \frac{rD}{L(L - r)}$$

carrying capacity as pure membranes (no moment resistance), shown in Table 1 as  $p^u D / 2\sigma_d$  and plotted on some of the graphs at  $l/D = 0$ , is extremely low. Actually, a very thin shell acting as a membrane would buckle in circumferential compression.

As the pressure builds up, it tends to force the spherical cap outward along the axis and the meridional membrane tensions pull the toroidal knuckle inward toward the axis. If the torus wall is thick enough to avoid buckling but thin compared with the radius of the knuckle, and the material does not work-harden, a plastic hinge circle will form at B, Fig. 1, to permit the central region of the knuckle to compress in the circumferential direction and bend inward. A hinge circle will form at C in the spherical cap and the third hinge circle A usually forms in the cylinder. The entire knuckle region between A and C is plastic because inward motion of appreciable extent means plastic contraction of the circumference. A thin-walled sharply curved knuckle region is far weaker than the main part of the spherical cap or the cylindrical portion of the vessel. On the other hand, if the torus wall is not so thin compared with the knuckle radius, the knuckle region is stiff and strong and acts somewhat like a stiffening ring at the junction of a spherical cap and a cylinder. The ASME Code which requires very little variation of  $np^u D / \sigma_d$  with  $l/D$  apparently contains the implicit assumption that ordinarily the resistance to inward motion of the knuckle region is ade-

quately high. Although true for vessels designed to carry large pressure, the assumption is not valid for many storage vessels and other low-pressure containers. For these thin-walled vessels there is a large variation of the value of  $np^u D / 2\sigma_d$  with  $l/D$  as shown in Figs. 2-5. On the other hand, the dotted lines for values of  $np^u D / 2\sigma_d$  greater than unity show that, for less sharply curved knuckles and for relatively thick knuckles, the knuckle region is stronger than the main cylindrical part of the vessel.

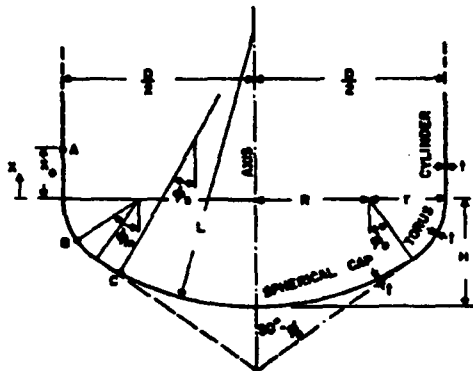


Fig. 1 Torispherical head, showing dimensions and locations of hinge circles A, B, C. (The equivalent toriconical head is shown by the dashed line which is tangent to the torus at its lower end.)

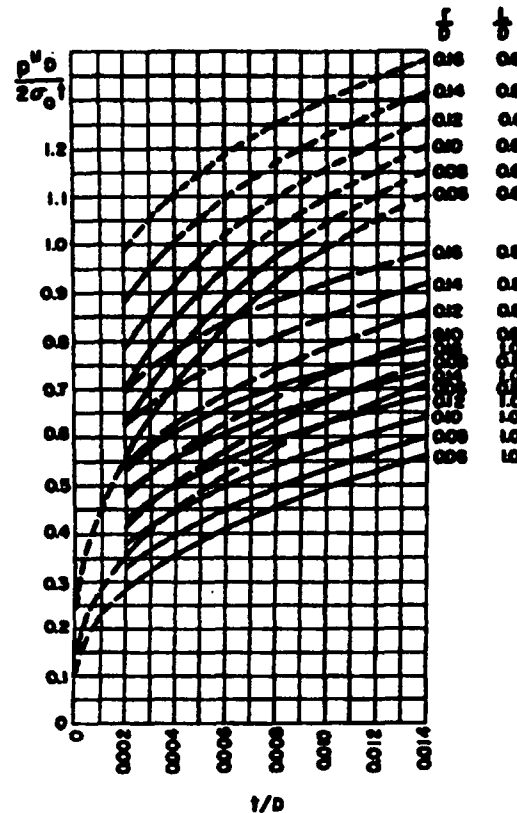


Fig. 2 Upper (unsafe) bound on limit pressure.  $l/D = 0.6, 0.8, 1.0$ .

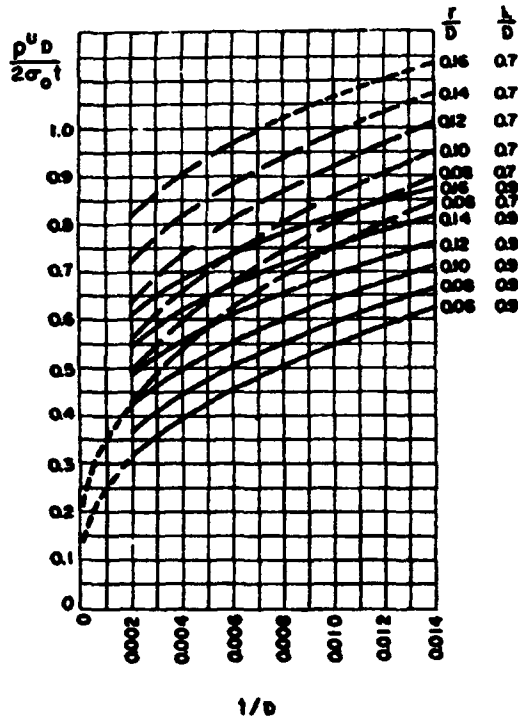


Fig. 3 Upper (unsafe) bound on limit pressure.  $L/D = 0.7, 0.9$ .

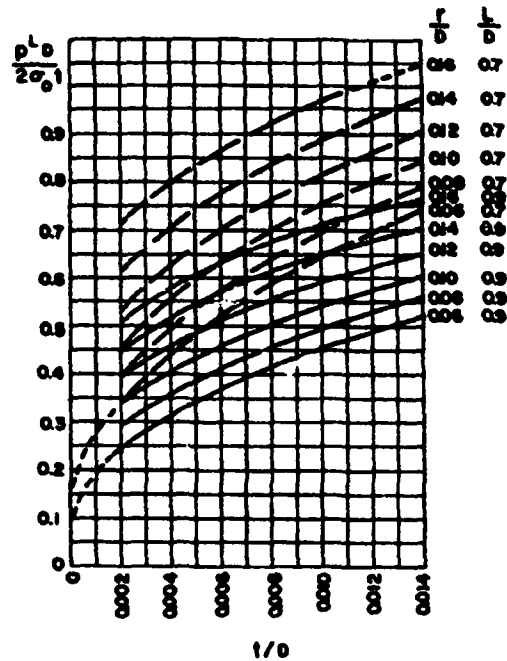


Fig. 5 Lower (safe) bound on limit pressure.  $L/D = 0.7, 0.9$ .

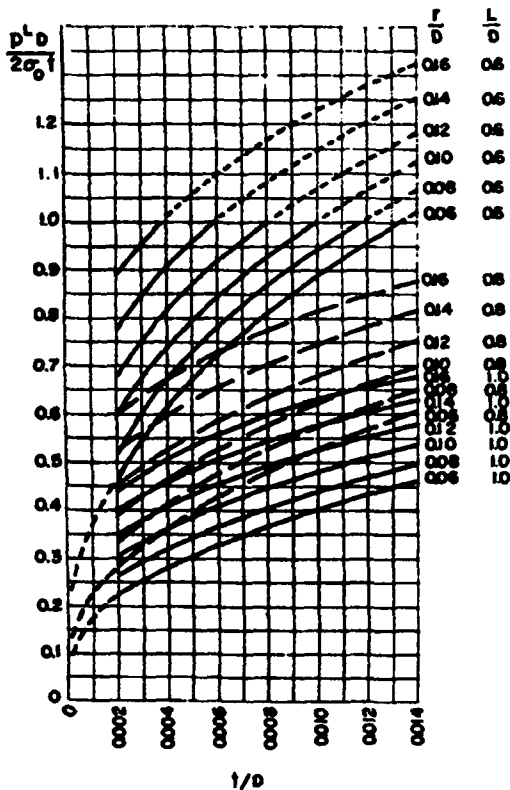


Fig. 4 Lower (safe) bound on limit pressure.  $L/D = 0.6, 0.8, 1.0$ .

#### Design Curves and Formula

The upper and lower bound theorems of limit analysis and design<sup>2</sup> were used to calculate the limit pressure. Therefore, even within the usual idealizations of the theory of plasticity, the exact answer is bounded rather than determined directly. Curves are plotted in Figs. 2 and 3 for  $p^u D/2\sigma_0 t$ , the upper (unsafe) values computed for  $np^u D/2\sigma_0 t$ , and in Figs. 4 and 5 for  $p^l D/2\sigma_0 t$ , the lower (oversafe) values. The designer then can make an independent judgment of the appropriate values to use.

However, if moderate accuracy is good enough or if a preliminary design is sought, Fig. 6 should prove a very helpful alternative. An approximate plot of  $t/D$  versus  $H/D$  for discrete values of  $np^u D/\sigma_0$ , it gives a clear picture of the penalty to be paid for the advantage of decreasing the axial length of the vessel. The agreement with the mean of the upper and lower bound calculations, also shown in Fig. 6, varies with  $r/D$  and  $L/D$  but to a much smaller extent than might be expected.

Remarkably good agreement with the limit calculations can be achieved through use of the variable  $t/L$  which is of prime importance in the ASME Code. The excellent fit of the simple formula

$$\frac{np^u D}{\sigma_0} = \left(0.33 + 5.5 \frac{r}{D}\right) \frac{t}{L} + 28 \left(1 - 2.2 \frac{r}{D}\right) \left(\frac{t}{L}\right)^2 - 0.00001$$

is illustrated in Fig. 7, a plot of  $t/L$  versus  $np^u D/\sigma_0$  for two values of  $r/D$ . The relatively minor variation with  $L/D$  is also a feature of the Code. However, the Code calls for a linear variation of  $t/L$  with increasing pressure, and there is no way of adjusting a straight line to the proper curves without being unsafe or far too safe. The lack of safety is all too evident in Fig. 8, a

<sup>2</sup> D. C. Drucker, W. Prager, and H. J. Greenberg, "Extended Limit Design Theorems for Continuous Media," *Quarterly of Applied Mathematics*, vol. 9, 1952, pp. 381-389.

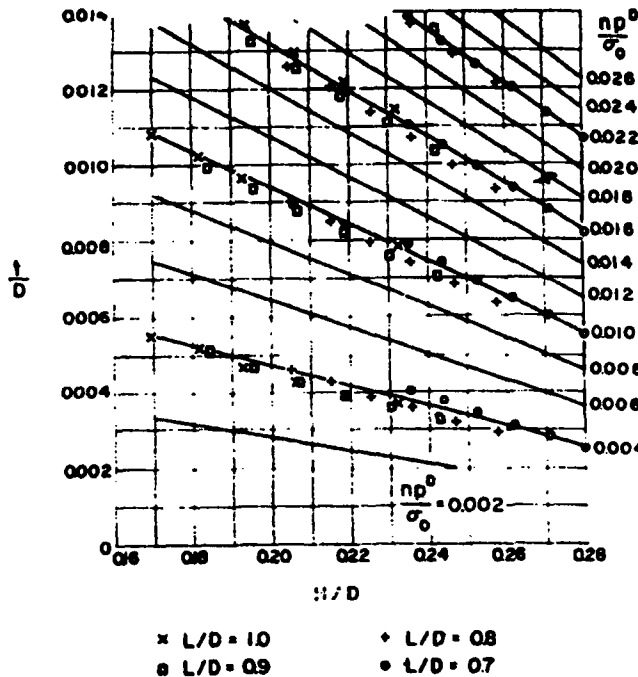


Fig. 6 Approximate curves for  $t/D$  versus  $H/D$  for constant  $np^0/\sigma_0$  (for  $L/D = 0.6$ ,  $H/D$  varies from 0.29 to 0.32)

plot of the formula for discrete values of  $r/D$ , which permits the designer to select  $t \cdot L$  for a given pressure or to check the pressure-carrying capacity of an existing design. Again the designer is urged to return to Figs. 2-5 to obtain upper and lower bounds on his factor of safety if he is forced to design with a very small margin.

The Appendix contains detailed information on the basis and the methods of calculation of Figs. 2-5. It supplements the discussion contained in the earlier papers<sup>3</sup> and is not complete in itself. In essence, the Tresca or maximum shearing stress criterion of yield is employed and the yield surface for the shell is a cut-off parabolic approximation to the exact shape for a symmetrically loaded cylindrical shell.

**Toriconical Heads**

The values of  $t \cdot L$  and  $np^0/\sigma_0$  plotted for a given torus apply equally well to torispherical and to toriconical heads. Table 1 can be used to obtain the appropriate interpolated value of  $L/D$  for Figs. 2-5 if desired. The angle  $\varphi_0$  is the complement of the torus angle and therefore the complement of the half angle of the cone.

**APPENDIX**

The equations of equilibrium for the various portions of the vessel, cylinder, torus and sphere are given in the references of footnote 5. The term involving the circumferential bending moment  $M_\theta$  is omitted from the equations of equilibrium for the torus and the sphere as  $M_\theta$  has little influence in carrying load for thin shells at sections not too near the axis of symmetry. The meridional bending moment  $M_\varphi$  is similarly omitted but its derivative is retained.

As  $M_\theta$  is considered as a passive moment in the curved portions of the shell as well as in the cylinder, full use of  $M_\varphi$  and the meridional and circumferential force resultants  $N_\varphi$  and  $N_\theta$  in carrying the internal pressure  $p$  is obtained by using the yield condition on  $N_\varphi$ ,  $N_\theta$ ,  $M_\varphi$  for the cylinder. In order to approximate to this yield condition or surface, the circumscribing surface

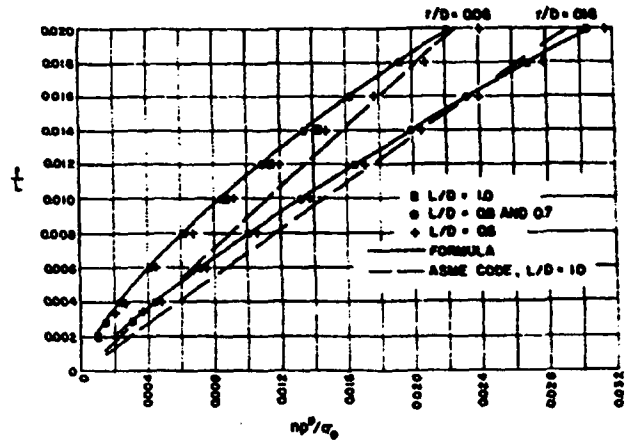


Fig. 7 Comparison of formula with average of upper and lower bounds and with ASME Code for  $r/D = 0.06$  and  $0.16$

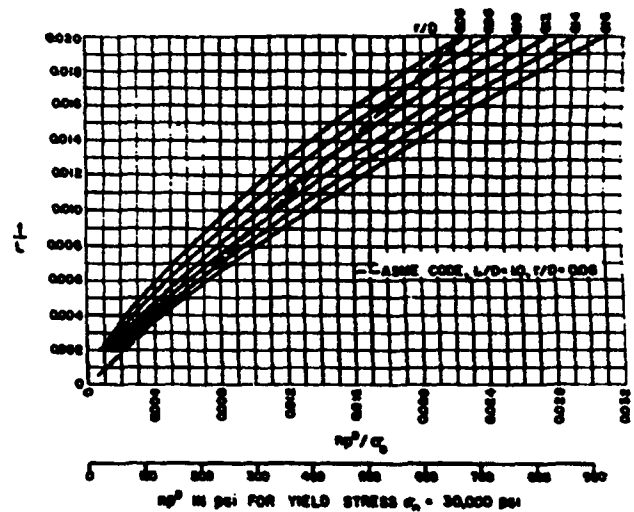


Fig. 8 Plot of  $np^0/\sigma_0 = (0.33 + 5.5 r/D)/L + 28 (1 - 2.2 r/D)(t/L)^2 - 0.0006$ ;  $np^0/\sigma_0$  must not exceed  $2t/D$

consisting of a parabolic cylinder with four cut-off planes is used.<sup>5</sup> In the region of interest between the hinge circles A, B, C of Fig. 1,  $N_\varphi$  is tensile and  $N_\theta$  is compressive. For this region to be at yield, the parabolic prism yield surface requires

$$N_\varphi - N_\theta = \sigma_d, \quad |M_\varphi| \leq \frac{1}{4} \sigma_d^2 \{1 - (N_\varphi/\sigma_d)^2\} \quad (1)$$

It is assumed that at the hinge circles A and C in the cylinder and the sphere,  $M_\varphi$  attains its largest negative value, and at hinge circle B in the torus,  $M_\varphi$  attains its largest positive value. The shear force  $Q$  is zero at the hinge circles. Under these conditions the equations of equilibrium can be integrated to provide the distribution of  $N_\theta$ ,  $N_\varphi$ ,  $M_\varphi$ , and  $Q$  in the plastic region.

It is found that in the cylinder,

$$M_\varphi = -\frac{1}{4} \sigma_d^2 \left\{ 1 - \left( \frac{pD}{4\sigma_d} \right)^2 \right\} + \frac{1}{2} \sigma_0 \frac{t}{D} \left( 2 + \frac{pD}{2\sigma_d} \right) (x_0 - x)^2 \quad (2)$$

$$Q = -\sigma_0 \frac{t}{D} \left( 2 + \frac{pD}{2\sigma_d} \right) (x_0 - x) \quad (3)$$

## DESIGN DATA AND METHODS

where  $x$  measures distance from the junction with the torus and  $x_0$  defines the location of the hinge circle A. In the torus,

$$\frac{M_\varphi}{r\sigma_d} = \frac{1}{4} \frac{t}{r} \left\{ 1 - \left( \frac{pD}{2\sigma_d} \right)^2 \frac{(R + r \sin \varphi_m)^2}{D^2 \sin^2 \varphi_m} \right\} - \frac{pR}{2\sigma_d} \frac{[1 - \cos(\varphi - \varphi_m)]}{\sin \varphi_m} + \frac{r}{R} \cos \varphi [k(\varphi) - k(\varphi_m)] + \log \left\{ \frac{R + r \sin \varphi}{R + r \sin \varphi_m} \right\}, \quad (4)$$

$$\frac{Q}{\sigma_d} = \frac{pR}{2\sigma_d} \frac{\sin(\varphi_m - \varphi)}{\sin \varphi_m} + \frac{r}{R} \sin \varphi [k(\varphi) - k(\varphi_m)], \quad (5)$$

where

$$k(\varphi) = \int_{\varphi_0}^{\varphi} \frac{Rd\varphi}{R + r \sin \varphi} = \frac{2R}{(R^2 - r^2)^{1/2}} \left[ \tan^{-1} \left\{ \frac{r + R \tan \frac{1}{2} \varphi}{(R^2 - r^2)^{1/2}} \right\} \right]_{\varphi_0}^{\varphi}, \quad (6)$$

$\varphi$  is the angle between the meridional normal and the axis of the shell, and  $\varphi_m$  is the location of the hinge circle B. In the sphere, with the assumption that  $\varphi - \varphi_0$  is small,

$$\frac{M_\varphi}{L\sigma_d} = -\frac{1}{4} \frac{t}{L} \left\{ 1 - \left( \frac{pL}{2\sigma_d} \right)^2 \right\} + \frac{1}{2} (\varphi - \varphi_0)^2, \quad (7)$$

$$\frac{Q}{\sigma_d} = \varphi - \varphi_0, \quad (8)$$

where  $\varphi_0$  defines the location of the hinge circle C.

The four quantities  $p$ ,  $\varphi_m$ ,  $\varphi_0$ , and  $x_0$  are determined from the conditions that  $M_\varphi$  and  $Q$  are continuous at the junctions of the cylinder and torus ( $x = 0$ ,  $\varphi = \pi/2$ ) and the torus and sphere ( $\varphi = \varphi_0$ ). These conditions can be written

$$\left( 2 + \frac{pD}{2\sigma_d} \right) \left( \frac{x_0}{D} \right)^2 = j(\varphi_m) \left( \frac{pD}{2\sigma_d} \right)^2 + a(\varphi_m) \frac{pD}{2\sigma_d} + b(\varphi_m), \quad (9)$$

$$\left( 2 + \frac{pD}{2\sigma_d} \right) \frac{x_0}{D} = c(\varphi_m) \frac{pD}{2\sigma_d} + d(\varphi_m), \quad (10)$$

$$(\varphi_0 - \varphi_m)^2 = l(\varphi_m) \left( \frac{pD}{2\sigma_d} \right)^2 + e(\varphi_m) \frac{pD}{2\sigma_d} + f(\varphi_m), \quad (11)$$

$$\varphi_0 - \varphi_m = g(\varphi_m) \frac{pD}{2\sigma_d} + h(\varphi_m), \quad (12)$$

where the functions not previously defined are given by

$$a(\varphi_m) = -2 \frac{rR}{D^2} \frac{(1 - \sin \varphi_m)}{\sin \varphi_m}, \quad (13)$$

$$b(\varphi_m) = 2 \frac{r}{D} \log \left\{ \frac{R + r}{R + r \sin \varphi_m} \right\} + \frac{t}{D}, \quad (14)$$

$$c(\varphi_m) = \frac{R}{D} \cot \varphi_m, \quad (15)$$

$$d(\varphi_m) = -\frac{r}{R} [k(\pi/2) - k(\varphi_m)], \quad (16)$$

$$e(\varphi_m) = -2 \frac{rR}{lD} \frac{[1 - \cos(\varphi_m - \varphi_0)]}{\sin \varphi_m}, \quad (17)$$

$$f(\varphi_m) = 2 \frac{r^2}{LR} \cos \varphi_0 k(\varphi_m) + 2 \frac{r}{L} \log \left\{ \frac{R + r \sin \varphi_0}{R + r \sin \varphi_m} \right\} + \frac{t}{L}, \quad (18)$$

$$g(\varphi_m) = \frac{R}{D} \frac{\sin(\varphi_m - \varphi_0)}{\sin \varphi_m}, \quad (19)$$

$$h(\varphi_m) = -\frac{r}{R} \sin \varphi_0 k(\varphi_m), \quad (20)$$

$$j(\varphi_m) = -\frac{1}{2} \frac{t}{D} \left\{ \frac{1}{4} + \frac{(R + r \sin \varphi_m)^2}{D^2 \sin^2 \varphi_m} \right\}, \quad (21)$$

$$l(\varphi_m) = -\frac{1}{2} \frac{t}{L} \left\{ \left( \frac{L}{D} \right)^2 + \frac{(R + r \sin \varphi_m)^2}{D^2 \sin^2 \varphi_m} \right\}. \quad (22)$$

Equations (9)–(12) were solved for  $pD/2\sigma_d$ ,  $\varphi_m$ ,  $\varphi_0$ , and  $x_0/D$  for given values of the parameters  $t/D$ ,  $L/D$ , and  $r/D$  which define the geometry of the vessel. The following values of the parameters were used:

$$t/D = 0.002, 0.004, 0.006, 0.008, 0.010, 0.012, 0.014$$

$$L/D = 1.0, 0.9, 0.8, 0.7, 0.6$$

$$r/D = 0.06, 0.08, 0.10, 0.12, 0.14, 0.16$$

In the numerical method used, a trial value  $\varphi_m^*$  was chosen for  $\varphi_m$  and the functions of  $\varphi_m$  occurring on the right-hand sides of equations (9)–(12) were evaluated. By elimination of  $\varphi_0 - \varphi_m$  between (11) and (12), a quadratic equation was obtained for  $pD/2\sigma_d$ . The positive root of this equation was then substituted in (9) and (10) to give two values of  $(x_0/D)^2$ . The difference between these two values was evaluated and the procedure was repeated with another trial value  $\varphi_m^*$  for  $\varphi_m$ , and again the difference between the two values of  $(x_0/D)^2$  was found. Linear interpolation between  $\varphi_m^*$  and  $\varphi_m^*$  was then used to give a better approximation to the true value of  $\varphi_m$ . The process was repeated until the magnitude of the difference between the two values of  $(x_0/D)^2$  as provided by (9) and (10) was less than  $10^{-2}$ .

For a few of the thinner vessels (12 out of the 210 considered), the upper hinge circle A does not lie in the cylinder but is located in the torus, and the analysis requires a straightforward modification. The details of this modification will not be given here.

The value of the pressure  $p$  obtained from equations (9)–(12) (or from the modified analysis) is the limit pressure  $p^U$  for the head with the parabolic yield surface. As this surface circumscribes the exact yield surface for the cylinder,  $p^U$  is an upper bound to the true limit pressure. The values of  $p^U$  are shown in Figs. 2 and 3. A lower bound  $p^L = \lambda p^U$  is obtained by choosing the factor  $\lambda$  so that the stress points  $\lambda N_\varphi$ ,  $\lambda N_\theta$ ,  $\lambda M_\varphi$  lie within the yield surface for the cylinder for all sections of the plastic region. The factor is given by

$$\lambda = (P^2 - 4P + 12)/2(P^2 - 4P + 8), \quad (23)$$

where  $P = p^U D/2\sigma_d$ , the critical section being the hinge circle A in the cylinder. The factor varies from 0.82 to 0.90 as  $P$  varies from 0.5 to 1.0, and the values of  $p^L D/2\sigma_d$  are given in Figs. 4 and 5. The average of the upper and lower bounds will be sufficiently close to the true limit pressure for practical purposes. Thus we put  $n p^D = (p^U + p^L)/2$ , where  $p^D$  is the design pressure and  $n$  the factor of the safety against collapse.

For a given thickness ratio  $t/D$ , the limit pressure  $n p^D$  increases as  $r/D$  increases, and decreases as  $L/D$  increases. The ratio  $H/D$  of the height of the head to the diameter depends similarly on the ratios  $r/D$ ,  $L/D$ , as can be seen from Table 1. In Fig. 6, approximate curves for  $t/D$  versus  $H/D$  for constant

values of  $np^D/\sigma_0$  are shown for the range  $0.17 < H/D < 0.28$  covered by the ranges 0.06 to 0.16 for  $r/D$  and 0.7 to 1.0 for  $L/D$ . Actual points for  $np^D/\sigma_0 = 0.004, 0.010, 0.016,$  and  $0.022$  are also shown for comparison with the approximate curves.

It was found that, for a fixed value of  $r/D$ , the variation of  $np^D/\sigma_0$  with  $t/L$  is almost independent of the ratio  $L/D$ . For  $L/D = 0.7$  and  $0.8$ , the formula

$$\frac{np^D}{\sigma_0} = \left(0.33 + 5.5 \frac{r}{D}\right) \frac{t}{L} + 28 \left(1 - 2.2 \frac{r}{D}\right) \left(\frac{t}{L}\right)^2 - 0.0006 \quad (24)$$

provides values of  $np^D/\sigma_0$  which are very close (e.g., within 3 per cent for  $t/L = 0.010$ ) to the values calculated from  $np^D = (p^U + p^L)/2$ . Formula (24) is also adequate for  $L/D = 1.0, 0.9,$

and 0.6 as can be seen from Fig. 7, in which the formula (24) is compared with the values calculated from  $np^D = (p^U + p^L)/2$  for the cases  $r/D = 0.06$  and  $0.16$ . Comparison with the ASME Code for Unfired Pressure Vessels is also made in Fig. 7. The ASME Code gives

$$\frac{p^D}{SE} = 2 \frac{t}{L} / \left(M + 0.2 \frac{t}{L}\right), \quad (25)$$

where  $M = \frac{1}{2}[3 + (L/r)^{1/2}]$ ,  $S$  is the maximum allowable stress, and  $E$  is the efficiency of the welded joints. For the present purposes,  $SE$  was taken to be  $\sigma_0/n$ .

#### Acknowledgment

The authors would like to thank Mrs. Lois Paul for her assistance with the computations.

## Hydrodynamic Lubrication of a Roller Bearing— Introduction of Parameters to Obtain Charts for Calculation

### F. W. v. HACKEWITZ<sup>1</sup>

#### Nomenclature

- $E$  = modulus of elasticity (21,000 kg./sq. mm for steel), kg./sq. mm  
 $P$  = radial load on cylindrical roller per unit effective roller length, kg./mm  
 $P^*$  = relative load on cylindrical roller  $P/R_0$ , kg./sq. mm  
 $R$  = radius of cylindrical roller, mm  
 $R_i$  = radius of inner ring raceway, mm  
 $R^*$  = relative radius of cylindrical roller  $\frac{R/R_i}{1 + R/R_i}$   
 $h$  = smallest oil-film thickness to be found at contact between rolling body and inner ring, mm  
 $h^*$  = relative oil-film thickness  $h/R_i$   
 $k_1, k_2, k_3$  = constant coefficients  
 $n$  = resultant rotating speed of the bearing, i.e., rotating speed of inner ring relative to outer ring, rpm  
 $p_m$  = peak pressure in contact area between roller and inner ring, kg./sq. mm  
 $u$  = parameter, angle deg  
 $\alpha$  = reduction parameter  $R^* p_m^2 / k_1^2 k_2$   
 $\beta$  = reduction parameter  $h^* / k_3$   
 $\gamma$  = pressure coefficient of viscosity of lubricating oil at operating temperature [2],<sup>2</sup> sq. mm/kg. The coefficient  $\gamma$  supposes an oil where  $\log [\eta(p)/\eta_0]$  is proportional to the pressure  $p$  as to justify  $\eta(p) = \eta_0 e^{\gamma p}$ . Some lubricating oils obey this law, but there are other oils in use, which show deviation. Thus a verification of the proper pressure dependence of viscosity is advisable for each particular case.  
 $\eta_0$  = viscosity of lubricating oil at atmospheric pressure and operating temperature, kg. sec./sq. mm  
 $\eta_r$  = resultant viscosity of lubricating oil at the rolling contact [3], kg. sec./sq. mm  
 $\mu$  = deformation parameter which is defined in Dörr's

work [1]. The parameter's definition fixes two limiting end points: One for  $\mu = 0$ , where no elastic deformation occurs at the rolling contact, and the other for  $\mu = 2$ , with maximum elastic deformation, i.e., no oil film separating the contacting rolling bodies (Hertzian case). Dörr derives simplified formulas valid for  $0 \leq \mu \leq 1.7$ , thus covering the greatest part of the parameter range. Our calculation is based on these simplified formulas.

$\nu$  = Poisson's ratio (0.303 for steel)

$\pi = 3.14159 \dots$

$e = 2.71828 \dots$

#### Introduction

IN A recent note [3] hydrodynamic formulas have been proposed to calculate contact pressure and oil-film thickness in a lubricated cylindrical roller bearing. These formulas use Dörr's derivations for elastic deformation at the rolling contact [1], and a pressure-dependent viscosity [2]. Their numerical evaluation is cumbersome, demanding extensive calculation.

Relative and dimensionless magnitudes are introduced in the following. They help to establish charts which represent isothermal results for different bearing design and various running conditions, thus aiding in the engineer's rapid investigation.

The charts show a minimum oil-film thickness at certain combinations of roller load and running speed.

#### General Calculation

Conditions are more severe at the inner contact than at the outer contact. We calculate, therefore, relationships for the inner contact only. Introducing the following reduction parameters

$$R^* \equiv \frac{R/R_i}{1 + R/R_i} \quad (1)$$

$$P^* \equiv P/R_0, \text{ kg./sq. mm} \quad (2)$$

$$h^* \equiv h/R_i \quad (3)$$

$$k_1 \equiv \frac{\pi E}{12(1 - \nu^2)}, \text{ kg./sq. mm} \quad (4)$$

<sup>1</sup> SKF Central Laboratoriet, Göteborg, Sweden.

<sup>2</sup> Numbers in brackets indicate References at end of paper.

Manuscript received by ASME Applied Mechanics Division, June 9, 1960; final draft, January 17, 1961.

# Torispherical shells under internal pressure—failure due to asymmetric plastic buckling or axisymmetric yielding

G D Galletly, ScD, DEng, FICE, FIMechE and J Blachut, PhD  
Department of Mechanical Engineering, University of Liverpool

*In the diameter-to-thickness range  $250 < D/t < 1000$ , internally pressurized torispherical shells can fail either by plastic buckling or by axisymmetric yielding. However, the present Code rules cater only for the axisymmetric yielding mode and they also restrict the  $D/t$  ratios to being less than 500. The rules are based on limit analysis results and these can be conservative for this problem. With regard to internal pressure buckling, there are as yet no design rules in either the American or the British pressure vessel Codes to prevent its occurrence.*

*To provide guidance for a more accurate formulation of design rules for both of these failure modes over the range  $300 < D/t < 1500$ , the authors have made a series of calculations to determine the values of  $p_{cr}$  (the internal buckling pressure) and  $p_s$  (the axisymmetric yielding pressure) for perfect torispherical shells. The availability of these results, obtained with a finite-deflection shell theory, enables curves to be drawn showing when buckling is the controlling failure mode and when axisymmetric yield controls.*

*A comparison is also made, for  $D/t < 600$ , between the controlling failure pressures mentioned above and the Drucker-Shield limit pressures. The ratio between the former and the latter varied between 1.2 and 1.8, depending on the geometry of the shell and the magnitude of the yield point,  $\sigma_{yp}$ . Considerable economies in the designs of many torispherical shells could, therefore, be achieved if the relevant sections of the Codes were to be modified to take advantage of the foregoing results.*

*The controlling failure pressure curves also indicate how Code rules to prevent plastic buckling for  $D/t > 500$  might be formulated. For the benefit of designers, the numerical values of  $p_{cr}$  and  $p_s$  were transformed, using curve-fitting techniques, into simple approximate equations. Although these equations are for perfect torispherical shells, they should be very beneficial when analysing the related problems of fabricated torispheres in practice.*

## NOTATION

$p$	internal pressure
$p_{cr}$	internal buckling pressure of torispherical shell (usually plastic buckling herein)
$p_{cr}^D, p_{cr}^F$	$p_{cr}$ obtained using the deformation or flow theory options in BOSOR 5
$p_{yp}$	pressure at yield (see Fig. 4)
$p_{c1}, p_{c2}$	axisymmetric yielding pressures of a torispherical shell (see Fig. 4)
$p_c$	$p_{c1}$ or $p_{c2}$
$p_{DS}$	Drucker-Shield limit pressure
$p_{contr}$	controlling failure pressure
$r$	radius of toroidal portion (knuckle) of torisphere (see Fig. 2)
$t$	thickness of cylinder and torispherical shell
$D$	diameter of attached cylinder (see Fig. 2)
$E$	modulus of elasticity
$L$	length of attached cylinder (see Fig. 2)
$\alpha$	angle used in definition of $p_{c2}$ (see Fig. 4)
$\delta$	deflection of the crown of the torisphere
$\sigma_{yp}$	yield point of material

Note:  $1 \text{ N/mm}^2 \approx 145 \text{ lbf/in}^2$

## 1 INTRODUCTION

Torispherical shells are frequently used as end closures on cylinders subjected to internal pressure and applications can be found in various fields, for example the

aerospace, brewing, food processing, chemical, nuclear and oil industries. In the first three industries cited the vessels usually do not exceed 5 m in diameter whereas the diameters can be greater than 20 m in the others.

One well-known failure of a torispherical shell occurred in 1956 during the hydrostatic proof test of a 15 m diameter fluid coker at Avon, California. An elastic stress analysis of this head was carried out subsequently by Galletly (1, 2) and it showed that (a) the direct hoop stresses in the knuckle were compressive and exceeded the yield point of the material at a number of locations and (b) buckling of the knuckle in the hoop direction was a definite possibility for some geometries. Metallurgical information about the brittle failure of this head may be found in (3).

The buckling prediction in (2) was verified experimentally in (4). Another case of buckling under internal pressure occurred with a 20 m diameter oil-storage vessel and is described in (5). Since that time, the only internal pressure buckling failures of torispheres to have been reported in the literature are those on the small diameter (3–5 m) heads used for brewing vats and food processing vessels (see, for example, Fig. 1). However, internally pressurized torispheres having larger diameters have been used in recent years on pressure vessels in the nuclear industry, for example in the vessels containing the liquid sodium in fast-breeder reactors and as roof structures for containment vessels of pressurized water reactors. As an agreed set of design rules for this internal pressure buckling problem is still not available, nuclear engineers sometimes have to test fairly large-scale models of their vessels in order to satisfy the certifying authorities of the integrity of their designs.

The MS was received on 8 October 1984 and was accepted for publication on 18 January 1985.

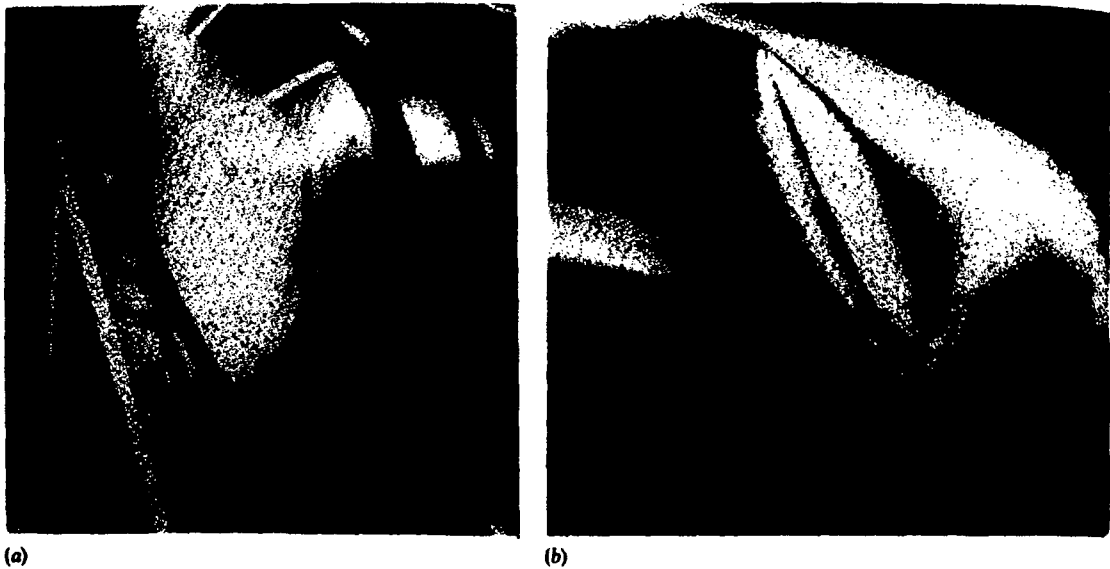


Fig. 1 Plastic buckling due to internal pressure in a 3 m diameter stainless steel torisphere:  
(a) outward buckles (b) inward buckle

With regard to the yielding of the foregoing torisphere at Avon, an elastic-plastic stress analysis of it should have been carried out. This would have been difficult to do at the time and Drucker and Shield (who were consulted about the problem) therefore undertook a limit analysis of the torispherical head (6). In their analysis, they assumed that failure would occur when three plastic hinge circles developed in the head.

One result of both the elastic and the limit analyses of the Avon vessel was that it showed that the then current edition of the ASME Code was in need of revision for certain torispherical geometries. The aspect of the problem which Drucker and Shield chose to investigate was the axisymmetric yielding mode. They were able to calculate the limit pressures for a wide range of torispherical geometries and presented their results in the form of design curves (7). These curves were restricted to diameter-to-thickness ( $D/t$ ) ratios which were less than 500, as it was thought that buckling might occur for torispheres having  $D/t > 500$  (it is now known that circumferential buckling can occur in some torispheres which have  $D/t < 500$ ). Drucker and Shield did not investigate the buckling problem.

Nowadays, there are several sophisticated shell buckling computer programs available and, in principle, one can compute (for perfect torispheres) the internal buckling pressures  $p_{cr}$  and the axisymmetric collapse (yielding) pressures  $p_c$ . The problem is non-linear, both geometrically and materially, and, when calculating the internal buckling pressures (for which both the pressure  $p$  and the number of circumferential waves at buckling have to be estimated), the solutions can sometimes be rather time consuming to obtain. Nevertheless, some numerical solutions for both  $p_{cr}$  and  $p_c$ , for torispherical shells with  $D/t$  ratios in the range  $500 < D/t < 1500$ , were published in the literature several years ago (8-10); similar solutions for 2:1 ellipsoidal shells were given in (11-13).

As there are two possible static failure modes for

torispheres under internal pressure (corresponding to  $p_{cr}$  or  $p_c$ ), a designer will need to know which of the two is the lower, as it will be the controlling one. A few approximate controlling failure mode curves have been given before for perfect torispheres (14, 15) but more accurate ones need to be determined.

With regard to Code rules, there are, as yet, no design rules for the prevention of internal pressure buckling of torispherical shells in either the British (BS 5500) or American (ASME) Codes. Work on the problem is under way, but residual stresses, strain-hardening, etc. [see (15)] complicate the issue. Some possible design equations for preventing buckling in internally pressurized torispheres having  $D/t > 500$  have been discussed within the British Standards Institution (BSI) already. These equations were compared with all known test results on internal pressure buckling of fabricated torispheres (mainly for  $D/t > 450$ ) and seem quite satisfactory (15). However, when the proposed buckling rules were compared with the provisions of BS 5500, at the maximum value of  $D/t$  allowed by the Code (that is  $D/t = 500$ ), it was found that, in many cases, the buckling rules would have permitted smaller shell thicknesses than would have been allowed by the Code.

It was, therefore, decided to extend the earlier calculations (8, 9) to lower values of  $D/t$  and more values of  $\sigma_{yp}$ . It is clearly of interest to resolve the above anomaly, both from the scientific and economic points of view.

## 2 OBJECTIVES AND SCOPE OF THE PRESENT STUDY

The primary aims of the present study on perfect torispheres under internal pressure are:

- (a) to determine, over the range  $300 < D/t < 1500$ , when plastic buckling controls the failure mode and when axisymmetric yielding controls it,

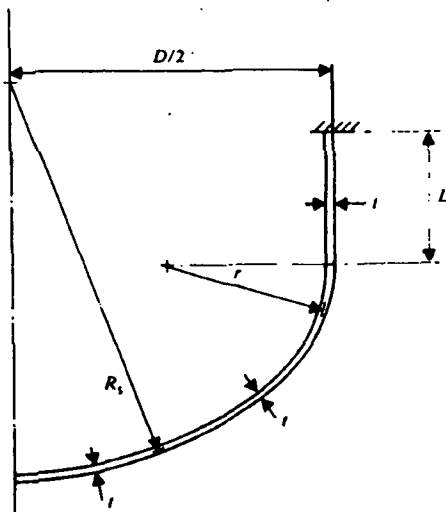


Fig. 2 Torispherical shells considered in computer analyses

- (b) to resolve the discrepancy, mentioned in the previous section, between the limit pressure predictions and the buckling predictions at  $D/t = 500$  and
- (c) to derive simple approximate equations for  $p_c$  and  $p_{cr}$  which will be of assistance to designers and to Code-writing bodies.

The range of the torispherical shell parameters investigated in the study were as follows (see Fig. 2):

Geometric	$\left\{ \begin{array}{l} R_s/D = 1.0 \text{ and } 0.8 \\ r/D = 0.05-0.20 \\ D/t = 300-1500 \end{array} \right.$	
Material		$\left\{ \begin{array}{l} \sigma_{yp} = 207 \text{ N/mm}^2, 310 \text{ N/mm}^2 \text{ and } 414 \text{ N/mm}^2 \\ E = 207\,000 \text{ N/mm}^2 \end{array} \right.$

The material of the shell wall was taken to be elastic, perfectly plastic and the finite-deflection BOSOR 5 program (16) was used to determine the values of  $p_c$  and  $p_{cr}$ . Although not considered in this paper, materials which strain-harden can be handled by BOSOR 5. The strain-hardening is assumed to be isotropic and the von Mises yield criterion is used. Some calculations on torispheres incorporating strain-hardening are given in (8, 9).

A sketch of the torispherical shells employed in the analyses appears in Fig. 2. As may be seen, the thicknesses of the spherical cap, the torus and the cylinder are the same and are constant throughout. This is not always the case in practice, of course. The  $L/D$  ratio used in all the calculations was 1.0.

With regard to the structural design problems of actual welded torispheres in practice (as opposed to perfect ones), these will be discussed in a companion paper.

### 3 BRIEF RÉSUMÉ OF PREVIOUS WORK

#### 3.1 Circumferential buckling

The first theoretical solution for the buckling of perfect internally pressurized torispheres appears to be that

given in 1962 by Mescall (4) of Watertown Arsenal. He became interested in the problem after the failure of the vessel in Avon, California, and the prediction of buckling in (2). His solution was a small-deflection elastic one, obtained with the aid of the Rayleigh-Ritz method. An elastic finite-deflection numerical solution of the problem was given a few years later by Thurston and Holston (17). Brown and Kraus (18) discussed the internal pressure buckling of the related ellipsoidal shells and, in 1976, Bushnell published his shell buckling computer program BOSOR 5 (16). With the availability of this program, it became possible to solve elastic-plastic buckling problems of perfect shells of revolution incorporating finite deflections. The BOSOR 5 program has been used in several investigations of internally pressurized torispheres, for example (8-10, 19-22). Nowadays, there are some finite element programs which will also solve the problem, for example (23, 24).

Some simple equations for the internal plastic buckling pressures  $p_{cr}$ , which were derived from the BOSOR 5 computer results were suggested in 1979 by Galletly and Radhamohan (8). However, the lowest value of  $D/t$  considered in that investigation was 500 and the main value of  $\sigma_{yp}$  investigated was the relatively low one of 207 N/mm<sup>2</sup>. The elastic internal buckling pressures of internally pressurized torispheres and the pressures at which first yielding occurred were also determined by Aylward and Galletly and are given in (13). Some additional results for the plastic buckling pressures  $p_{cr}$  were given in a recent publication of the Liverpool group (25) and the problem is under study in Germany (24), France (26), Austria (27), the United States (28) and Sweden.

In addition to the numerical computer studies, some small-scale experimental work has been carried out on 0.14 m diameter machined torispherical shells under internal pressure at Manchester (29, 30) and Liverpool (31, 32). These tests will be discussed briefly later.

#### 3.2 Axisymmetric yielding

As mentioned earlier, the pioneering work on the limit pressures of internally pressurized torispheres was done by Drucker and Shield in the early 1960s. In the decade that followed, several elastic-plastic finite element programs appeared which enabled the elastic-plastic stress analysis (but not the buckling analysis) of perfect shells to be undertaken. One such investigation, applied to ASME standard torispherical heads, was carried out by Popov, Khojasteh-Bakht and Sharifi (33). Using the small-deflection theory of shells, and assuming an elastic, perfectly plastic steel, they confirmed the conclusions of Galletly and Drucker-Shield on this problem. They were also able to follow the development of plastic zones through the thickness of the shell and to make reasonably accurate plots of the load-deflection behaviour of the shell. In all the cases investigated by them, yielding began at the inner face of the toroidal knuckle and, with increasing internal pressure, propagated along and across the thickness of the wall. At a load level which varied between 1.5 and 2.0 times the elastic load limit, a single hinge circle formed in the torus.

One of the problems encountered in their analysis was how the collapse load should be defined, since the load-deflection curve keeps rising (even though at a

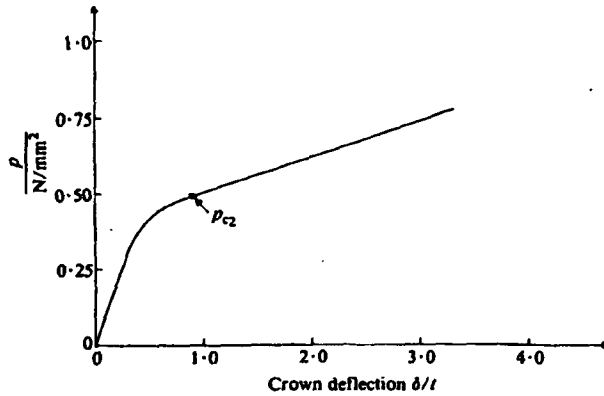


Fig. 3 Crown deflection versus internal pressure for a torispherical shell ( $D/t = 300$ ,  $R_s/D = 1.0$ ,  $r/D = 0.06$ ,  $\sigma_{yp} = 207 \text{ N/mm}^2$ )

reduced rate); see Fig. 3. Gerdeen (34) has discussed various possible solutions to this problem and two of the possibilities will be used in this paper. These are outlined in the next section.

The next step was to include finite deflections in the analysis and this was done by several investigators. The BOSOR 5 computer program was one of these programs and was the one used by Radhamohan and Galletty (9) to calculate the axisymmetric  $p_c$  values for some torispherical geometries.

Experimental information on the finite-deflection axisymmetric yielding pressures is rather sparse, particularly in the region  $300 < D/t < 600$ , where some circumferential buckling failures can occur. The few tests reported in the literature are discussed in (9).

#### 4 DEFINITIONS OF $p_{c1}$ AND $p_{c2}$ USED IN THE PAPER

A detailed description of the BOSOR 5 program is available in Bushnell (16). It is a variational finite-difference program; earlier versions of the method, as applied to shells, appeared independently in (35) for buckling and vibrations and in (36) for vibrations. The BOSOR 5 program has been used by a number of investigators on many different problems (37) and it is accepted in the profession as being reasonably accurate.

When BOSOR 5 is used for plastic stress analyses, any strain-hardening which occurs is assumed to be isotropic. With plastic buckling analyses, flow (incremental) theory is used for the prebuckling phase and, in the bifurcation buckling phase, one can select either the flow or the deformation theory of plasticity. However, the shear modulus used in the flow theory for the buckling phase is that corresponding to deformation theory. Bushnell's reason for incorporating this modification into his program was to eliminate much of the discrepancy between the flow and the deformation theories in buckling predictions [see (38)].

The practical effect of having two buckling options in BOSOR 5 is that one can usually obtain two predictions for  $p_{c1}$ , with the one from deformation theory being the lower. In addition, sometimes a prediction of buckling is obtained when the deformation theory is used but not when the flow theory is used (examples

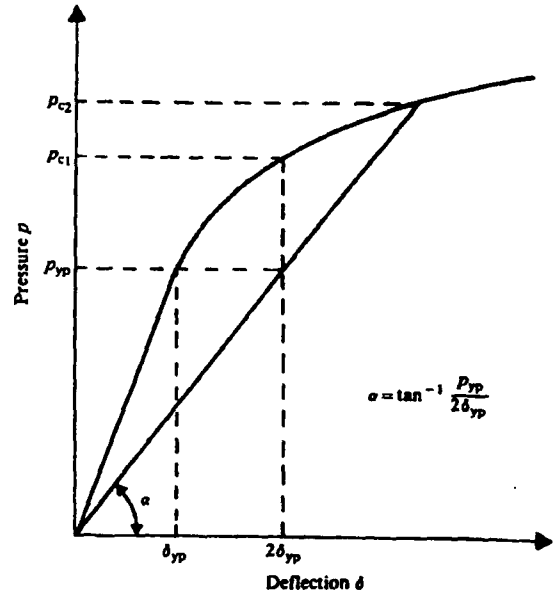


Fig. 4 Definition of the axisymmetric yielding pressures  $p_{c1}$  and  $p_{c2}$  used in the paper

will be given later). These points were noted in (20). The flow theory (modified) predictions are presumably more correct than the deformation theory ones but there is very little experimental evidence on shells available on this point.

With regard to the determination of the axisymmetric yielding pressure  $p_c$ , a typical plot of internal pressure  $p$  versus the crown deflection  $\delta$  of a torispherical shell is shown in Fig. 3. Even though elastic, perfectly plastic (no strain-hardening) materials are being considered, the knee of the  $p$ - $\delta$  curve will be rounded, as shown in Fig. 3 (it is assumed that buckling does not occur for these cases). As may be seen, there is no pressure which could definitely be called the collapse pressure. The two definitions used in this paper for the axisymmetric yielding pressure  $p_c$  are shown in Fig. 4. They are:

- $p_{c1}$ , which is the internal pressure at which the crown deflection reaches twice the yield point deflection, that is  $\delta = 2\delta_{yp}$ , and
- $p_{c2}$ , which is the internal pressure at which a line drawn from the origin and having a slope of  $\alpha$  meets the  $p$ - $\delta$  curve.

The above definitions of  $p_c$  were used in (9, 12) and were suggested by Gerdeen, who studied various definitions of collapse in (34). As may be seen, the definitions of  $p_c$  given above are somewhat arbitrary; they also underestimate the collapse pressure.

In determining the  $p_c$  values which are given later in the paper, the values of  $\delta$  corresponding to a given internal pressure were found from the finite-deflection BOSOR 5 program. The  $p$ - $\delta$  curves were then drawn using increments of pressure, and yield was assumed to have occurred when the deflections started to increase substantially.

With regard to the development of plastic zones in the shell at  $p = p_{c2}$ , two sample torispherical shells were

considered. Both of them had  $R_p/D = 1.0$  and  $\sigma_{yp} = 207$  N/mm<sup>2</sup> and the other geometric ratios were  $r/D = 0.06$ ,  $D/t = 300$  and  $r/D = 0.10$ ,  $D/t = 500$ . In both cases, the plastic zones propagated right across the shell thickness but, at these pressure levels, only a single hinge circle had formed.

### 5 EXPERIMENTS ON 'NEAR-PERFECT' INTERNALLY PRESSURIZED TORISPHERICAL SHELLS

Torispherical shells in practice contain residual stresses (due to the welding and/or forming operations) and initial shape imperfections; also, if they are cold-spun from austenitic stainless steel, their stress-strain curves will, due to strain-hardening, be considerably different from those of the 'as-received' plate material. In consequence, tests on fabricated torispheres are not very suitable when one is attempting to assess the adequacy of any theoretical treatment of the buckling of perfect torispheres.

However, some small (0.137 m diameter) machined 'near-perfect' torispheres have been made at UMIST and the University of Liverpool. Most of the models were machined from 0.15 m diameter solid billets of an aluminium alloy and had a wall thickness of  $\frac{1}{2}$  mm ( $D/t$  was about 540). Some mild steel models were also made and some models had  $\frac{1}{4}$  mm wall thickness. Unfortunately, it was not possible to achieve a reasonably constant thickness in the hoop direction with the  $\frac{1}{4}$  mm thick models.

The UMIST tests (29, 30) have been analysed by Lagae and Bushnell (21) using the BOSOR 5 program. The overall agreement was reasonably good, the ratio  $P_{exp}/P_{theo}$  varying from 0.82 to 1.05. The experimental/theoretical ratios found in the Liverpool tests on aluminium alloy models (31, 32) were broadly similar (that is 0.90-0.98), although higher values were found for some mild steel models.

Even though the above agreement between experiment and theory is quite good, it should be noted that

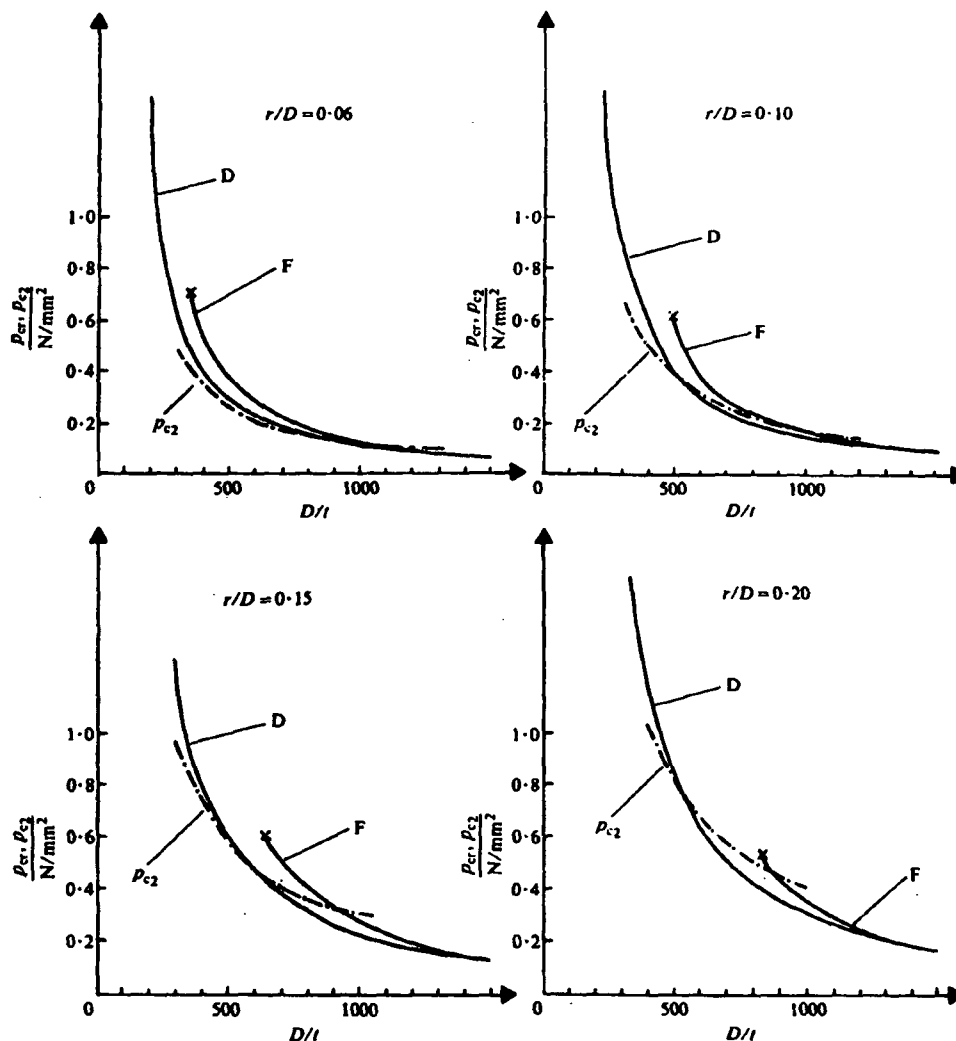


Fig. 5 Curves of  $p_{er}$  (F = flow theory, D = deformation theory) and  $p_{c2}$  for internally pressurized torispheres ( $R_p/D = 1.0$ ,  $\sigma_{yp} = 207$  N/mm<sup>2</sup>)

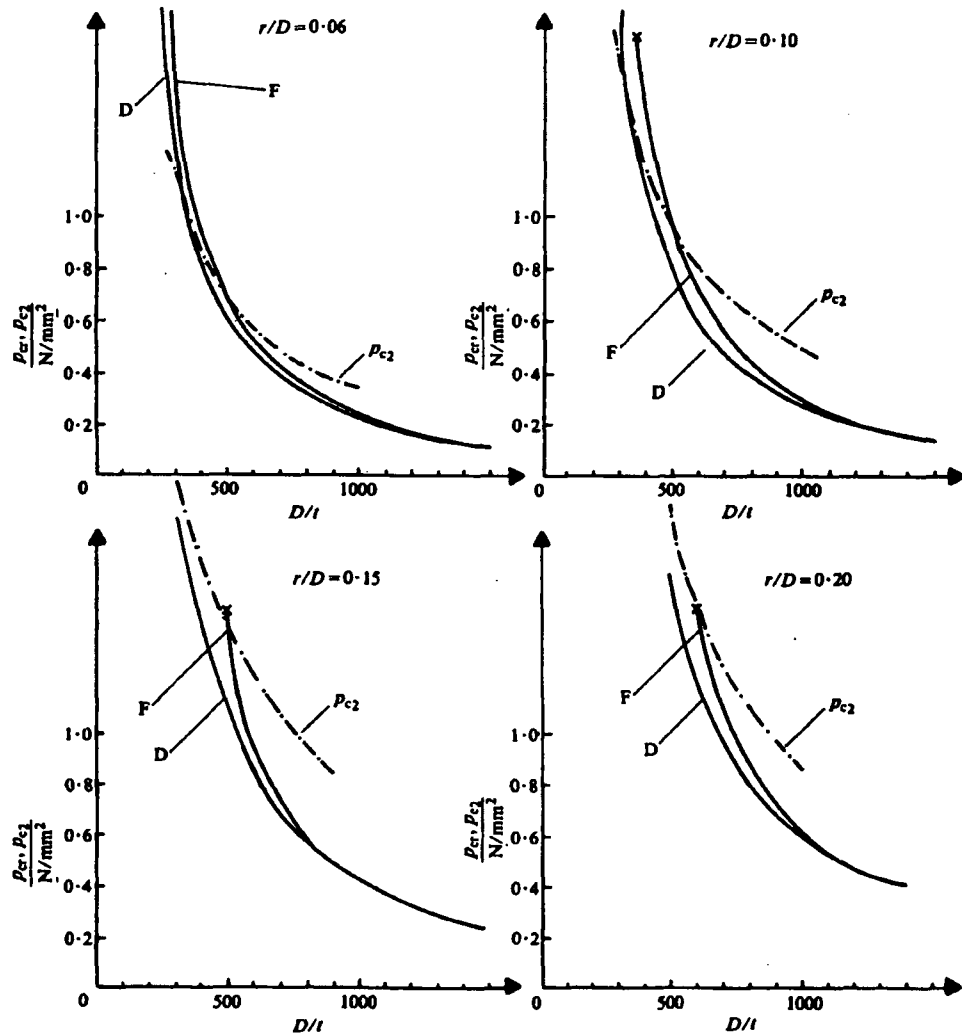


Fig. 6 Curves of  $p_{cr}$  (F = flow theory, D = deformation theory) and  $p_{c2}$  for internally pressurized torispheres ( $R_j/D = 1.0$ ,  $\sigma_{yp} = 414 \text{ N/mm}^2$ )

the number of tests which have been conducted to date on near-perfect models is quite small. In the main, only aluminium alloy models having  $D/t \approx 540$  and  $R_j/D = 1.0$  have been investigated, with  $\sigma_{yp} \approx 310 \text{ N/mm}^2$ .

## 6 NUMERICAL RESULTS FOR PERFECT TORISPHERES

The BOSOR 5 finite-deflection computer program was employed to obtain the numerical results in this section. It would be useful to have an independent check of some of these results using one of the finite element programs which are available. However, the only cross-checks known to the authors are those carried out by Wunderlich (39).

### 6.1 Unsymmetric plastic buckling

Numerical values of the internal buckling pressures,  $p_{cr}/\sigma_{yp}$ , for perfect steel torispherical shells are given in

Table 1 for  $R_j/D = 1.0$  and Table 2 for  $R_j/D = 0.8$ . Both the deformation and the flow theories of plasticity were used in the calculations (as noted before, the flow theory option in BOSOR 5 uses the deformation theory shear modulus in the bifurcation buckling calculations). The plastic buckling results for  $R_j/D = 1.0$  are also shown graphically in Figs 5 and 6 for  $\sigma_{yp} = 207$  and  $414 \text{ N/mm}^2$  respectively (on these figures, D = deformation theory and F = flow theory).

From the tables and figures it may be seen that:

1. The internal buckling pressures predicted by deformation theory are less than, or equal to, those predicted by flow theory (this is the usual situation with the two plasticity theories).
2. For some values of the geometric parameters and  $\sigma_{yp}$ , buckling is predicted by the deformation theory whereas flow theory does not predict any buckling.
3. The values of  $p_{cr}/\sigma_{yp}$  predicted by the deformation theory are not, over the range of yield points studied,

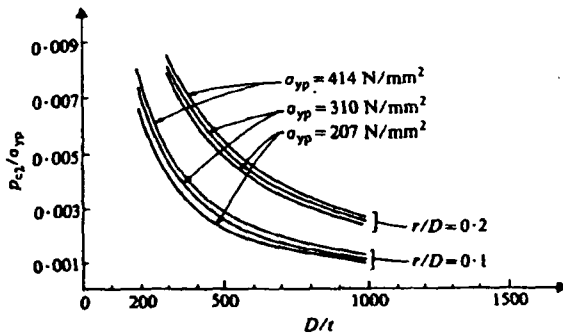


Fig. 7 The variation of  $p_{cr}/\sigma_{yp}$  with  $\sigma_{yp}$  for two values of  $r/D$  ( $R_j/D = 1.0$ )

very sensitive to the value of  $\sigma_{yp}$  chosen in the calculations. With the flow theory predictions, the values of  $p_{cr}/\sigma_{yp}$  vary slightly with  $\sigma_{yp}$ , with the higher  $\sigma_{yp}$  values giving the lower values of  $p_{cr}/\sigma_{yp}$ .

## 6.2 Axisymmetric yielding mode

Two values of the axisymmetric yielding pressure were calculated for all the torispheres investigated. These were designated  $p_{c1}$  and  $p_{c2}$  (see Fig. 4) and the values obtained from BOSOR 5 are given in Tables 3 and 4. From these tables it may be noted that  $p_{c1} > p_{c2}$  (as it should) and both  $p_{c1}/\sigma_{yp}$  and  $p_{c2}/\sigma_{yp}$  are slightly dependent on the value of  $\sigma_{yp}$ . As an example, Fig. 7 shows how  $p_{c2}/\sigma_{yp}$  varies with  $D/t$  and  $\sigma_{yp}$  for shells having  $R_j/D = 1.0$ ,  $r/D = 0.10$  and  $0.20$ . As may be seen, the lowest values of  $p_{c2}/\sigma_{yp}$  occur with the lowest value of  $\sigma_{yp}$ .

The theoretical internal pressure-crown deflection curve for a torisphere having  $R_j/D = 1.0$ ,  $r/D = 0.06$ ,  $D/t = 300$  and  $\sigma_{yp} = 207 \text{ N/mm}^2$  is shown in Fig. 3 and the pressure  $p_{c2}$  is marked on the curve. It may be observed that  $p_{c2}$  is well below the failure pressure. Also, at this pressure level, it can be shown that only one plastic zone has propagated through the shell thickness.

## 6.3 Axisymmetric yielding ( $p_{c2}$ ) or asymmetric plastic buckling ( $p_{cr}$ )

The  $p_{c2}$  curves have been plotted with the plastic buckling curves in Figs 5 and 6. The intersection of the  $p_{c2}$  curve with the  $p_{cr}$  curves indicates the approximate transition between the axisymmetric yielding mode and the plastic buckling mode. As is evident, the  $D/t$  values at which the transition in failure mode occurs depends on  $\sigma_{yp}$  and the geometry of the torispherical shell. The transitional values of  $D/t$  also depend on whether the flow or deformation theory values of  $p_{cr}$  are employed in the analysis. In what follows, the deformation theory values of  $p_{cr}$  will be chosen, as they are always lower than the flow theory values. As may be seen from Figs 5 and 6, this will mean that the failure mode is not always predicted correctly (the flow theory values of  $p_{cr}$  could, of course, be used if this should prove desirable).

## 6.4 The controlling failure pressure curves

As has been discussed, a torispherical shell subjected to internal pressure can fail by asymmetric buckling ( $p_{cr}$ )

Table 1 Values of  $p_{cr}/\sigma_{yp} \times 10^3$  for steel internally pressurized torispheres having  $R_j/D = 1.0$

$D/t$	Deformation theory			Flow theory		
	207	310	414	207	310	414
$r/D = 0.06$						
1500	0.30	0.29(109)	0.28	0.33	0.32(98)	0.29
1200	0.43	0.40(97)	0.38	0.47	0.44(85)	0.43
1000	0.53	0.53(86)	0.52	0.57	0.58(73)	0.58
800	0.73	0.71(60)	0.70	0.83	0.80(60)	0.78
600	1.07	1.09(59)	1.10	1.23	1.16(49)	1.23
500	1.40	1.42(49)	1.47	1.73	1.60(43)	1.57
400	1.93	2.00(44)	2.00	2.53	2.31(34)	2.23
300	3.10	3.1 (34)	3.27	NB	4.18(25)	3.87
$r/D = 0.10$						
1500	0.42	0.41(76)	0.40	0.45	0.40(75)	0.40
1200	0.57	0.52(69)	0.53	0.62	0.58(65)	0.53
1000	0.73	0.71(61)	0.68	0.83	0.78(61)	0.72
800	1.00	0.98(56)	0.95	1.20	1.04(52)	1.03
600	1.53	1.47(46)	1.47	1.87	1.87(33)	1.82
500	2.00	1.96(41)	1.95	2.93	2.44(28)	2.35
400	2.80	2.76(34)	2.75	NB	3.96(21)	3.63
300	4.37	4.36(27)	4.37	NB	NB	NB
$r/D = 0.15$						
1500	0.60	0.60(60)	0.58	0.63	0.60(69)	0.62
1200	0.83	0.80(49)	0.80	0.93	0.80(49)	0.80
1000	1.07	1.02(42)	1.00	1.25	1.07(39)	1.00
800	1.47	1.42(37)	1.37	1.70	1.56(37)	1.43
600	2.27	2.13(33)	2.08	NB	2.80(21)	2.27
500	2.87	2.76(29)	2.67	NB	NB	3.53
400	3.93	3.78(25)	3.73	NB	NB	NB
300	6.20	6.04(20)	6.00	NB	NB	NB
$r/D = 0.20$						
1500	0.82	0.87(57)	0.88	0.83	0.88(60)	0.88
1200	1.15	1.11(43)	1.17	1.23	1.11(40)	1.17
1000	1.47	1.42(33)	1.43	1.73	1.47(30)	1.43
800	2.07	1.96(27)	1.93	NB	2.27(25)	2.03
600	3.10	3.04(23)	3.05	NB	NB	3.52
500	4.00	3.96(21)	3.90	NB	NB	NB
400	5.93	5.71(18)	5.60	NB	NB	NB
300	NB	NB	NB	NB	NB	NB

### Notes

- Numbers in parentheses are the predicted number of circumferential waves at buckling. They are shown only for  $\sigma_{yp} = 310 \text{ N/mm}^2$ .
- NB = no buckling found.

or axisymmetric yielding ( $p_c$ ). The mode which occurs will be the one which has the lower failure pressure; that is, this will be the controlling one. From the values given in Tables 1 to 4, it is possible to construct the controlling failure pressure curves for the various values of  $r/D$ . Figures 8 and 9 show these normalized curves for  $R_j/D = 1.0$  and  $\sigma_{yp} = 207$  and  $414 \text{ N/mm}^2$  (for the  $p_{cr}$  curves, the averages of the deformation theory values given in Table 1 were used). The approximate location of the transition in the failure mode is shown by vertical arrows on the curves; the arrow pointing downwards refers to the  $\sigma_{yp} = 414 \text{ N/mm}^2$  curve while the upwards-pointing arrow refers to the  $\sigma_{yp} = 207 \text{ N/mm}^2$  curve. To the right of any arrow plastic buckling is the failure mode which will occur, whereas axisymmetric yielding occurs to the left of it. As may be seen, an increase in  $\sigma_{yp}$  moves the transitional  $D/t$  to the left. This is, of course, what one would expect.

From these curves for  $R_j/D = 1.0$ , it may be observed that the effect of  $\sigma_{yp}$  is not very pronounced and also

Table 2 Values of  $p_{cr}/\sigma_{yp} \times 10^3$  for steel internally pressurized torispheres having  $R_1/D = 0.8$

D/t	$\sigma_{yp}$ N/mm <sup>2</sup>	Deformation theory			Flow theory		
		207	310	414	207	310	414
<i>r/D = 0.05</i>							
1500	0.35	0.34(129)	0.33	0.38	0.37(90)	0.38	
1300	0.43	0.42(125)	0.42	0.45	0.47(87)	0.45	
1000	0.60	0.62(99)	0.62	0.63	0.62(75)	0.65	
800	0.80	0.87(81)	0.85	0.93	0.89(66)	0.93	
600	1.27	1.29(65)	1.30	1.60	1.42(51)	1.42	
500	1.73	1.76(54)	1.88	2.20	2.04(45)	2.00	
400	2.40	2.40(46)	2.48	NB	NB	NB	
300	3.93	3.91(37)	3.98	NB	NB	NB	
<i>r/D = 0.10</i>							
1500	0.53	0.51(101)	0.51	0.53	0.51(84)	0.51	
1300	0.63	0.60(77)	0.61	0.66	0.62(64)	0.63	
1000	0.93	0.88(62)	0.90	1.20	1.02(53)	1.13	
800	1.26	1.24(51)	1.26	1.80	1.60(38)	1.50	
600	2.00	1.91(46)	1.90	NB	NB	NB	
500	2.60	2.58(39)	2.55	NB	NB	NB	
400	3.67	3.69(33)	3.63	NB	NB	NB	
300	6.00	5.91(26)	5.87	NB	NB	NB	
<i>r/D = 0.15</i>							
1500	0.80	0.80(72)	0.80	0.93	0.85(72)	0.83	
1300	0.96	0.93(67)	0.96	1.00	0.97(50)	0.96	
1000	1.30	1.33(42)	1.30	1.46	1.33(41)	1.30	
800	1.80	1.77(36)	1.73	1.93	1.91(33)	1.87	
600	2.67	2.62(30)	2.57	NB	NB	NB	
500	3.46	3.38(27)	3.38	NB	NB	NB	
400	5.00	4.89(23)	4.77	NB	NB	NB	
300	NB	NB	NB	NB	NB	NB	
<i>r/D = 0.20</i>							
1500	1.15	1.17(56)	1.16	1.06	1.02(55)	1.06	
1300	1.40	1.37(45)	1.43	1.50	1.37(44)	1.43	
1000	2.00	1.91(31)	1.91	2.20	1.95(30)	1.91	
800	2.53	2.56(26)	2.50	NB	2.84(24)	2.63	
600	3.93	3.85(23)	3.86	NB	NB	NB	
500	4.93	4.89(20)	4.83	NB	NB	NB	
400	NB	NB	NB	NB	NB	NB	
300	NB	NB	NB	NB	NB	NB	

Notes

- Numbers in parentheses are the predicted number of circumferential waves at buckling. They are shown only for  $\sigma_{yp} = 310$  N/mm<sup>2</sup>.
- NB - no buckling found.

that plastic buckling occurs for  $D/t > 400$  and most values of  $r/D$  when  $\sigma_{yp} = 414$  N/mm<sup>2</sup>. Whereas, for  $\sigma_{yp} = 207$  N/mm<sup>2</sup>, axisymmetric yielding occurs for  $D/t < 800$  when  $r/D = 0.06$  and for  $D/t < 500$  when  $r/D = 0.20$ . For  $D/t > 800$ , plastic buckling is the controlling failure mode for both values of  $\sigma_{yp}$  and all four values of  $r/D$ .

The situation with respect to the normalized controlling failure pressure curves for  $R_1/D = 0.8$  is broadly similar to that for  $R_1/D = 1.0$ .

7 A COMPARISON OF THE DRUCKER-SHIELD LIMIT PRESSURES WITH THE CONTROLLING FAILURE PRESSURES

The Drucker-Shield limit pressures ( $p_{DS}$ ) for torispherical shells were published more than twenty years ago (7) and were obtained using small-deflection shell theory and limit analysis techniques. However, in the last

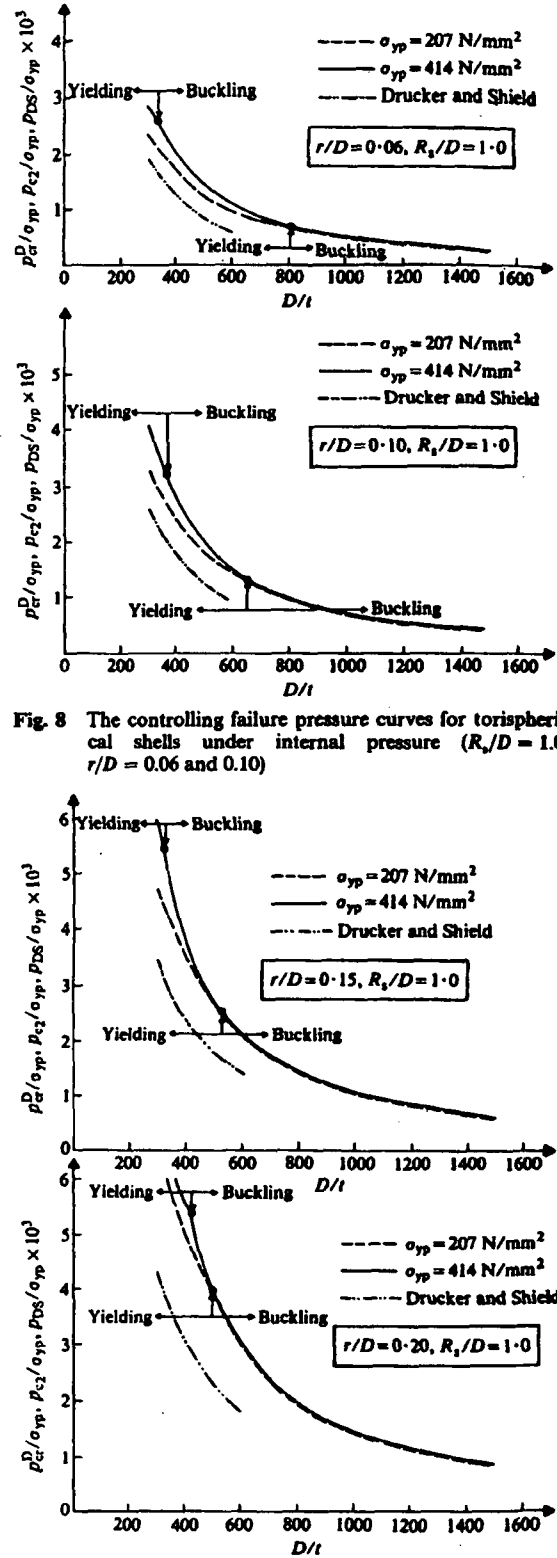


Fig. 8 The controlling failure pressure curves for torispherical shells under internal pressure ( $R_1/D = 1.0$ ,  $r/D = 0.06$  and  $0.10$ )

Fig. 9 The controlling failure pressure curves for torispherical shells under internal pressure ( $R_1/D = 1.0$ ,  $r/D = 0.15$  and  $0.20$ )

**Table 3** Axisymmetric yielding ( $R_0/D = 1.0$ ). Values of  $p_{c1}/\sigma_{yp}$  ( $\times 10^3$ ) and  $p_{c2}/\sigma_{yp}$  ( $\times 10^3$ ) for steel internally pressurized torispherical shells

$D/t$	$\sigma_{yp} = 207 \text{ N/mm}^2$		$\sigma_{yp} = 310 \text{ N/mm}^2$		$\sigma_{yp} = 414 \text{ N/mm}^2$	
	$p_{c1}/\sigma_{yp}$	$p_{c2}/\sigma_{yp}$	$p_{c1}/\sigma_{yp}$	$p_{c2}/\sigma_{yp}$	$p_{c1}/\sigma_{yp}$	$p_{c2}/\sigma_{yp}$
$r/D = 0.06$						
900	0.57	0.60	0.58	0.71	0.67	0.88
700	0.73	0.80	0.80	0.93	0.85	1.08
500	1.13	1.23	1.18	1.4	1.30	1.65
300	2.07	2.33	2.22	2.58	2.35	2.82
$r/D = 0.10$						
900	0.80	0.95	0.90	1.10	1.05	1.34
700	1.13	1.23	1.20	1.42	1.33	1.68
500	1.67	1.80	1.80	2.07	1.87	2.35
300	2.93	3.27	2.89	3.51	3.33	4.10
$r/D = 0.15$						
990	1.20	1.53	1.38	1.78	1.63	2.00
700	1.53	1.93	1.82	2.33	2.00	2.57
500	2.40	2.73	2.76	3.20	3.00	3.43
300	4.07	4.73	4.40	5.29	4.87	5.93
$r/D = 0.20$						
900	1.90	2.17	2.02	2.33	2.23	2.40
700	2.33	2.77	2.71	3.02	2.87	3.03
500	3.47	3.93	3.78	4.22	4.07	4.50
300	5.50	6.80	5.75	7.30	6.10	7.60

**Table 4** Axisymmetric yielding ( $R_0/D = 0.8$ ). Values of  $p_{c1}/\sigma_{yp}$  ( $\times 10^3$ ) and  $p_{c2}/\sigma_{yp}$  ( $\times 10^3$ ) for steel internally pressurized torispherical shells

$D/t$	$\sigma_{yp} = 207 \text{ N/mm}^2$		$\sigma_{yp} = 310 \text{ N/mm}^2$		$\sigma_{yp} = 414 \text{ N/mm}^2$	
	$p_{c1}/\sigma_{yp}$	$p_{c2}/\sigma_{yp}$	$p_{c1}/\sigma_{yp}$	$p_{c2}/\sigma_{yp}$	$p_{c1}/\sigma_{yp}$	$p_{c2}/\sigma_{yp}$
$r/D = 0.05$						
900	0.62	0.70	0.80	0.72	0.73	1.07
700	0.73	0.93	0.96	1.18	0.98	1.32
500	1.17	1.40	1.29	1.58	1.37	1.75
300	2.07	2.73	2.40	3.07	2.63	3.27
$r/D = 0.10$						
1000	0.83	0.97	0.93	1.11	1.05	1.30
800	1.20	1.33	1.24	1.47	1.38	1.72
600	1.60	1.83	1.69	2.04	1.87	2.33
400	2.66	2.90	2.86	3.24	3.00	3.77
200	5.73	6.66	5.91	7.38	6.73	8.07
$r/D = 0.15$						
1000	1.46	1.70	1.58	1.84	1.76	2.08
800	1.86	2.00	2.00	2.31	2.23	2.60
600	2.47	2.73	2.66	3.20	2.96	3.50
400	3.87	4.27	3.91	4.71	4.46	5.20
200	8.00	9.07	8.44	9.68	9.40	10.6
$r/D = 0.20$						
600	3.47	4.07	3.69	4.20	4.10	4.40
500	4.13	4.80	4.51	5.0	4.95	5.30
400	5.47	6.13	5.60	6.33	6.33	6.67
300	7.33	8.0	7.56	8.18	8.13	8.53

Table 5 A comparison of  $p_{cs}/\sigma_{yp}$ ,  $p_{cs}^D/\sigma_{yp}$  and  $p_{DS}/\sigma_{yp}$  ( $\times 10^3$ ) for internally pressurized steel torispherical shells over the range  $300 < D/t < 600$

D/t	300			400			500			600		
	$p_{cs}/\sigma_{yp}$	$p_{cs}^D/\sigma_{yp}$	$p_{DS}/\sigma_{yp}$									
$R/D = 1.0$												
0.06	2.33*			1.70			1.23			0.97		
	2.58	3.12	1.87	1.84	1.98	1.25	1.40	1.43	0.82	1.11	1.09	0.60
	2.82			2.17			1.65			1.30		
0.10	3.27			2.37			1.80			1.43		
	3.51	4.37	2.57	2.62	2.77	1.74	2.07	1.97	1.25	1.71	1.49	0.93
	4.10			2.90			2.35			1.97		
0.15	4.73			3.57			2.73			2.27		
	5.29	6.08	3.46	3.91	3.81	2.41	3.20	2.77	1.79	2.71	2.16	1.38
	5.93			4.43			3.43			2.83		
0.20	6.80			5.00			3.93			3.20		
	7.30	NB	4.29	5.29	5.75	3.07	4.22	3.95	2.32	3.42	3.06	1.83
	7.60			5.55			4.50			3.60		
$R/D = 0.8$												
0.05	2.73			1.93			1.40			1.10		
	3.07	3.93	2.27	2.09	2.43	1.48	1.58	1.78	1.03	1.29	1.29	0.75
	3.27			2.47			1.85			1.50		
0.10	4.30			2.90			2.2			1.83		
	4.80	5.93	3.37	3.24	3.66	2.32	2.5	2.58	1.71	2.04	1.91	1.31
	5.20			3.77			2.8			2.33		
0.15	5.9			4.27			3.3			2.73		
	6.7	NB	4.47	4.71	4.87	3.16	3.8	3.41	2.38	3.2	2.62	1.88
	7.5			5.20			4.2			3.5		
0.20	8.10			6.13			4.8			4.07		
	8.18	NB	5.51	6.33	NB	3.99	5.0	4.88	3.05	4.2	3.89	2.44
	8.53			6.67			5.3			4.4		

\* Three values are shown for  $p_{cs}/\sigma_{yp}$ , corresponding to  $\sigma_{yp} = 207, 310$  and  $414$  N/mm<sup>2</sup>. NB = no buckling found.

decade, several authors have used large-deflection shell theories to analyse torispherical shells. Due to the changes in shape which occur under pressure, the torispheres are stronger than predicted by linear theories. Several authors [for example (31)] have noted that some of the Drucker-Shield limit pressures are lower than the corresponding axisymmetric yielding pressures obtained from finite-deflection shell theories.

Since several national pressure vessel Codes (for example the American, the British, the French) incorporate the Drucker-Shield limit pressures in their regulations for torispherical shells, it is of considerable interest to know how conservative the limit pressures are. In consequence, they were determined over the range  $300 < D/t < 600$ , using equation (25) of (7) with  $n = 1$ . The  $p_{DS}$  values thus found are approximately  $\frac{1}{2}(p^u + p^l)$ , where  $p^u$  and  $p^l$  are the upper and lower bounds to the limit pressures. The values of  $p_{DS}/\sigma_{yp}$  do not depend on  $\sigma_{yp}$ .

The values of  $p_{DS}$  are given in Table 5 (Drucker and Shield actually limited their analysis to  $D/t = 500$ ). In addition, three values of the finite-deflection axisymmetric yielding pressure ( $p_{cs}/\sigma_{yp}$ ) are given for each torisphere. The upper value is for  $\sigma_{yp} = 207$  N/mm<sup>2</sup>, the middle one for  $\sigma_{yp} = 310$  N/mm<sup>2</sup> and the lower one for  $414$  N/mm<sup>2</sup>. The values of  $p_{cs}$  in Table 5 are the averages of the deformation theory values in Tables 1 and 2 and they are denoted by  $p_{cs}^D$ .

Comparing the various quantities in Table 5, it may be seen that:

1. All the Drucker-Shield limit pressures ( $p_{DS}$ ) are lower than their corresponding  $p_{cs}$  values.
2. All the  $p_{DS}$  values are lower than their corresponding plastic buckling pressures found from deformation theory, that is  $p_{cs}^D$ .
3. From 1 and 2 the lowest predicted failure pressures for all the shells in Table 5 are the  $p_{DS}$  values. However, this predicted failure mode cannot always be correct, as the controlling failure mode is plastic buckling for several of the shells in Table 5 when  $\sigma_{yp} = 414$  N/mm<sup>2</sup>. Some experimental results on shells which failed by buckling and had  $D/t$  ratios in the range  $350 < D/t < 500$  (40) tend to support this observation.

The Drucker-Shield limit pressures have also been plotted on Figs 8 and 9 and it is again clear that the  $p_{DS}$  values are always lower than the controlling failure pressures. The ratios between the two vary with  $\sigma_{yp}$  and the geometric parameters, and some values are listed in Table 6. As the values given for  $D/t = 500$  vary between 1.2 and 1.8, this means that the shell thicknesses calculated from the limit pressures (on which the relevant section in BS 5500 is based in part) will be greater than those found from the buckling rules (41). Hence, a mismatch in the required thicknesses will occur unless steps

**Table 6** Ratios of the controlling failure pressures ( $p_{cont}$ ) to the Drucker-Shield limit pressures ( $p_{DS}$ )

$r/D$	$D/t = 300$		$D/t = 500$	
	$p_{cont}/p_{DS}$		$p_{cont}/p_{DS}$	
	$\sigma_{yp} = 207 \text{ N/mm}^2$	$\sigma_{yp} = 414 \text{ N/mm}^2$	$\sigma_{yp} = 207 \text{ N/mm}^2$	$\sigma_{yp} = 414 \text{ N/mm}^2$
	$R_0/D = 0.8$			
0.05	1.36	1.72	1.21	1.44
0.10	1.29	1.49	1.28	1.54
0.15	1.39	1.45	1.32	1.68
0.20	1.57	1.57	1.47	1.55
	$R_0/D = 1.0$			
0.06	1.50	1.74	1.25	1.51
0.10	1.44	1.58	1.27	1.60
0.15	1.53	1.55	1.37	1.71
0.20	1.70	1.70	1.59	1.77

are taken to prevent it. This explains the anomaly mentioned in the Introduction.

The ratios in Table 6 are also very relevant to a number of national pressure vessel Codes, as their rules for internally pressurized torispheres are, for  $D/t < 500$ , based on the Drucker-Shield limit pressures. As may be seen from Table 6, considerable economies could be obtained by modifying the relevant sections of the Codes in line with the finite-deflection results given herein.

It should be noted that, even though the present investigation has been limited to steel shells, some of the results will carry over to other metallic shells. For instance, the plastic buckling  $p_{cr}$  values of aluminium shells are not very different from those of steel shells (8), despite the threefold difference in  $E$  values. Again, the axisymmetric yielding pressures of aluminium shells are somewhat higher than those of comparable steel shells (9). Thus, the above conclusion on more economic designs of torispheres will not be limited to steel shells only. With materials having low  $E$  values, the possibility of elastic buckling should also be checked (13).

### 8 SIMPLE APPROXIMATE EQUATIONS FOR PREDICTING $p_{cr}$ AND $p_{c2}$ FOR PERFECT TORISPHERICAL SHELLS

It is very helpful to designers of fabricated torispherical shells to have simple approximate equations available for predicting both the plastic buckling pressures and the axisymmetric yielding pressures of internally pressurized torispheres. Some equations in this category, for perfect torispheres and for the range  $500 < D/t < 1500$ , were given by Galletly and Radhamohan in (8, 9) (for  $p_{cr}^D$  and  $p_{c1}$ ).

The present calculations have extended the previous results in several respects, particularly to lower values of  $D/t$ . One could perhaps have improved the simple equations in (8, 9) using this information. However, the modified flow theory in BOSOR 5 does not predict any buckling for certain values of  $r/D$ ,  $D/t$  and  $\sigma_{yp}$  (see Figs 5 and 6) and various limits would have to be placed on the equation for  $p_{cr}^D$ .

A simpler way of proceeding is to utilize the internal buckling pressures calculated using deformation theory, that is  $p_{cr}^D$ . As noted earlier, the quantities  $p_{cr}^D/\sigma_{yp}$  are

almost independent of  $\sigma_{yp}$  and this makes the functional relationship between them and the geometric parameters a little simpler. The  $p_{cr}^D$  values are always lower than the  $p_{cr}^F$  values, so this approach will be on the conservative side.

With regard to the axisymmetric yielding mode, the  $p_{c2}$  values depend on  $\sigma_{yp}$  to some extent. What was done, therefore, was to determine an approximate equation for  $p_{c2}$  from the lowest values obtained, that is for  $\sigma_{yp} = 207 \text{ N/mm}^2$ . The effect of  $\sigma_{yp}$  was considered later.

From previous work, it was known that  $D/t$  and  $r/D$  were important geometric parameters and that  $R_0/D$  also had a noticeable effect on the failure pressures. However, the functional forms of the desired equations were not known and some were, therefore, assumed. The equations which follow may not be the best ones that could be found. However, they are reasonably satisfactory approximations to the computer results, and the errors involved in using them, over the ranges studied, are as indicated.

For the internal buckling pressures, the following equation was found:

$$\frac{p_{cr}^D}{\sigma_{yp}} \approx \frac{120(r/D)^{0.81}}{(D/t)^{1.46}(R_0/D)^{1.18}} \quad (1)$$

and, for the axisymmetric yielding pressures,

$$\frac{p_{c2}}{\sigma_{yp}} \approx \frac{10(r/D)^{0.85}}{(D/t)^{1.10}(R_0/D)^{0.93}} (1 + 0.001\sigma_{yp}^{1.09}) \quad (2)$$

The errors in equation (1) over the range  $300 < D/t < 1500$  are +12 and -16 per cent and in equation (2) are  $\pm 16$  per cent.

An equation for  $p_{cr}^D$  which gives errors within  $\pm 10$  per cent is

$$\frac{p_{cr}^D}{\sigma_{yp}} \approx \frac{200(r/D)^{1.5}}{(D/t)^{1.42}(R_0/D)^{1.17}} \left\{ 1 + 0.05 \left( \frac{r}{D} \right)^{-1.315} \right\} \quad (3)$$

and an equation for  $p_{c2}$  which agrees with the computer results for  $\sigma_{yp} = 207 \text{ N/mm}^2$  and  $\sigma_{yp} = 414 \text{ N/mm}^2$  to within  $\pm 8$  per cent is

$$\frac{p_{c2}}{\sigma_{yp}} \approx \frac{20(r/D)^{1.78}}{(D/t)^{1.08}(R_0/D)^{0.87}} \left\{ 1 + 0.1 \left( \frac{r}{D} \right)^{-1.37} \right\} \times (1 + 0.001\sigma_{yp}^{1.1}) \quad (4)$$

Comparing equations (1) and (3), it may be seen that the former is not just a simplified version of the latter. This is also the case with equations (2) and (4). The minimization routine used to derive the exponents in the equations has, presumably, arrived at different local minima for the various cases (one can also vary the magnitudes of the exponents and constants slightly and obtain equations which give errors that are not much larger than those quoted above).

It would have been preferable to arrive at simpler equations than those given above and which perhaps incorporated other groupings of the geometrical parameters. This has not been accomplished so far. For the internal buckling pressures for a constant  $R_0/D$ , it has, however, been observed that the quantities  $p_{cr}^D/\sigma_{yp}$

Table 7 Controlling failure pressures ( $p_{cr}/\sigma_{yp}$  or  $p_{cr}^D/\sigma_{yp}$ )  $\times 10^3$  for  $R_2/D = 0.8$  and 1.0. A comparison of BOSOR 5 predictions with those of equations (3) and (4)

$r/D$ $D/t$	0.05		0.10		0.15		0.20	
	BOSOR 5	Equations (3) and (4)	BOSOR 5	Equations (3) and (4)	BOSOR 5	Equations (3) and (4)	BOSOR 5	Equations (3) and (4)
$R_2/D = 0.8$								
300	2.73(Y) 3.27(Y)	2.40(Y) 3.13(Y)	4.30(Y) 5.20(Y)	3.91(Y) 5.10(Y)	5.90(Y) 7.50(Y)	5.65(Y) 7.37(Y)	8.00(Y) 8.99(Y)	7.68(Y) 10.01(Y)
400	1.93(Y) 2.45(B/Y)	1.76(Y) 2.31(B/Y)	2.90(Y) 3.66(B)	2.87(Y) 3.57(B)	4.27(Y) 4.87(B)	4.15(Y) 5.06(B)	6.13(Y) 6.67(Y)	5.63(Y) 6.78(B)
500	1.40(Y) 1.75(B/Y)	1.38(Y) 1.70(B)	2.20(Y) 2.58(B)	2.26(Y) 2.60(B)	3.30(Y) 3.41(B)	3.26(Y) 3.69(B)	4.80(Y) 4.88(B)	4.43(Y) 4.94(B)
600	1.10(Y) 1.29(B)	1.14(Y) 1.31(B)	1.83(Y) 1.91(B)	1.85(Y) 2.01(B)	2.62(B) 2.62(B)	2.68(Y) 2.84(B)	3.89(B) 3.89(B)	3.64(Y) 3.81(B)
800	0.80(Y) 0.84(B)	0.83(Y) 0.87(B)	1.25(B) 1.25(B)	1.33(B/Y) 1.33(B)	1.77(B) 1.77(B)	1.89(B) 1.89(B)	2.53(B) 2.53(B)	2.53(B) 2.53(B)
1000	0.60(B/Y) 0.63(B)	0.63(B) 0.63(B)	0.90(B) 0.90(B)	0.97(B) 0.97(B)	1.31(B) 1.31(B)	1.38(B) 1.38(B)	1.94(B) 1.94(B)	1.84(B) 1.84(B)
1300	0.42(B)	0.44(B)	0.61(B)	0.67(B)	0.95(B)	0.95(B)	1.40(B)	1.27(B)
1500	0.34(B)	0.36(B)	0.52(B)	0.55(B)	0.80(B)	0.80(B)	1.16(B)	1.04(B)
$R_2/D = 1.0$								
$r/D$ $D/t$	0.06		0.10		0.15		0.20	
300	2.33(Y) 2.82(Y)	2.22(Y) 2.89(Y)	3.27(Y) 4.10(Y)	3.22(Y) 4.14(B)	4.73(Y) 5.93(Y)	4.66(Y) 5.87(B)	6.80(Y) 7.60(Y)	6.32(Y) 7.86(B)
400	1.70(Y) 1.98(B)	1.63(Y) 1.97(B)	2.37(Y) 2.77(B)	2.36(Y) 2.75(B)	3.57(Y) 3.81(B)	3.41(Y) 3.90(B)	5.00(Y) 5.55(Y)	4.64(Y) 5.22(B)
500	1.23(Y) 1.43(B)	1.28(Y) 1.43(B)	1.80(Y) 1.97(B)	1.86(Y) 2.00(B)	2.73(Y) 2.77(B)	2.68(Y) 2.84(B)	3.93(Y) 3.95(B)	3.65(Y) 3.80(B)
600	0.97(Y) 1.09(B)	1.05(Y) 1.11(B)	1.43(Y) 1.49(B)	1.53(B/Y) 1.54(B)	2.16(B) 2.16(B)	2.19(B/Y) 2.19(B/Y)	3.06(B) 3.06(B)	2.93(B) 2.93(B)
700	0.80(Y) 0.87(B)	0.89(B/Y) 0.89(B)	1.18(B) 1.18(B)	1.24(B) 1.24(B)	1.72(B) 1.72(B)	1.76(B) 1.76(B)	2.40(B) 2.40(B)	2.36(B) 2.36(B)
900	0.60(B/Y) 0.60(B)	0.62(B) 0.62(B)	0.82(B) 0.82(B)	0.87(B) 0.87(B)	1.20(B) 1.20(B)	1.23(B) 1.23(B)	1.67(B) 1.67(B)	1.65(B) 1.65(B)
1200	0.40(B)	0.41(B)	0.54(B)	0.58(B)	0.81(B)	0.82(B)	1.14(B)	1.10(B)
1500	0.29(B)	0.30(B)	0.41(B)	0.42(B)	0.59(B)	0.60(B)	0.86(B)	0.80(B)

## Notes

- Y = axisymmetric yielding collapse  
B = unsymmetric plastic buckling
- In each column with two entries, the first entry is for  $\sigma_{yp} = 207 \text{ N/mm}^2$  and the second is for  $\sigma_{yp} = 414 \text{ N/mm}^2$ .
- The BOSOR 5 buckling pressures (marked B) are the average  $p_{cr}^D$  values in Table 5.

$(D/t)^{3/2}$  are approximately constant for each value of  $r/D$ . This result is, of course, consistent with equation (1).

#### 9 A COMPARISON OF THE PREDICTIONS OF EQUATIONS (3) AND (4) WITH THE COMPUTER RESULTS

Equations (3) and (4) were employed to determine the controlling failure pressures for all the perfect torispheres considered in this paper. The predictions of the equations were then compared with the computer results for  $p_{cr}$  and  $p_{cr}^D$ . The results of this exercise are given in Table 7 for  $\sigma_{yp} = 207$  and  $414 \text{ N/mm}^2$ . For each value of  $r/D$ , two columns are given. The first columns are the BOSOR 5 computer results and give the lower of  $p_{cr}$  and  $p_{cr}^D$  (the latter being the average of the corresponding value in Tables 1 and 2). The second columns come from equations (3) and (4) and, in each case, the lower value is recorded. The letter B after an entry signifies that the buckling mode is predicted to

control and the letter Y means that axisymmetric yielding controls.

For  $R_2/D = 1.0$ , the computer results and the approximate predictions of the controlling failure pressures are compared graphically in Figs 10 and 11. From these figures and Table 7, it may be seen that the overall agreement between the predictions of equations (3) and (4) and the computer results is fairly satisfactory and the errors are smaller with the higher value of  $\sigma_{yp}$ . The prediction of the controlling failure mode may also be seen to be usually correct (it will be recalled that the computer results from deformation theory are being employed in this discussion).

#### 10 CONCLUSIONS

- Using the BOSOR 5 computer program, values of the internal buckling pressures ( $p_{cr}$ ) and the axisymmetric yielding pressures ( $p_c$ ) have been obtained for perfect steel torispheres over the range  $300 < D/t < 1500$ .

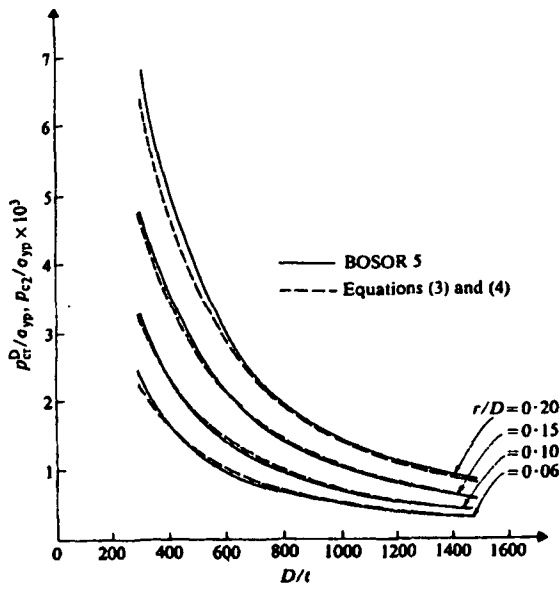


Fig. 10 A comparison of the predictions of equations (3) and (4) with the computer results ( $R_e/D = 1.0$ ,  $\sigma_{yp} = 207$  N/mm<sup>2</sup>)

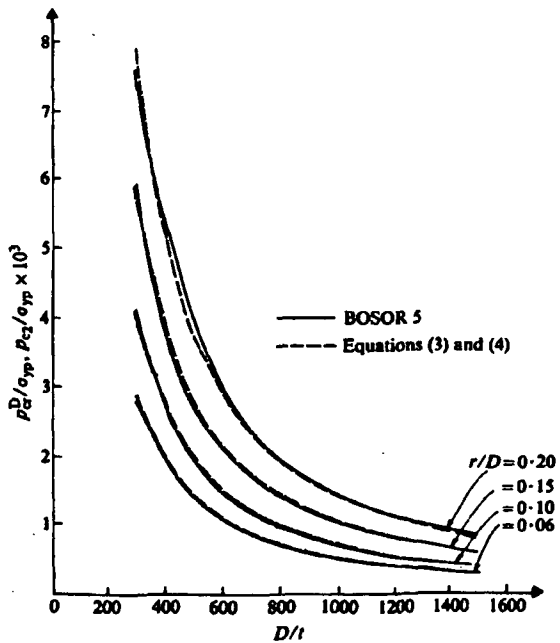


Fig. 11 A comparison of the predictions of equations (3) and (4) with the computer results ( $R_e/D = 1.0$ ,  $\sigma_{yp} = 414$  N/mm<sup>2</sup>)

2. From the above results, the controlling failure pressure curves (that is the lower of  $p_{cr}$  and  $p_{c2}$ ) for perfect steel torispheres under internal pressure can be determined. Over the range  $300 < D/t < 600$ , the Drucker-Shield limit pressures were compared with these controlling failure pressures and the ratio

between the two varied between 1.2 to 1.8. These results indicate that considerable economies could be achieved in the design of many torispherical shells if the various national Codes took advantage of the foregoing.

3. Using curve-fitting methods, simple approximate equations for  $p_{cr}^D$  and  $p_{c2}$  were determined over the range  $300 < D/t < 1500$ . These equations give adequate predictions of the failure pressures and modes for perfect internally pressurized torispherical shells. They should be a useful guide to similar equations for fabricated torispheres.

REFERENCES

- 1 Galletly, G. D. Stress failure of large pressure vessels—recommendations resulting from studies of the collapse of a 68 ft high x 45 ft dia. pressure vessel. Shell Development Corporation, Emeryville, California, Tech. Rep. 45-57, March 1957.
- 2 Galletly, G. D. Torispherical shells—a caution to designers. *Trans. ASME, J. Engng Ind.*, 1959, 81, 51-56. Also published in *Pressure Vessel and Piping Design—Collected Papers 1927-1959*, 1960, ASME, New York.
- 3 Harding, A. G. and Ehmke, E. F. Brittle failure of a large pressure vessel. *Proc. Am. Petrol. Inst.*, 1962, 42(3), 107-117.
- 4 Mescall, J. Stability of thin torispherical shells under uniform internal pressure. *Collected Papers on Instability of Shell Structures*, NASA Tech. Note D-1510, 1962.
- 5 Fiso, A. and Schneider, R. W. Wrinkling of a large thin code head under internal pressure. *Bull. Weld. Res. Coun.*, June 1961, 69, 11-13.
- 6 Drucker, D. C. and Shield, R. T. Limit analysis of symmetrically loaded shells of revolution. *Trans. ASME, J. Appl. Mech.*, 1959, 81, 61-68.
- 7 Shield, R. T. and Drucker, D. C. Design of thin-walled torispherical and toriconical pressure-vessel heads. *Trans. ASME, J. Appl. Mech.*, 1961, 83, 292-297.
- 8 Galletly, G. D. and Radhamohan, S. K. Elastic-plastic buckling of internally-pressurized thin torispherical shells. *Trans. ASME, J. Press. Vess. Tech.*, 1979, 101, 216-225.
- 9 Radhamohan, S. K. and Galletly, G. D. Plastic collapse and the controlling failure modes of internally-pressurized thin torispherical shells. *Trans. ASME, J. Press. Vess. Tech.*, 1979, 101, 311-320.
- 10 Galletly, G. D. Buckling and collapse of thin internally-pressurized dished ends. *Proc. Instn. Civ. Engrs.*, 1979, 67(2), 607-626.
- 11 Galletly, G. D. Elastic and elastic-plastic buckling of internally-pressurized 2:1 ellipsoidal shells. *Trans. ASME, J. Press. Vess. Tech.*, 1978, 100, 335-343.
- 12 Galletly, G. D. and Aylward, R. W. Plastic collapse and the controlling failure pressures of thin 2:1 ellipsoidal shells subjected to internal pressure. *Trans. ASME, J. Press. Vess. Tech.*, 1979, 101, 64-72.
- 13 Aylward, R. W. and Galletly, G. D. Elastic buckling of, and first yielding in, thin torispherical shells subjected to internal pressure. *Int. J. Press. Vess. Piping*, 1979, 7, 321-336.
- 14 Galletly, G. D. A comparison of the plastic buckling behaviour of 2:1 ellipsoidal and 2:1 torispherical shells subjected to internal pressure. *Proc. IUTAM Symp. on Physical Non-Linearities in Structural Analysis*, Senlis, France, May 1980, pp 85-88.
- 15 Galletly, G. D. The buckling of fabricated torispherical shells under internal pressure. *Buckling of Shells—Proc. of a State-of-the-Art Colloquium*, Stuttgart (Ed. E. Ramm), 1982, pp 429-466 (Springer-Verlag, Berlin).
- 16 Bushnell, D. BOSOR 5—program for buckling of elastic-plastic shells of revolution including large deflections and creep. *Comput. Structs.*, 1976, 6, 221-239.
- 17 Thurston, G. A. and Holston, Jr, A. A. Buckling of cylindrical shell end closures by internal pressure. NASA CR 540, 1966.
- 18 Brown, K. W. and Kraus, H. Stability of internally-pressurized vessels with ellipsoidal heads. *Trans. ASME, J. Press. Vess. Tech.*, 1976, 98, 157-161.
- 19 Galletly, G. D. Plastic buckling of torispherical and ellipsoidal shells subjected to internal pressure, *Proc. Instn. Mech. Engrs.*, 1981, 195, 329-345.

- 20 Bushnell, D. and Galletly, G. D. Stress and buckling of internally-pressurised elastic-plastic torispherical vessel heads—comparisons of test and theory. *Trans. ASME, J. Press. Vess. Tech.*, 1977, 99, 39–53.
- 21 Lagae, G. and Bushnell, D. Elastic-plastic buckling of internally-pressurised torispherical vessel heads. *Nucl. Engng and Des.*, 1978, 48, 405–414.
- 22 Bushnell, D. Non-symmetric buckling of internally-pressurised ellipsoidal and torispherical elastic-plastic pressure vessel heads. *Trans. ASME, J. Press. Vess. Tech.*, 1977, 99, 54–63.
- 23 Kanodia, V. L., Gallagher, R. H. and Mang, H. A. Instability analysis of torispherical pressure vessel heads with triangular thin-shell finite elements. *Trans. ASME, J. Press. Vess. Tech.*, 1977, 99, 64–74.
- 24 Rensch, H. J. and Wunderlich, W. A semi-analytical finite element procedure for non-linear elastoplastic analysis of arbitrarily loaded shells of revolution. *Proc. 6th Int. SMIRT Conf.*, Paris, 1981, Paper M4/1, pp 1–8 (North Holland Publishing Co.).
- 25 Galletly, G. D. and Beachut, J. Plastic buckling of internally-pressurised torispherical shells. *3rd Int. Colloquium on the Stability of Metal Structures*, Paris, November 1983, Final Report, pp 179–184 (CTICM).
- 26 Cantos, B. et al. Elastic and elastic-plastic buckling of vessel heads. Computation by the CEASEMT system. *Proc. 4th Int. SMIRT Conf.*, San Francisco, 1977, Paper G7/4.
- 27 Unger, C. and Mang, H. A. Zum spannungs- und stabilitätsproblem von kesselböden unter innendruck. *Der Stahlbau*, 1980, 12, 373–379.
- 28 Steele, C. R. and Ranjna, G. V. Effect of stiffening rings on the stability of torispherical heads. *Pressure Vessel Design* (Ed. G. E. O. Widera), 1982, PVP-57, pp 67–84 (ASME, New York).
- 29 Kirk, A. and Gill, S. S. The failure of torispherical ends of pressure vessels due to instability and plastic deformation—An experimental investigation. *Int. J. Mech. Sci.*, 1975, 17, 525–544.
- 30 Patel, P. R. and Gill, S. S. Experiments on the buckling under internal pressure of thin torispherical ends of cylindrical pressure vessels. *Int. J. Mech. Sci.*, 1978, 20, 159–175.
- 31 Galletly, G. D. Internal pressure buckling of very thin torispherical shells—a comparison of experiment and theory. *Proc. 3rd Int. Conf. Struct. Mech. Reactor Technol. (SMIRT)*, London, 1975, Paper G2/3.
- 32 Galletly, G. D. Some experimental results on the elastic-plastic buckling of thin torispherical and ellipsoidal shells subjected to internal pressure. *2nd Int. Colloquium Stability of Steel Structures*, Liège, 1977, Preliminary Report, pp 619–626.
- 33 Popov, E. P., Khojasteh-Bakht, M. and Sharif, P. Elastic-plastic analysis of some pressure vessel heads. *Trans. ASME, J. Engng Ind.*, May 1970, 309–316.
- 34 Gerdeen, J. C. A critical evaluation of plastic behaviour data and a unified definition of plastic loads for pressure components. *WRC Bull.*, NY, 1979, 254, 1–64.
- 35 Bushnell, D. Buckling and vibration of ring-stiffened segmented shells of revolution—Numerical results. *Proc. 1st Int. Conf. on Press. Vess. Tech.*, Delft, October 1969, pp 255–268 (ASME, New York).
- 36 Abdulla, K. M. and Galletly, G. D. Free vibrations of cones, cylinders and cone/cylinder combinations. *Symp. on Struct. Dynamics*, Loughborough University of Technology, March 1970, Paper B2, pp B.2.1–B.2.20.
- 37 Bushnell, D. Buckling of shells—pitfall for designers. *AIAA J.*, September 1981, 19 (9), 1183–1226.
- 38 Bushnell, D. Plastic buckling. *ASME PVP 'Decade of Progress'*, 1982, pp 47–117 (ASME, New York).
- 39 Wunderlich, W. Discussion of (19) in *Proc. Instn Mech. Engrs*, 1981, S39.
- 40 Roche, R. L., Altx, M. and Austrussen, B. Design rules against buckling of dished heads; *Proc. 5th Int. Conf. on Press. Vess. Tech.*, San Francisco, 1984, pp 274–289.
- 41 Galletly, G. D. The background to forthcoming design proposals for two shell buckling problems. *Behaviour of thin-walled structures* (Eds J. Rhodes and J. Spence), 1985, pp 179–210, (Elsevier Applied Science Publications).